UNIVERSITÀ POLITECNICA DELLE MARCHE

Engineering Faculty

Master Degree in Biomedical Engineering

Analysis of functional connectivity in healthy subjects with intact brain and in patients with surgical resection of the corpus callosum

Supervisor: *Professor Laura Burattini*

Candidate: *Elena Vitti*

Co-Supervisors: *Professor Mara Fabri*

Ilaria Marcantoni, PHD

A.Y. 2021/2022

Abstract

One of the most complex organs of the human body is the brain both from an anatomical and physiological point of view; it is divided into two hemispheres (right and left) and consists of different structures that continuously exchange information thanks to the presence of neurons, cells found at the base of nervous tissue, which generate and receive electrical impulses. The two hemispheres communicate with each other to exchange information necessary to perform numerous neural functions. This communication takes place through the cerebral commissures, of which the largest and the most important is the corpus callosum. The resection of the corpus callosum is a surgical technique that was introduced in the past to be able to cure severe forms of epilepsy. Since the corpus callosum is the main communication route between the two hemispheres, its partial or total resection will cause different effects on the brain. Patients in whom the corpus callosum was resected for therapeutic reasons (split-brain patients) provide a unique opportunity of research. This pilot study investigates the interhemispheric functional connectivity in callosotomized patients operated in adult age. Connectivity between left and right hemispheres is studied through functional magnetic resonance images whose operating principle is based on nuclear magnetic resonance. The functional magnetic resonance is a non-invasive method of imaging, which is based on the BOLD signal, and which allows to obtain images showing brain activity. This technique was used to obtain the resting state data that are analyzed in this study. Resting state networks are anatomically separated, but functionally linked, brain regions that interact continuously even when the brain is at rest and the acquisition of resonance images takes place in absence of any stimulus to the subjects. FSL software was used for the data analysis, specifically created for the analysis of magnetic resonance images, and equipped of various useful tools for this purpose. The patients analyzed are between 40 and 50 years of age and have undergone callosotomy about 20/25 years earlier. While the healthy subjects are between 30 and 70 years of age, none with regressed pathologies and with correct neuronal activity. In the subject analysis step, the evaluation of interhemispheric functional connectivity and the recognition of the resting state networks were performed by using the probabilistic independent component analysis. Independent components were obtained using the ICA technique, among which,

at first, it was possible to identify signal and noise components. Subsequently 10 resting-state networks are identified in both patients and controls characterizing brain activity in a of each subject in state of rest.

Multi-subject analysis on healthy subjects allowed to identify three activations resting state networks: medial visual, default mode, and sensory motor. Both patients showed a bilateral brain activity in the medial visual network, comparable to healthy subjects. In the sensory motor and the default mode networks the activation was unilateral, at variance with controls. In this thesis work, some subjects showed a certain degree of bilaterality of the activated regions, even after callosotomy surgery. It is therefore possible to hypothesize a capacity for readaptation of the brain as regards communication between the two hemispheres, once the callosal resection has taken place, through subcortical networks.

TABLE OF CONTENTS

“Un vincitore è semplicemente
un sognatore che non si è mai arreso”
N. Mandela

“Ridere ci ha resi invincibili.
Non come coloro che vincono sempre,
ma come coloro che non si arrendono”
F. Kahlo

Alla mia bellissima famiglia

Introduction

The brain is a complex organ, both from an anatomical and physiological point of view. It is divided into two hemispheres, and it is formed by different structures that constantly exchange information thanks to the neurons, which generate and receive electrical impulses. The brain is the center of many functions, such as sensory and motor, and each is controlled predominantly by either the right or left hemisphere according to the principle of hemispheric lateralization. This exchange of information takes place through the cerebral commissures, of which the largest and most important is the corpus callosum. The corpus callosum is a large white matter tract and it represents the main link between the right hemisphere and the left hemisphere, allowing both hemispheres to communicate and send neural signals to each other. Thus, sensory, motor, and cognitive information are continuously exchanged between the two hemispheres via this neural pathway, and a damage to the corpus callosum can lead to hemispheric miscommunication and loss of functions such as vision, speech, and memory.

The cut of the corpus callosum is a surgical technique introduced, in the past, for the treatment of severe forms of epilepsy. Epilepsy is a chronic disease that causes recurrent violent seizures in the patient's brain, and it is usually treated with medication. Callosotomy was used if the patient did not respond to antiepileptic drugs. However, this kind of intervention is rarely done today because of the introduction of drugs that can control epileptic seizures. The cut of the corpus callosum shows that in addition to a possible beneficial effect for the treatment of epilepsy, alterations could be found in the subjects involved, therefore there will be different effects depending on whether the resection is partial or total.

Subjects who underwent corpus callosotomy in their young life, that are still alive, are adjudged to be fit with corpus callosum studies that aim to determine how the different brain areas interact with each other and whether there are other mechanisms by which the two halves of the brain communicate without the information passing through the corpus callosum.

Interhemispheric connectivity is mainly studied through functional magnetic resonance imaging (fMRI), which allows us to investigate the functional connections of the brain.

It is a non-invasive method with high spatial resolution that allows to obtain images showing brain activity based on the BOLD signal, which depends on the level of blood oxygenation in response to neural activity.

The aim of this present work is to understand how information passes between the two cerebral hemispheres in patients in whom the corpus callosum is surgically cut and compare the functional connectivity of patients with the one of healthy subjects.

Furthermore, healthy subjects were considered as a comparison method for pathological subjects, to understand whether or not there is a bilateral network in patients with callosotomy, i.e., if there is a reorganization of the fibers in the brain despite the corpus callosum having been severed, allowing to neuronal signals to travel from one hemisphere to the other via subcortical pathways.

Functional magnetic resonance imaging was used to acquire DICOM images of the subjects considered in this study, while the FSL software, created specifically for the analysis of magnetic resonance images and equipped with different useful tools, was used for the data analysis of the present study. The data used in this study were acquired from two right-handed patients, P1, P2, P3, P4, P5 (age: 30-60 years; M/F=4/1) who had severe epilepsy episodes in their history, and healthy subjects S1, S2, S3, S4 (age: 31-70 years; F/M= 2/4). The callosotomy surgery was done in 2018 for all patients.

Chapter 1 *"Anatomy and Physiology of the Brain"*

1.1 The Nervous System

The nervous system is the main system that receives, processes, and responds to internal and external stimuli and it is the center of controlling, regulatory, and communicating system in the body. It controls complicated processes like movement, thought and memory and it plays an essential role in the activities done without thinking, such as breathing, blushing, and blinking. It is made up of nerve tissue, brain, spinal cord and peripheral nerves. The nervous system has two main parts, and each part contains billions of cells called neurons, or nerve cells. These special cells send and receive electrical signals through the body. The nervous system is divided in *Central nervous system* and *Peripheral nervous system* (***Figure 1***) (Ambrosi et al., 2010).

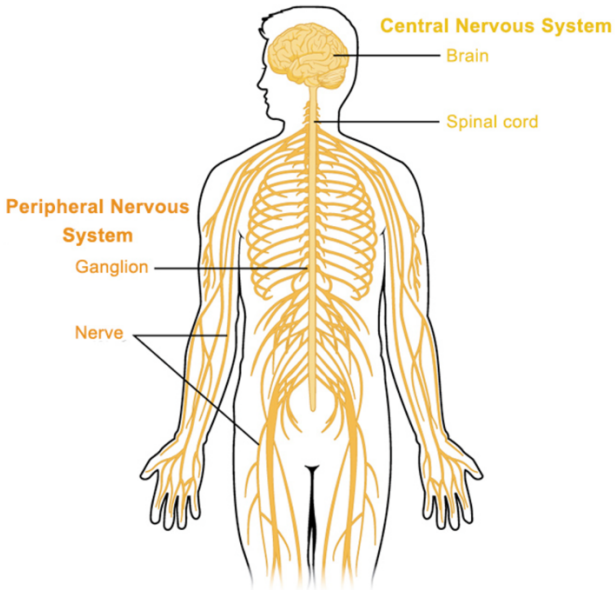

Figure 1 *Central nervous System which includes the brain and spinal cord, and Peripheral Nervous system, which encompasses nerves outside the brain and spinal cord* (From Farlex Partner Medical Dictionary, 2012)

The *Central nervous system* (CNS) comprises the brain and spinal cord. It receives information from the entire body and coordinates activity across the whole organism, constantly adapting it to the continuous environmental variations. The brain is contained in the skull. The *spinal cord* is located within the vertebral canal and forms the caudal part of the central nervous system. Supported by the vertebrae, the spinal cord carries messages to and from the brain and the rest of the body. The *Peripheral nervous system*

(PNS) consists of many nerves that branch out from the CNS all over the body. This system transmits information from the brain and spinal cord, generated at the level of the CNS, to all other organs of the body, and vice versa. The peripheral nervous system is further subdivided into *Somatic nervous system* and *Autonomic nervous system*. The *Somatic nervous system* consists of nerves that go to the skin and muscles, and it is involved in conscious perception and voluntary activities. The *Autonomic nervous system* consists of nerves that connect the CNS to the visceral organs such as the heart, stomach, and intestines, and it mediates unconscious perception and unvoluntary activities (Ambrosi et al., 2010).

1.1.1 Cells of Nervous System

There are two cell types in the nervous system: neurons specialized in the generation and conduction of nerve impulses and glial cells that perform support functions and intervene in reparative processes, in the inflammatory response and in immune processes (Anastasi et al., 2012).

1.1.1.1 Glial Cells

The glia cells are non-neuronal cells located in the CNS and PNS that do not produce any electrical impulses. They have four main functions:

- surround the neurons to protect and support them;
- deliver nutrients and oxygen to neurons;
- isolate one neuron from another;
- destroy pathogens and remove dead neuron.

Glial cells are divided into three groups: *macroglia*, (astrocytes and oligodendrocytes*)*, *ependymal cells* and *microglia cells*. *Astrocytes* carry out a protective action against neurons by producing growth factors and by modeling the formation of scar tissue. *Oligodendrocytes* perform the fundamental function of producing myelin in the CNS, similar function to the Schwann cells in PNS. The *ependymal cells* line the spinal cord and the ventricular system of the brain. These cells are involved in the creation and secretion of cerebrospinal fluid (CSF) and beat their cilia to help circulate the CSF and make up the blood-CSF barrier (Johansson et al., 1999). The *microglia* are specialized macrophages

capable of phagocytosis that protect neurons of the central nervous system (Brodal, 2010).

1.1.1.2 Neurons

The neuron is a specialized cell that has the fundamental task of generating and conducting an electrical signal along its membrane and transmitting it to other neurons or effector cells. For this reason, the nerve cell, is made up of a cell body (*soma*) that contains the nucleus, and extensions: the dendrites and the axon.

The *dendrites* receive signals from neighboring neurons, the *axon* generates and transmits the nerve signal over a distance, and the *axon terminal* transmits signals to other neuron dendrites or tissues. The cell body is delimited by a simple plasma membrane; the axon membrane can be covered by one or more layers of myelin forming a sheath. The *myelin sheath* speeds up signal transmission along the axon; it is produced by the wrapping of oligodendrocytes (in the central nervous system) or *Schwann cells* (in the peripheral nervous system).

Along the course of the axon there are points of interruption of the myelin sheath, called *Ranvier nodes,* which correspond to the region where a Schwann cell or an oligodendrocyte takes over from the previous one. This allows the electrical impulse to run along the axon, "jumping" from one node to another, with a mode of propagation called “saltatorial” which is much faster (10-120 m/s) than those of unmyelinated fibers (0.5-1.6 m/s) (Anastasi et al., 2012) (***Figure 1.2***).

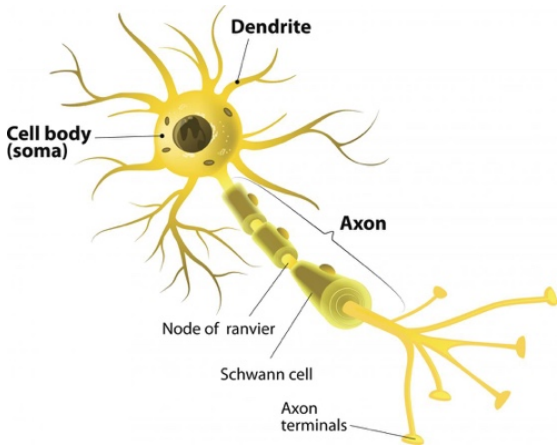

Figure 1.1 *Diagram of a section of a neuron represented in its different parts* (From Anastasi et al., 2012)

1.1.1.2.1 Types of Neurons

Neurons can be classified into three basic groups depending on their function: sensory neurons, motor neurons and relay neurons (***Figure 1.2***) (Ambrosi et al., 2010).

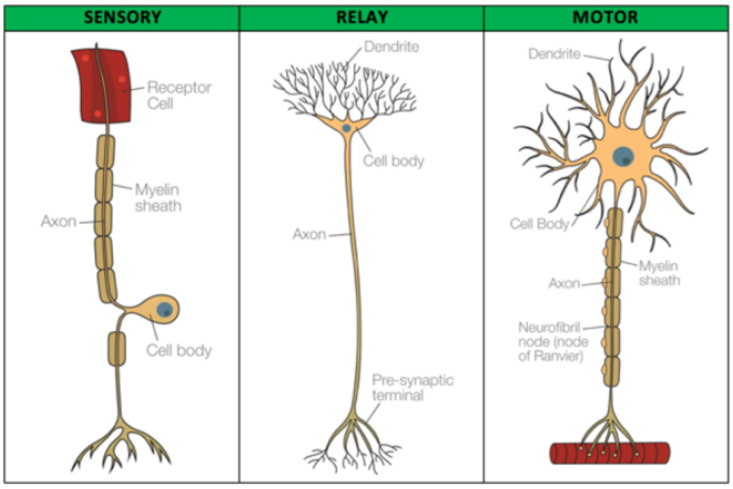

Figure 1.2 *Sensory Neurons, Relay Neurons and Motor Neurons morphology* (From Anastasi et al., 2012)

Sensory Neurons (afferent neurons) are nerve cells carrying nerve impulses from sensory receptors towards the central nervous system and brain. When these nerve impulses reach the brain, they are translated into 'sensations', such as vision, hearing, taste, and touch. This sensory information can be either physical (sound, heat, touch, and light), or chemical (taste or smell). An example of this can be when touching an extremely hot surface. Once this happens, the sensory neurons will be sending signals to the central nervous system about the information they have received. Most sensory neurons are characterized as being pseudo-unipolar. This means that they have one axon which is split into two branches (Ambrosi et al., 2010).

Motor neurons (efferent neurons) are the nerve cells responsible for carrying signals away from the central nervous system towards muscles to cause movement. They release Acetylcholine (Ach) as neurotransmitters to trigger responses leading to muscle movement. Motor neurons are in the brainstem or spinal cord and connect to skeletal muscles throughout the body. These types of neurons transmit signals from the spinal cord and brainstem to skeletal and smooth muscle to either directly or indirectly control

muscle contraction. Motor neurons are defined as multipolar. This means that they have one axon and several dendrites emerging from the cell body.

Interposed between the sensory neurons and the motor neurons are the interneurons or relay neurons which constitute the largest group. They allow sensory and motor neurons to communicate each other, and they connect various neurons within the brain and spinal cord. They are easy to recognize, due to their short axons. Interneurons, in addition to mediating simple reflexes, are also implicated in higher brain functions (Ambrosi et al., 2010).

1.1.1.2.2 Neurons Action Potential

Neurons are electrically excitable, reacting to input with the production of electrical impulses, propagated as action potentials throughout the cell and its axon. To begin conduction, an action potential is generated near the cell body portion of the axon. The action potential is generated and propagated by means of changes of the plasma membrane permeability to sodium and potassium. The action potentials finally reach the axonal terminal and transmit the signal to neighboring cells through synapses. This action is the way these cells can interact with each other, i.e., at synapses via synaptic transmission. The protein membrane of a neuron acts as a barrier to ions.

Normally, the cell's interior is negative, compared to its outside. This state is the resting membrane potential of about -60/-70 mV (Chen et al., 2021). When ions move across the membrane through ion channels that open and close due to the presence of neurotransmitter, the influx and outflux of ions will make the inside of the target neuron more positive. This change in membrane potential will open voltage-gated cationic channel (sodium channel) resulting in the process of depolarization and when this depolarization reaches a point of no return, called a threshold, a large electrical signal is generated. This is a generation of the neuronal action potential. An action potential is a rapid rise and subsequent fall in voltage or membrane potential across a cellular membrane with a characteristic pattern (***Figure 1.3***) (Chen et al., 2021).

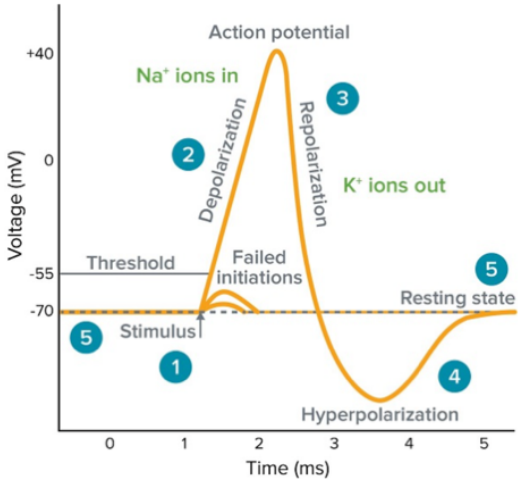

Figure 1.3 *Action Potential phases* (From Chen et al., 2021)

The stimulus starts the rapid change in voltage or action potential (1). Sufficient current must be administered to the cell to raise the voltage above the threshold to start membrane depolarization; if the current is insufficient to depolarize the membrane to the threshold level, an action potential will not fire. The depolarization is caused by a rapid rise in membrane potential opening of sodium channels in the cellular membrane, resulting in a large influx of sodium ions (2).

Membrane repolarization results from rapid sodium channel inactivation as well as a large efflux of potassium ions resulting from activated potassium channels (3), while the hyperpolarization is a lowered membrane potential caused by the efflux of potassium ions and closing of the potassium channels (4). The phase of resting state is when membrane potential returns to the resting voltage that occurred before the stimulus occurred (5) (Chen et al., 2021).

1.2 Human Brain

The brain is the most developed and functionally most important part of nervous system, and its functioning constitutes the primary foundation of biological individuality and personal identity. It is a complex organ that controls thought, memory, emotion, touch, motor skills, vision, breathing, temperature, hunger, and every process that regulates our body. Together, the brain and spinal cord that extends from it make up the central nervous system. The brain is constituted about 60% of fat and the remaining 40% is a combination of water, protein, carbohydrates, and salts. The brain itself is a not a muscle.

It contains blood vessels and nerves fibers, including neurons and glial cells (Seitun, 2019). The brain is made up of many specialized areas that work together (***Figure 1.4***).

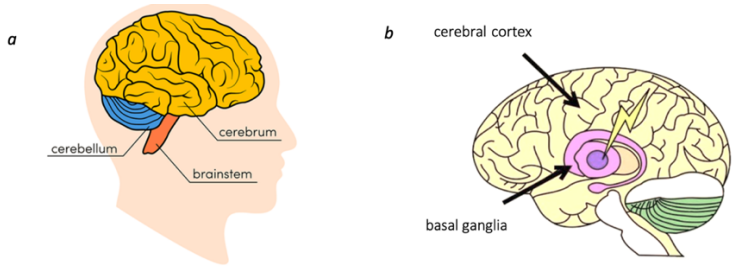

Figure 1.4 *Human Brain Anatomy: (a) At high level, the brain can be divided into the cerebrum, brainstem, and cerebellum. (b) Basal ganglia located at the bottom of the cerebral cortex, near the base of the brain* (From Seitun, 2019).

The cerebrum is the largest and highest portion of the brain and accounts for two thirds of the total weight of the brain. The cerebrum consists of two hemispheres, divided by the deep interhemispheric fissure that ends at the level of the corpus callosum, which is a commissural structure made up of myelinated and unmyelinated fibers.

One hemisphere, usually the left, is functionally dominant, controlling language and speech. Both hemispheres interpret visual and spatial information.

The cerebral hemispheres consist of an inner core of myelinated nerve fibers, white matter, and an outer cortex of gray matter.

The gray matter contains of the cell bodies of the neurons, the dendrites that extend from them and the proximal tract of the axons. The white matter consists of bundles of nerve fibers (axons) of neurons whose soma is localized in the gray matter (Ambrosi et al., 2010).

The cerebrum is formed by:

- The *cortex* is the outermost layer of brain cells. Thinking and voluntary movements begin in the cortex
- The *basal ganglia* are a cluster of structures in the center of the brain. The basal ganglia coordinate messages between multiple other brain areas

The cerebellum is located near the brainstem, and it is the part of the brain contributing to the control of voluntary movements and involved in control of balance, coordination, and posture.

Each hemisphere is also divided into several lobes (***Figure 1.5***):

- The *frontal lobe* is responsible for problem solving and judgment and motor function
- The *parietal lobe* manages sensation, handwriting, and body position
- The *temporal lobe* is involved with memory and hearing
- The *occipital lobe* contains the brain's visual processing system.

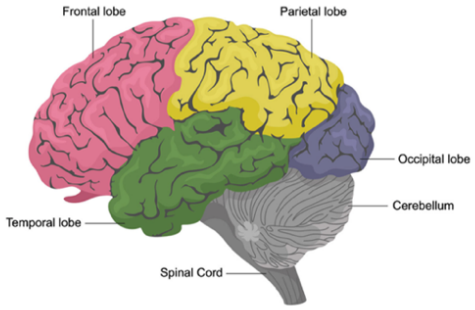

Figure 1.5 *Human Brain Anatomy: four sections of the Brain called Lobes: (pink): Frontal Lobe; (yellow): Parietal Lobe; (green) Temporal Lobe; (blue) Occipital Lobe* (From Seitun, 2019).

Between the cerebrum and the spinal cord is present the brainstem, which participates in the transport of sensory and motor stimuli from and to the head region, by means of afferent and efferent fiber bundles (Ambrosi et al., 2010).

1.2.1 Lobes of the Brain

Frontal lobe constitutes the anterior part of the brain and contains the motor cortical area and the premotor cortex. The frontal lobe participates in learning and memory processes, while in the left side words are formed and controlled. Therefore, in the anterior part of the frontal lobe (prefrontal cortex) higher cognitive functions are performed; in the posterior part the movements are controlled and modified (***Figure 1.11, blue***) (Binder et al., 1997).

Parietal lobe is situated in the middle part of the brain. It helps to identify objects and understand spatial relationships (where one's body is compared with objects around the person). The parietal lobe is also involved in interpreting pain and touch in the body (***Figure 1.11, yellow***) (Russell et al., 1992).

Temporal lobe is in the lower part of the cerebral hemispheres, and it is seat of the acoustic area. The temporal lobe is involved in short-term memory, speech, musical rhythm, and some degree of smell recognition. An integral part of the temporal lobe is

the limbic system. The temporal lobe houses Wernicke's area, which helps the brain understand spoken language (***Figure 1.11, green***) (Binder et al., 1997).

Occipital lobe is in the posterior part of the brain and its main activity is to process visual information. There are many neurons specialized in recognizing and processing the details of an image. All visual information is integrated into the occipital lobes, including those that influence posture and balance (***Figure 1.11, pink***) (Russell et al., 1992).

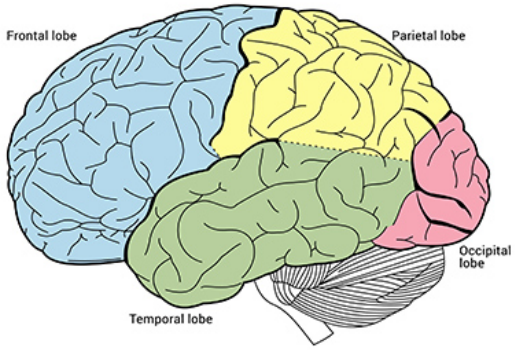

Figure 1.11 *Brain's Lobes* (From Russell et al., 1992).

1.2.2 Cerebral Cortex

The *cerebral cortex* is the outermost layer of the brain, associated with the highest mental capabilities. The cerebral cortex constitutes the highest level of integration and planning of the motor system; it also controls consciousness, thought, memory and intelligence.

The cerebral cortex is primarily composed of grey matter. Although the cerebral cortex is only a few millimeters in thickness, it consists of approximately half the weight of the total brain mass. The cerebral cortex has a wrinkled appearance, consisting of bulges, also known as gyri, and deep furrows, known as sulci.

The many folds and wrinkles of the cerebral cortex allow for an increased number of neurons to live there, permitting large amounts of information to be processed. The cortex is present in both hemispheres, right and left, separated by a large groove called interhemispheric fissure. The right hemisphere controls the left side of the body, and the left half controls the right side of the body. The two hemispheres are connected via the corpus callosum, formed by bundles of nerve fibers, to allow both hemispheres of the cerebral cortex to communicate with each other and to establish further connections (Ambrosi et al., 2010).

1.2.2.1 Cerebral Cortex Areas

The cerebral cortex is composed by different areas, with different organization and functions. They were originally defined by the German anatomist Korbinian Brodmann based on their cytoarchitectonic (histological) characteristics (***Figure 1.6***) (Finger, 2013). The cerebral cortex can be characterized as being made up of three types of divisions, which serve different purposes: sensory, motor, and association areas. The combination of these three areas account for most of human's cognition and behavior (Ambrosi et al., 2010).

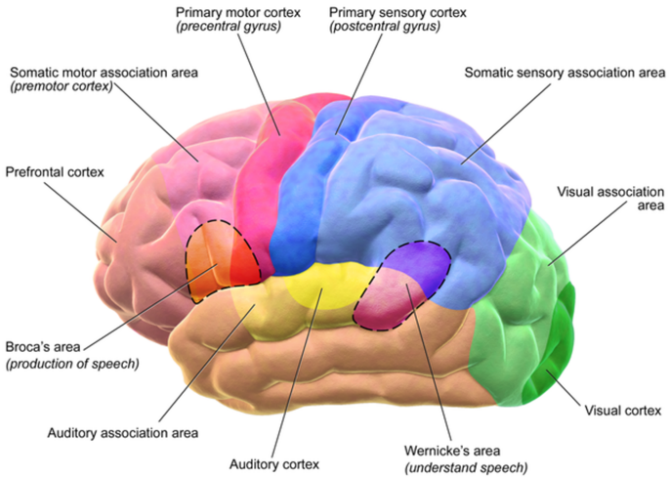

Figure 1.6 *Motor and Sensory areas of the Cerebral Cortex* (From Finger, 2013)

1.2.2.1.1 Sensory Areas

The sensory areas of the cerebral cortex are responsible for general somatic sensitivity: they deal with the conscious perception of elementary stimuli, and with the reception and interpretation of sensory information from different parts of the body such as touch, pressure, temperature, and pain, from different parts of the body. The sensory areas ca be divided into a primary and a secondary area: the primary areas directly receive signal from different receptors through subcortical relays structures. The secondary areas are involved in the encoding and decoding of sensory stimuli allowing their recognition following the attribution of a meaning based on experience.

The *sensory areas* include the visual cortex, the somatosensory cortex, the auditory cortex, and the gustatory cortex (***Figure 1.7***).

The *visual cortex* is in the occipital lobes, and it is essential to the conscious processing of visual stimuli. It is important for making sense of visual information and plays a role in

object recognition and representation. There is a visual cortex in each hemisphere: the visual cortex in the left hemisphere receives information from the right visual field, the visual cortex in the right hemisphere receives information from the left visual field (Ambrosi et al., 2010).

The somatosensory cortex is in the parietal lobe and receives tactile information from the body. This information can include temperature, touch, and pain, all of which are then integrated in the somatosensory cortex to produce a 'map' of the body.

The *auditory cortex* is an area within the temporal lobes which is responsible for processing auditory information. This cortex can perform basic and higher functions relating to hearing, including the ability for some people to language switch.

Finally, the *gustatory cortex* is a region in the frontal lobe which is responsible for the perception of taste (Ambrosi et al., 2010).

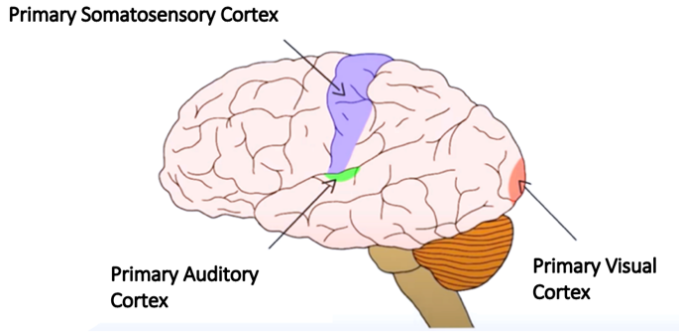

Figure 1.7 *Sensory areas of the Cerebral Cortex* (From Seitun, 2019).

1.2.2.1.2 Motor Areas

The motor areas are indispensable for the programming of voluntary movement, for the formulation of abstract thought and more generally for higher cognitive activities (ability to judge, to choose). These areas are mainly found within the frontal lobes and include the primary motor cortex, premotor cortex, and supplementary motor cortex. (***Figure 1.8***).

The *primary motor cortex* is associated with the coordination and initiation of motor movements. Each cerebral hemisphere of the primary motor cortex contains a motor-related representation of the opposite side of the body. The primary motor cortex, located in front of the central cleft, controls specific muscles in the body, and more cortical regions are assigned to those that cause fine movements (fingers, thumb, lips, mouth).

The *premotor cortex*, located in front of the motor cortex, controls coordinated movements: it is involved in preparing and executing limb movements, as well as using information from other regions of the cortex to select appropriate movements. It is also necessary for learning, especially through imitation, and social cognition, specifically empathy.

The *supplementary cortex* is responsible for the planning of complex movements and contributes to the control of movement (Ambrosi et al., 2010).

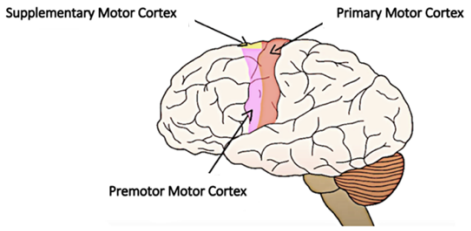

Figure 1.8 *Motor areas of the Cerebral Cortex* (From Seitun, 2019).

1.2.2.1.3 Association Areas

The association areas are present throughout the cerebral cortex in the four lobes. These areas act by integrating information from other brain regions, often adding more complexity to their functions. The association areas can form connections between sensory and motor areas to give meaning to and organize information in these areas.

Association areas within the frontal lobes are involved in key processes such as planning, thinking, and feeling; they also play a role in personality and controlling emotional behaviors. Association areas within the parietal lobe are involved in spatial skills such as spatial awareness and reasoning, as well as being responsible for paying attention to visual stimuli in the environment (***Figure 1.9***). In the temporal lobes, association areas function primarily in memory processes such as processing procedural and episodic memories.

Occipital lobe association areas contribute to facilitate memories associated with visuals to be retained as well as enabling us to think in a visual manner; they also communicate with other lobes of the cortex to assimilate visual information with memories, sounds, and language to understand visual stimuli (Ambrosi et al., 2010).

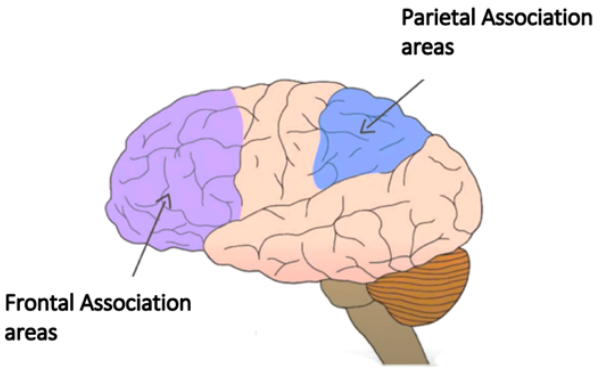

Figure 1.9 *Frontal and Parietal Association areas of the Cerebral Cortex* (From Seitun, 2019).

1.2.2.1.4 Broca and Wernicke's areas

Broca's area in the human prefrontal cortex and Wernicke's area in the human temporal lobe are the two most well-known cortical areas involved in the production and comprehension of speech (Chaplin et al., 2020).

The French physician and anatomist, Pierre Paul Broca, studied for the first time in 1861 the Broca's area, thanks to an examination of on a patient unable to reproduce words, despite understanding what was said to him. On physical examination, this patient's brain showed a lesion in the left frontal lobe. Thus, in 1863 Broca wrote an article in which he spoke about 8 clinical cases characterized by the presence of a lesion to the left frontal lobe, and which presented aphasia, literally the absence of language. From this, he deduced that the left hemisphere that controlled the production of the speech and this area is known as Broca's area (Mohr et al. 1978).

Broca's motor area is in the motor associative area that controls the mouth and lips (*Figure 1.10*).

The primary functions of the Broca area are both language production and comprehension through the activation of the motor neurons: it coordinates the movements of the larynx and the mouth generating the expression of words. Different regions of the Broca area are specialized in various aspects of comprehension: the anterior portion helps with word meaning, while the posterior is associated with phonology. The Broca area is also necessary for language repetition, gesture production, sentence grammar and fluidity, and the interpretation of others' actions (Stinnett et al., 2021). In contrast to Broca's area, which serves the expressive aspects of motor speech, Wernicke's area, located in the temporal lobe, is devoted to another major aspect of

language: comprehension of spoken and written language (***Figure 1.10***) (Russell et al., 1992).

The Wernicke area was discovered in 1874 by a German neurologist, Carl Wernicke, from whom it inherited the name. Wernicke's area is close to the auditory cortex (***Figure 1.10***) and it is associated with language comprehension, receiving information from the sensory association areas. It is important in a person's personality since it integrates sensory information and coordinates the access to auditory and visual memories (Moini, et al., 2020).

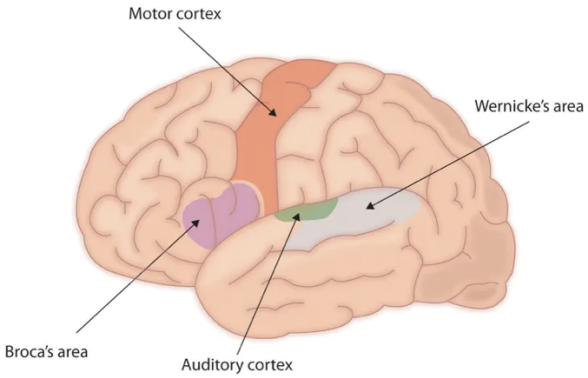

Figure 1.10 *Broca and Wernicke's areas* (From Moini et al., 2020)

The functions performed in the Wernicke area are:

- understanding of language, both written and spoken;
- management of the semantics of language, transforming words into their meaning.
- speech production planning

These functions form the basis of language understanding and are the basis of communication (Fiore, 2018).

In conclusion, Broca's and Wernicke's areas are the main language centers. The connections between these areas are considered as the primary or core language system (Binder et al., 1997). However, to be able to read, speak, and write, other areas of the brain need to function in coordination (Moini et al., 2020).

1.2.3 Cerebellum

The *cerebellum* ("little brain") is a structure located at the back of the brain, underlying the occipital and temporal lobes of the cerebral cortex (***Figure 1.12***). Although the cerebellum accounts for approximately 10% of the brain's volume, it contains over 50% of the total number of neurons in the brain (Vago et al., 2014).

Motor commands are not initiated in the cerebellum; rather, the cerebellum modifies the motor commands of the descending pathways to make movements more adaptive and accurate. The cerebellum is involved in the following functions:

- *Maintenance of balance and posture*: the cerebellum is important for making postural adjustments to maintain balance. Through its input from vestibular receptors and proprioceptors, it modulates commands to motor neurons to compensate for shifts in body position or changes in load upon muscles. Patients with cerebellar damage suffer from balance disorders, and they often develop stereotyped postural strategies to compensate for this problem (e.g., a wide-based stance) (Vago et al., 2014).

- *Coordination of voluntary movements*: most movements are composed of several different muscle groups acting together in a temporally coordinated fashion. One major function of the cerebellum is to coordinate the timing and force of these different muscle groups to produce fluid limb or body movements (Vago et al., 2014).

- *Motor learning*: the cerebellum is important for motor learning. The cerebellum plays a major role in adapting and fine-tuning motor programs to make accurate movements through a trial-and-error process (Vago et al., 2014).

- *Cognitive functions:* although the cerebellum is most understood in terms of its contributions to motor control, it is also involved in certain cognitive functions, such as language. Thus, the cerebellum is historically considered as part of the

motor system, but its functions extend beyond motor control in ways that are not well understood yet (Vago et al., 2014).

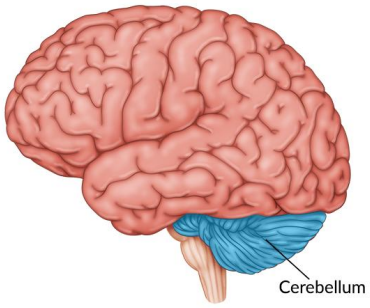

Figure 1.12 *Human Brain Anatomy: Cerebellum* (From Vago et al., 2014).

1.2.4 Corpus Callosum

The *Corpus Callosum* is a large white matter tract that connects the two hemispheres of the brain (***Figure 1.13***). It is the largest white matter structure in the brain both in size and number of axonal projections (200 million) between the two hemispheres (Baynes, 2013).

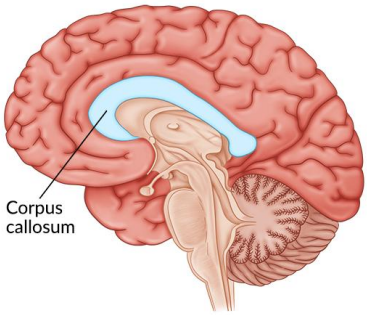

Figure 1.13 *Human Brain Anatomy: Corpus Callosum* (From Eccher, 2014)

The corpus callosum is composed of millions of nerve fibers that connect the two halves of the brain. Approximately half of these fibers are small and unmyelinated. These fibers transmit information more slowly than the larger myelinated axons, which are capable of extremely rapid transmission of information. Fast-conducting large fibers are typical of the interhemispheric connection between the primary and secondary sensory and motor cortices (Eccher, 2014).

The corpus callosum is divided into four parts: *rostrum, genu, body,* and *splenium* (***Figure 1.14***).

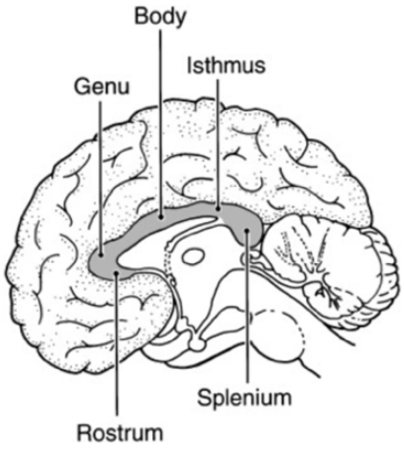

Figure 1.14 *Human Brain Anatomy: Sagittal section of the brain with major divisions of the corpus callosum labeled* (From Bayens, 2013)

The most anterior part of the callosum is the *rostrum*. Just behind the rostrum, the callosum bends to form the *genu* (or knee) and then extends posteriorly in the body. The *body* constricts slightly to become the isthmus and finally terminates in the slightly bulbous splenium. The rostrum is the floor of the frontal horn. The genu gives rise to a large fiber tract, which forms the anterior wall of the frontal horn, and the genu connects the frontal lobes (Baynes, 2013).

The *splenium* gives rise to a large tract, the forceps major, which forms a prominence called the *bulb of callosum* in the upper part of the medial wall of the atrium and occipital horn as it sweeps posteriorly to connect the occipital lobes. Another fiber tract, the tapetum, arises in the posterior part of the body and splenium and sweeps laterally and inferiorly to form the roof and lateral wall of the atrium and the temporal and occipital horns (Baynes, 2013).

1.2.5 Brainstem

The *Brainstem* connects the cerebrum to the spinal cord and plays a vital role in regulating some involuntary body actions, including heartbeat, and breathing (Ambrosi et al., 2010). The brainstem is composed by three regions: *midbrain, pons, and medulla* (***Figure 1.15***):

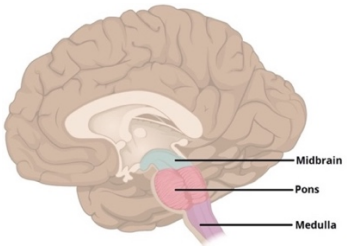

Figure 1.15 *Human Brain Anatomy: three major parts of the Brainstem* (From Bayens, 2013)

Midbrain, also called mesencephalon is a small region in the topmost part of the brainstem and it serves important functions in motor movement, it is crucial for regulating eye movements, and in auditory and visual processing (Ambrosi et al., 2010).

Pons is the intermediate part of the brainstem, just above the medulla oblongata. Named for the Latin word for "bridge," the pons is the connection between the midbrain and the medulla, so it links brain to spinal cord, and this makes the pons a vital section of nervous system, providing a route for signals to travel to and from the brain. The pons handles several important jobs thanks to several neurotransmitters: it influences the sleep cycle; it manages pain signals, and it works with other brain structures: it is a key connection point to cerebellum. It also works cooperatively with other parts of brainstem that manage breathing (Ambrosi et al., 2010).

Medulla is at the bottom of the brainstem, connecting spinal cord through the foramen magnum, an opening at the bottom of the skull. Functions of the medulla regulate many bodily activities, including heart rhythm, breathing, blood flow, and oxygen and carbon dioxide levels. The medulla produces reflexive activities such as sneezing, vomiting, coughing, and swallowing. The medulla also separates the nerves that control muscle movement, which are on the left side, and the nerves that control certain sensations like touch, temperature, or pain, which are on the right side (Ambrosi et al., 2010).

1.2.6 Ventricular System of the Brain

The *ventricular system* is a set of communicating cavities within the brain. These structures are responsible for the production, transport, and removal of cerebrospinal fluid (CSF), which bathes the central nervous system.

The brain's ventricular system is comprised of four ventricles as well as small structures which connect each ventricle called foramina of Monro. In this way, the ventricles communicate each other to function as they should.

The ventricles of the brain are cavities which produce and store cerebrospinal fluid (CSF). There are four ventricles of the brain: the 2 lateral ventricles, third ventricle, and fourth ventricle. The ventricles are lined with a specialized membrane called the choroid plexus, which is made up of ependymal cells, which are tailored to produce CSF and to secrete it into the ventricles at a relatively constant rate. (***Figure 1.16 and 1.17***) (Waxman, 2020).

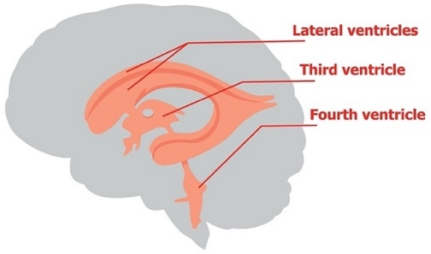

Figure 1.16 *Human Brain Anatomy: Brain Ventricles* (From Waxman, 2020)

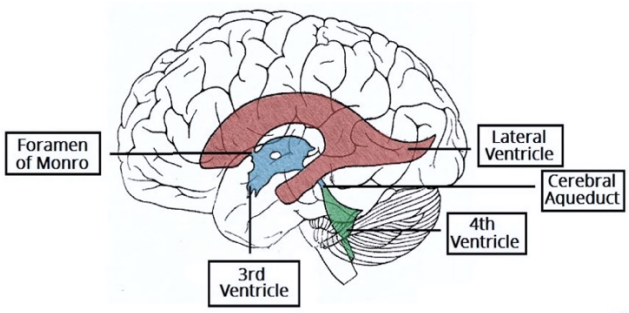

Figure 1.17 *Human Brain Anatomy: The anatomical positioning of the ventricles of the brain* (From Waxman, 2020)

1.2.6.1 Lateral Ventricles

The lateral ventricles are the largest in the series of four interconnecting fluid-filled cavities within the brain. The left and right lateral ventricles are located within their respective hemispheres of the cerebrum. The lateral ventricles are C-shaped structures and have three horns which project into the frontal, occipital, and temporal lobes. The volume of the lateral ventricles increases with age (Waxman, 2020).

The central part of the lateral ventricle is elongated antero-posteriorly. Anteriorly, it becomes continuous with the anterior horn at the level of the interventricular foramen

(*Figure 1.18*). The lateral ventricles are best seen in frontal sections, where their ventral surface is usually defined by the basal ganglia, their dorsal surface by the corpus callosum and their medial surface by the septum pellucidum, a membranous tissue sheet that forms part of the midline sagittal surface of the cerebral hemispheres (Purves et al., 2001)

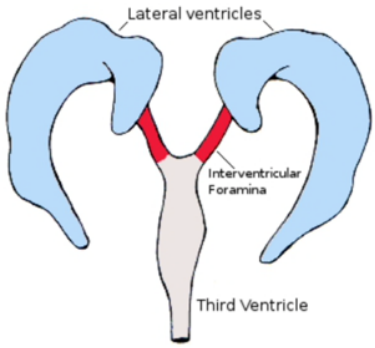

Figure 1.18 *Human Brain Anatomy: Lateral Ventricles in blue, Intraventricular Foramina in red* (From Purves et al., 2001)

The body of the lateral ventricle communicates with the atrium posteriorly from the foramina of Monro to the corpus callosum (Scelsi et al., 2020). The frontal or anterior horn extends anteriorly from the foramina of Monro and communicates with the body of the lateral ventricles posteriorly. The occipital or posterior horn curves posteriorly and medially from the atrium and varies in size. The temporal or inferior horn is the longest and largest horn, extending anteriorly from the atrium below the thalamus and terminating at the amygdala (Scelsi et al., 2020).

The lateral ventricle has been considered part of the limbic system and plays an important role in explicit, episodic, declarative, contextual, or relational forms of rapid encoding, consolidation, and retrieval processes related to memory and emotion. The anterior wall is formed by the genu of the corpus callosum, the roof is formed by the body of the corpus callosum, and the floor is formed by the thalamus.

The lateral wall is formed by the caudate nucleus and thalamus. The atrium is a triangular cavity that communicates with the body, temporal horn, and occipital horn. (***Figure 1.19***) (Scelsi et al., 2020).

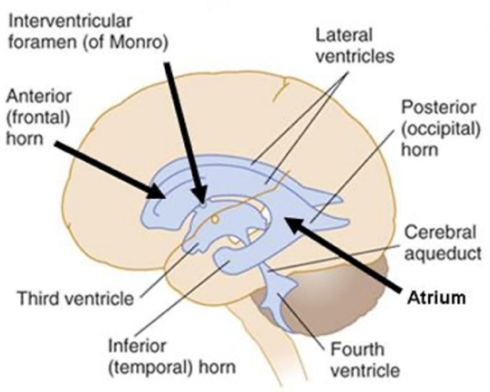

Figure 1.19 *Human Brain Anatomy: Different parts of Lateral Ventricles* (From Vago, et al., 2014)

1.2.6.2 Third Ventricle

The third ventricle is a very narrow, funnel-shaped structure situated between the right and left thalamus, in the midline between the right and left lateral ventricles, just above the brain stem (***Figure 1.20***). It directly communicates with other ventricles: it communicates with each lateral ventricle via the foramen of Monro, and with the fourth ventricle via the aqueduct of Sylvius. The boundaries of the third ventricle are formed by a variety of structures, the most important being the dorsal thalamus and hypothalamus, and by structures that form small outpocketings called recesses. The third ventricle has two lateral walls, a roof, a floor, an anterior and a posterior wall (Waxman, 2020).

The lateral wall of the third ventricle is formed inferiorly by the hypothalamus and superiorly and posteriorly by the thalamus.

The roof is composed by four layers: the first layer is formed by the fornices and the hippocampal commissure, the second layer by the superior membrane of tela choroidea, the third layer is a vascular layer, and the fourth layer is the inferior membrane of tela choroidea (Scelsi et al., 2020).

The posterior wall of the third ventricle begins at Sylvius' aqueduct anteriorly and inferiorly. Similar to the other brain ventricles, the main function of the third ventricle is to produce, secrete and convey cerebrospinal fluid (Vago, et al., 2014).

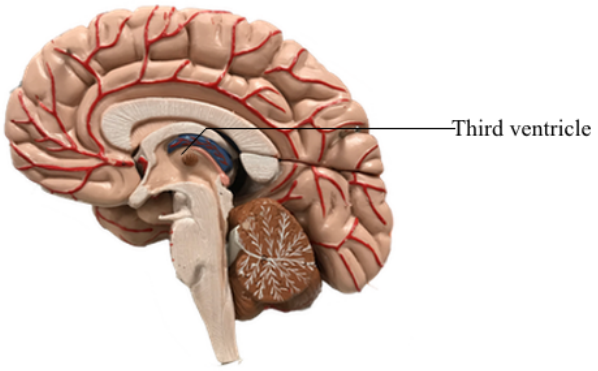

Figure 1.20 *Human Brain Anatomy: Third Ventricle* (From Vago, et al., 2014)

1.2.6.3 Fourth Ventricle

The fourth ventricle is the last ventricle of the system which receives CSF from the third ventricle via the cerebral aqueduct. It is a diamond-shaped structure which lies within the brain stem, at the junction between the pons and the medulla oblongata (***Figure 1.21***). It has four openings through which CSF drains into two places of the brain. CSF drains into the central spinal canal, bathing the spinal cord (Vago, et al., 2014).

It also drains into the subarachnoid cisterns, bathing the brain, between the arachnoid mater and pia mater. Here the CSF is absorbed back into the circulation.

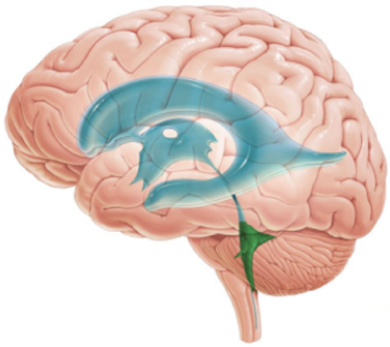

Figure 1.21 *Human Brain Anatomy: Fourth Ventricle in green* (From Vago, et al., 2014)

1.3 Structural and Functional Connectivity

Brain connectivity refers to the communication pathways groups of neurons. The connectivity studies the topography and organization of these connections which are dynamic, means that they change moment by moment to allow the connection of two or more neuronal groups necessary to perform a certain task (motor, sensitive, emotional, memorization). These links can change their topography and their characteristics with a

certain speed measurable in thousandths of a second. Obviously, experience, training and learning can model some connection structures over time that remain more or less fixed and stable but around which dynamic connections are articulated (Sporns, 2013). The human brain is characterized by structural and functional connectivity within and between regions.

Structural connectivity refers to the anatomical organization of the brain by means of fiber tracts. It plays a fundamental role in determining how neuron networks generate, process, and transfer information within and between brain regions. It describes anatomical connections linking a set of neural elements (Sporns, 2013).

Functional connectivity is defined as the temporal dependence of neuronal activity patterns of anatomically separated brain regions and refers to statistical dependence between time series of electrophysiological activity and (de)oxygenated blood levels in distinct regions of the brain. In the context of functional neuroimaging, functional connectivity is suggested to describe the relationship between the neuronal activation patterns of anatomically separated brain regions, reflecting the level of functional communication between regions. In fact, it has been observed that functional connectivity can be detected between brain regions in the absence of direct structural connectivity. In the past years an increasing body of neuroimaging studies has started to explore functional connectivity by measuring the level of co-activation of resting-state fMRI time-series between brain regions (van den Heuvel, 2010).

Chapter 2 *"Resection of the Corpus Callosum as a treatment for Epilepsy"*

2.1 Epilepsy

Epilepsy is one of the oldest diseases recorded in the history of medicine. Epilepsy is a chronic neurological disorder that affects the central nervous system in which an alteration of neuronal activity occurs (***Figure 2***). It is characterized by the presence over time of recurrent and unprovoked seizures, which are episodes of involuntary movement of short duration that may involve a part of the body (partial) or the entire body (generalized) and are sometimes accompanied by loss of consciousness and control of bowel or bladder function. In rare cases, these events can be short-lived, so much so that they go almost unnoticed, but they can last for long periods (King-Stephens, 2009).

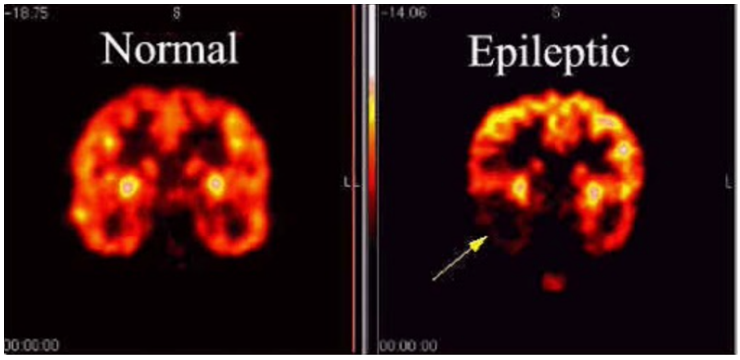

Figure 2. *Comparison between a brain with normal neuronal activity (left) and a brain during a seizure (right)* (From Beghi et al., 2015)

2.2 Pathogenesis

The behavioral characteristics of a seizure depend upon the location of the origin of the electrical abnormality and subsequent involvement of other structures (***Figure 2.1***)

In fact, different parts of the brain can be the site of these episodes. For example, in the *frontal lobe* (blue in ***Figure 2.1***), the seizures may cause loss of motor control, a change in behavior, or change in language expression. In the *occipital lobe* (green in ***Figure 2.1***), seizures can cause a person to see multi-colored shapes, such as circles and flashes, or experience temporary loss of vision. Regarding the *temporal lobe* (red in ***Figure 2.1***), the seizures that begin here may cause a person to experience an odd smell, odd taste,

buzzing or ringing in the ears, fear or panic, déjà vu, or abdominal discomfort. For the *parietal lobe* (yellow in ***Figure 2.1***), they cause a person to fell numbness or tilting, or feel burning or cold sensations (Stafstrom et al., 2015).

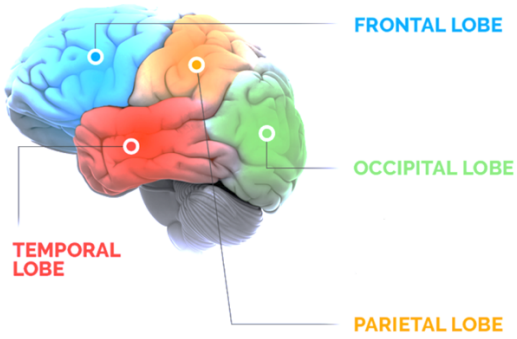

Figure 2.1 *A person will experience different symptoms depending on where a seizure starts in their brain* (From Stafstrom et al., 2015)

2.3 Role of Corpus Callosum in epilepsy and Callosotomy: the Split Brain

The corpus callosum is the main route for communication between both cerebral hemispheres. When epileptogenic foci occur near the portion of the corpus callosum, seizures with apparent generalized onset can occur. This results in an alteration of the electrical activity of the neurons and precisely from the fact that the neurons are all activated at the same time, causing an epileptic seizure (Seitun, 2019).

Corpus callosotomy is a surgical technique used in the palliative management of medically refractory cases of epilepsy in which focal resection surgery is not feasible (Vaddiparti et al., 2021). The seizures can be controlled with antiepileptic drug, but the occurrence of a single seizure does not always require initiation of antiepileptic drug (AED) therapy (Fisher et al., 2014), and surgical resection of the seizure focus is required.

2.3.1 Prevention for seizures: Split Brain

In an epileptic brain, focal seizures propagate to the contralateral hemispheres, resulting in secondary generalization mainly via the corpus callosum (Okanishi et al., 2021). The surgical intervention of the corpus callosum section, is a palliative procedure performed to reduce the severity of drug-resistant epilepsy and it is an effective treatment for intractable epilepsy (Luat et al., 2017).

The rationale for this procedure is based on the hypothesis that the corpus callosum is a critical pathway for interhemispheric spread of epileptic activity.

Split-brain (divided-brain) syndrome is also called callosal disconnection syndrome. It is a condition involving a cluster of neurological abnormalities caused by partial or complete severing or lesioning of the corpus callosum, both for natural pathological events (stroke, brain tumors), and for iatrogenic causes (surgical interventions of the corpus callosum section)

Neurological pathologies that damage the corpus callosum rarely cause the complete syndrome unlike the surgical section which, involving the whole corpus callosum, gives rise to complex symptoms with counterintuitive behaviors. The syndrome occurs in different channels: visual, sensorimotor, auditory (Moini et al., 2020).

Split-brain patients constitute a small subpopulation of epileptic patients who have received the surgical resection of the callosal fibers to reduce the spread of epileptic foci between the cerebral hemispheres (Prete et al., 2018).

Callosotomy best ameliorates drop attacks, absence, and frontal lobe complex partial seizures often respond as well. In addition to seizure reduction, behavior and quality of life may improve. Hence, callosotomy is justified as a therapy for appropriate patients with intractable epilepsy (Asadi-Pooya, et al., 2008).

2.3.2 History of Split Brain

William P. van Wagenen, chair of neurosurgery at the University of Rochester, identified a direct association between the frequency of epileptic attacks and the integrity of corpus callosum, thereby introducing the rationale behind corpus callosotomy in epilepsy management. On February 11, 1939, van Wagenen performed the first surgical division of the corpus callosum at the University of Rochester, Strong Memorial Hospital to limit the spread of the convulsive wave to one half of the cerebrum. Over the next 3 months, William P. van Wagenen performed nine more callosotomies with either partial or near-complete sectioning of the corpus callosum.

In 1940, van Wagenen and Herren reported their findings and concluded that sectioning of the corpus callosum is a safe procedure to disrupt contralateral seizure propagation, preventing generalized seizures or loss of consciousness (Vaddiparti et al., 2021).

In the 1950s and 1960s, Roger Sperry performed experiments on cats, monkeys, and humans to study functional differences between the two hemispheres of the brain. At the time, he knew that each hemisphere of the brain is responsible for movement and vision on the opposite side of the body, so the right hemisphere was responsible for the left eye and vice versa. Sperry severed the corpus callosum in cats and monkeys to study the function of each side of the brain. To test how the callosal resection affected mammals, Sperry cut the corpus callosum of many cats and had them perform some tasks involving their vision and response to a visual stimulus. He found that if hemispheres were not connected, they functioned independently, a condition that he called *split-brain.* Later, Sperry tested the same idea in humans with their corpus callosum severed as treatment for epilepsy, a seizure disorder. He noted that patients with a severed corpus callosum did not show any significant difference in function from individuals with intact corpus callosum, even though their hemispheres could not communicate because of the callosal resection (Lienhard et al, 2017).

Sperry and his graduate student Michael Gazzaniga performed experiments on human volunteers, with callosal resection performed to treat drug-resistant epilepsy, to whom he asked to execute multiple tests.

From his previous experiments with cats and monkeys, Sperry learned that each hemisphere would only analyze information from the contralateral visual field, and that each hemisphere could not communicate to the other what it saw (*Figure 2.2)*.

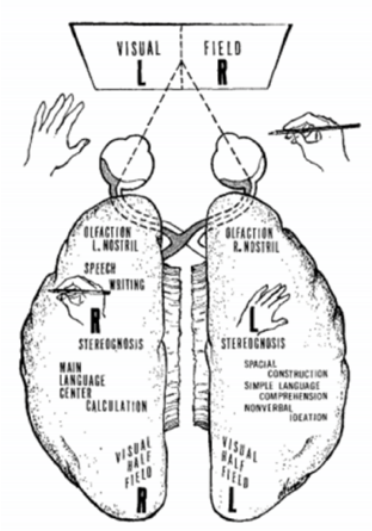

Figure 2.2 2 Human beings have two visual fields. These visual fields, which are different from the two eyes. The left visual field is what can be seen on the left, and the right visual field is what can be seen on the right (From Sperry,1968)

Sperry tested the function of the right hemisphere. He asked the participants to look at a white screen with a black dot in the middle. The black dot was the fixation point in the center of the visual field, so the right hemisphere of the brain analyzed everything to the left of the dot and the left hemisphere everything that appeared to the right of the dot (Lienhard et al., 2017).

Next, Sperry showed the participants a word on one side of the black dot for less than a second and asked them to say what they saw. When the participants saw the word with their right eye, the left hemisphere of the brain analyzed it and they were able to say what they saw (*Figure 2.3*). However, if the participants saw the word with their left eye, sending information to the right hemisphere, they could not know what the word was. Sperry concluded that the left hemisphere could recognize and articulate language, while the right one could not.

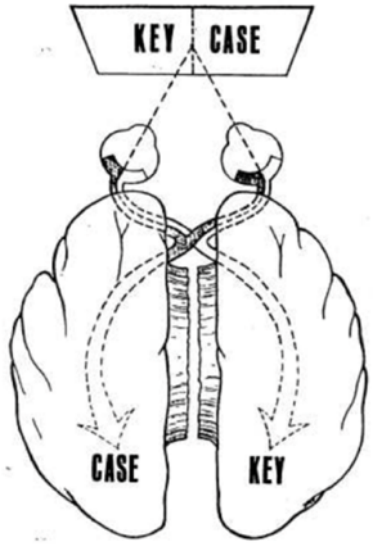

Figure 2.3 Two words were displayed in right and left side of a central dot. The word displayed in the left visual field was processed by the right hemisphere and vice versa (From Sperry, 1968)

In the second experiment, Sperry asked the volunteers to put their left hand in a box with several tools out of their sight. After that, the participants saw a word describing one of the objects in the box only in their left visual field (*Figure 2.4*).

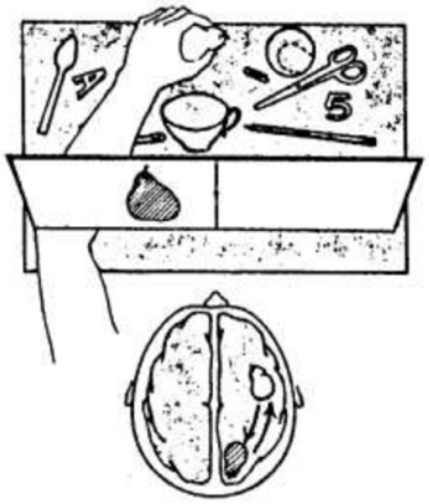

Figure 2.4 A word/image was displayed on the left side of the screen. By using the left hand, the subject picked up the object described on the screen and processed by the right hemisphere (From Sperry, 1968)

Sperry noted that most of the attendees picked up the item indicated by the box without seeing it, but when Sperry asked them for the item's name, they could not tell and didn't know why they were holding that item. Sperry concluded that the right hemisphere had some speech recognition ability, but no speech articulation, which meant that the right hemisphere could recognize or read a word, but could not pronounce it (Lienhard et al., 2017). In his latest series of experiments on humans, Sperry showed one object to the right eye of the participants and another object to the left eye. Then he asked the volunteers to draw what they saw only with their left hand, with their eyes closed. All participants drew the object they saw with their left eye, controlled by the right hemisphere, and described the object they saw with their right eye, controlled by the left hemisphere. This confirmed Sperry's hypothesis that the hemispheres of the brain functioned separately as two distinct brains and did not recognize the existence of the other hemisphere, as the description of the object did not match the design. He concluded that although there were no obvious signs of disability in people with the corpus callosum resected, the hemispheres did not communicate, thus compromising the full brain function. At the end, he discovered that the left hemisphere was responsible for language understanding and articulation; the right hemisphere could recognize a word but could not articulate it. Sperry received the 1981 Nobel Prize in Physiology and Medicine for his research on split-brain patients and the findings on the functions of the corpus callosum (Lienhard et al., 2017).

Chapter 3 "Functional Magnetic Resonance Imaging"

3.1 Outline of Magnetic Resonance Imaging

Magnetic resonance imaging (MRI) is a non-invasive modality which produces multiplanar and true 3D datasets of subjects in vivo, without relying on harmful ionizing radiation. It achieves a high spatial resolution, typically of the order of millimeters in the clinical setting (Cleary et al., 2014).

The major advantage of MRI over other modalities is direct multiplanar imaging, thanks to which the acquired data, for example from the axial plane, can then be directly converted to non-axial planes such as coronal, sagittal, or oblique. The basis of MRI is that certain atomic nuclei found in tissues, as those of hydrogen, which are positively charged protons, become magnetized when placed in an external magnetic field (Chan et al., 2019). These protons spin on their axis, producing a magnetic field (magnetic moment). When a patient is placed in a strong magnetic field in an MRI scanner, some H_1 protons align themselves with the field. When a radiofrequency pulse is applied, some of the protons aligned with the field will absorb energy and reverse direction. This absorbed energy is given off as a radiofrequency pulse as the protons relax (return to their original alignment), producing a voltage in the receiver coil (Bandettini,2012). After the radio-frequency pulse is turned off, the magnetization undergoes processes called relaxation and precession as it returns to its thermal equilibrium configuration. It is possible to detect the magnetization because the transverse component of processing magnetization induces an electromotive force in the receiver coil. The received signal can be spatially encoded by the application of magnetic field gradients that are superimposed on the uniform, main magnetic field. Excitation and detection modules are repeated until all data are collected and the data are recorded and processed to form an image (Chan et al., 2019).

3.1.1 Basic Principles of MRI

MRI systems include a 5– 10ton superconductive magnet, carefully designed to provide a strong magnetic field with high homogeneity inside the bore where the object to be imaged is positioned (Amaro et al., 2006). In an MRI exam, a person is lying on a motorized table that moves inside a narrow tubular scanner, producing a high magnetic

field. Each point within the body, represented in the final image as a particular 'pixel' (*picture element*) or 'voxel' (*volume element*), will have a certain number of protons aligned with the main magnetic field (Amaro et al., 2006). Normally, protons (positively charged parts of an atom) in tissues have no particular arrangement (***Figure 3.1 (a)***). However, when they are surrounded by a strong external magnetic field(B_0), such as in an MRI scanner, the nuclei adopt one of two possible orientations: parallel or antiparallel to the external field (***Figure 3.1 (b)***). Parallel alignment is the lower energy state and is thus the preferred alignment, whereas antiparallel alignment is the higher energy state. This results in a net magnetization vector (Mz) parallel to the external magnetic field (van Geuns et al., 1999).

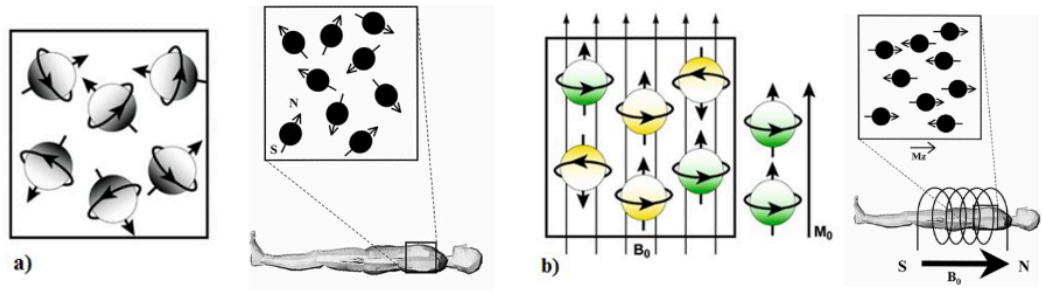

Figure 3.1 *Effect caused on protons by an external static magnetic field.* ***(a)*** *In the absence of a magnetic field, the spins are directed in all directions.* ***(b)*** *The magnetic field determines a magnetization with a parallel or antiparallel direction. This results in a net magnetization vector (M_0) parallel to the external magnetic field* (From van Geuns et al., 1999)

The amount of energy required to flip protons from the parallel to the antiparallel orientation is directly related to the magnetic field strength; stronger fields require more energy or higher frequency radiation. The net magnetization vector from the nuclei inside the magnet in its equilibrium state is static and does not produce a measurable signal. To obtain information from the spins, the direction of the net magnetization vector must be altered (van Geuns et al., 1999).

Individual nuclei do not actually line up with the magnetic field but wobble or precess around the direction of the external field (***Figure 3.2***). The frequency of this precession is given by the Larmor equation:

$$F = \frac{\gamma B_0}{2\pi} \qquad [1]$$

where F is the precessional frequency, B_0 is the strength of magnetic field, and γ is the gyromagnetic ratio of the nucleus (van Geuns et al., 1999).

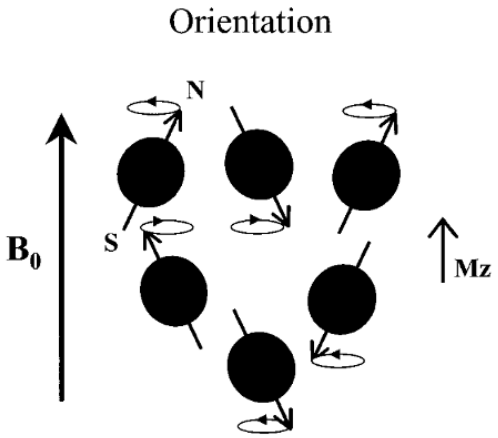

Figure 3.2 *In more detail the individual nuclei spin around their own axes and wobble or precess around the direction of the external field (B_0)* (From van Geuns et al., 1999)

When the scanner emits a pulse of radio waves, it momentarily misaligns the protons and two phenomena occur: first, enough protons absorb energy to jump from the parallel state to the higher level of the antiparallel state, and second, the spins are ‘‘whipped’’ to precess in phase. The effect of all this is that the net magnetization (Mz) flips 90° from the positive z-axis to transverse plane (***Figure 3.3***). The net magnetization in the transverse plane rotates around B_0 at the Larmor frequency. This rotating transverse magnetization can be measured because it will induce an alternating current (AC) in the receiver coil placed around the patient (van Geuns et al., 1999).

After the radio frequency (RF) transmitter is switched off, the equilibrium state will be sought. This means that the magnetization decays over time, which is represented by a decreasing magnitude of Mz in the transverse plane. This decreasing signal is called the free induction decay (FID). The protons will realign with the magnetic field releasing energy (called signals). The time required for the signal to return to equilibrium is the relaxation time (RT). The process of realignment to the external magnetic field is called longitudinal relaxation process (***Figure 3.4 (A)***) and the dephasing of the precessing spins that lead to transversal magnetization decay is called transverse relaxation (***Figure 3.4 (B)***) (van Geuns et al., 1999).

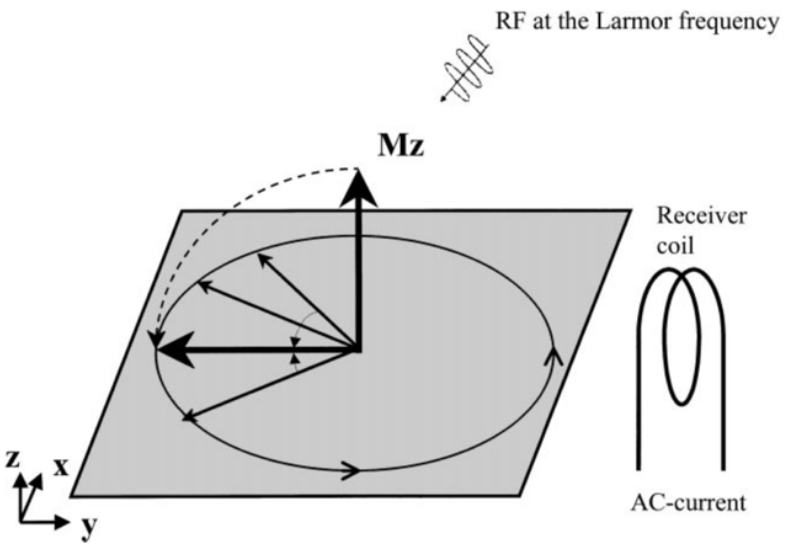

Figure 3.3 When the spins are exited with an RF pulse of exactly the Larmor frequency, the net magnetization flips 90° and the spins are ''whipped'' to precess in phase. The rotating net magnetization vector induces an AC in a receiver coil (From van Geuns et al., 1999)

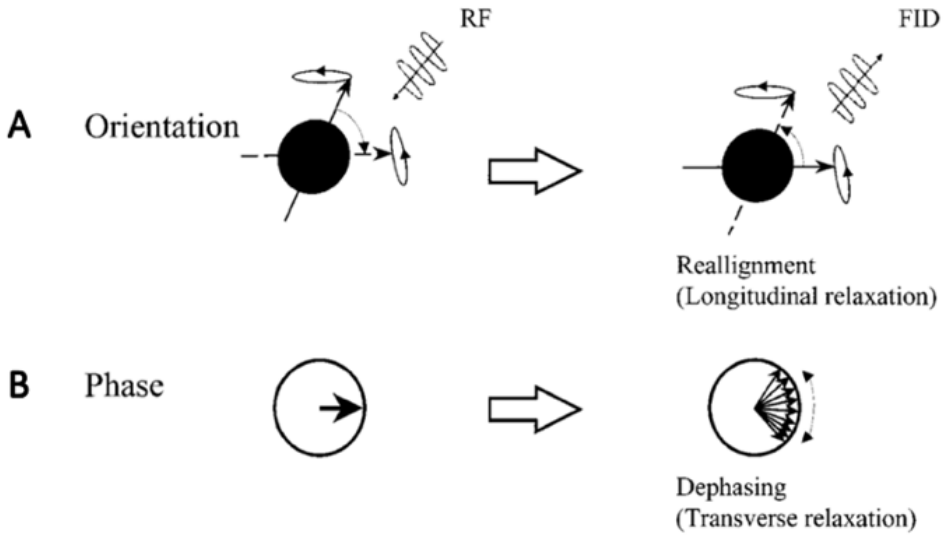

Figure 3.4 (A)Longitudinal relaxation: is the realignment of the net magnetization to the external magnetic field. (B) Transverse relaxation is the dephasing of the precessing spins (From van Geuns et al., 1999)

The longitudinal relaxation process is characterized by the T_1, relaxation time. The T_1 -RT is defined as the time required for the system to recover 63% of the original net magnetization vector, after it has been exposed to a 90° RF pulse (***Figure 3.5***). The second process of relaxation, also known as spin-spin relaxation or transverse relaxation, refers to the progressive dephasing of spinning protons resulting in decay in the magnetization in the transverse plane. The T_2-RT is the time it takes for dephasing to decay the signal to 37% of its original signal (***Figure 3.5***) (van Geuns et al., 1999).

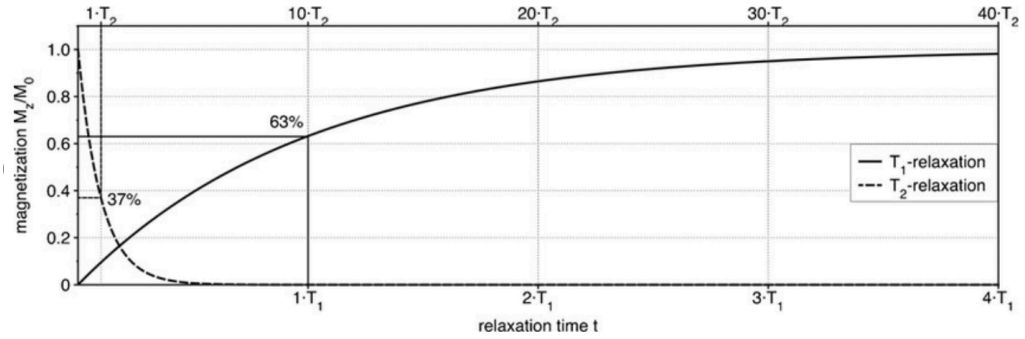

Figure 3.5 *Longitudinal relaxation characterized by the T1 relaxation time. Transverse relaxation characterized by the T2 time* (From van Geuns et al., 1999)

Various human tissues have different T_1 and T_2 values but the T_2 time is always shorter than the T_1 time (***Table 1***) (van Geuns et al., 1999).

Table 1. *T1 and T2 value of different tissues at 1.5T* (From van Geuns, et al., 1999)

Tissue	T1 (ms)	T_2 (ms)
Skeletal muscle	870	47
Myocardium	600	40
Liver	490	43
Fat	260	84
Blood	1,210	35
Venous arterial blood	1,210	250

The intensity of the signal varies from one tissue to another. The MRI scanner records these signals while a computer analyzes the signals and produces images. In conclusion, MRI is a method that allows you to obtain high-resolution images of the human body with a specific image contrast for the tissue under examination. The contrast is the result of the specific magnetic relaxation properties of the hydrogen nuclei present in the tissue water (Amaro et al., 2006).

3.1.2 MRI Imaging

Images creation through the principles of the magnetic resonance phenomenon is done exploiting the generation of the FID signals after the radiofrequency excitations. The contribution of FID to different voxels must be discriminated to distinguish different

tissues inside the area under investigation. To discriminate the contribution of different voxel (i.e. spatial position) to the recorded signals, the Larmor Law is used. Nuclei are excited with radio frequency (RF) pulses with a frequency equal, or near, their Larmor frequency in order to flip the magnetization vector in the transverse plane. In order to create a static magnetic field of spatially variant intensity, three magnetic field gradients (G_x, G_y , G_z) are added to B_0. The intensity of gradients G_x, G_y , G_z is small compared to the intensity of B_0 (Figure 3.6) (Amaro et al., 2006).

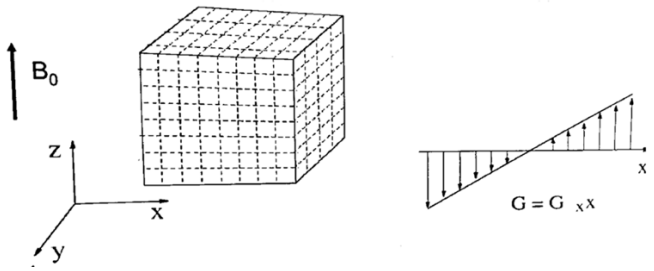

Figure 3.6 *Application of the G_x , G_y, G_z magnetic fields added to B_0 in order to distinguish the different slices* (From Amaro et al., 2006).

Since the Larmor frequency is proportional to the applied external magnetic field, using an added and spatially changing magnetic field (for all the three spatial orientation), it is possible to discriminate different spatial position according to the different resonance frequency.

$$f_{Larmor}(x) = \frac{\gamma(B_0+G_x x)}{2\pi} \qquad [2]$$

That is valid for every gradient direction.

3.1.2.1 Slice Selection

The fMR image formation process subdivides a section of the patient's body into a set of slices which are then cut into rows and columns to form a matrix of individual tissue voxels (Sahayaraj, 2015). To select a particular slice of tissue in the body we can turn on the set of electromagnets along the z-axis to create a magnetic gradient from head to feet (***Figure 3.7***).

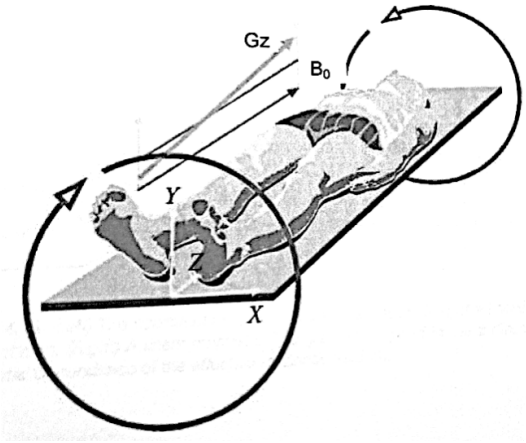

Figure 3.7 *Selection of slices along z-axis to create an image* (From Sahayaraj, 2015)

The spatial characteristics of an fMR image are produced by actions of the gradients applied during the acquisition phase. Magnetic field gradients are used to select slices and to give the RF signals the frequency and phase characteristics that create the individual voxels (***Figure 3.8***). The slices are separated by applying the RF pulses and detecting the signals from the different slices at different times, in sequence, during each imaging cycle (Sahayaraj, 2015).

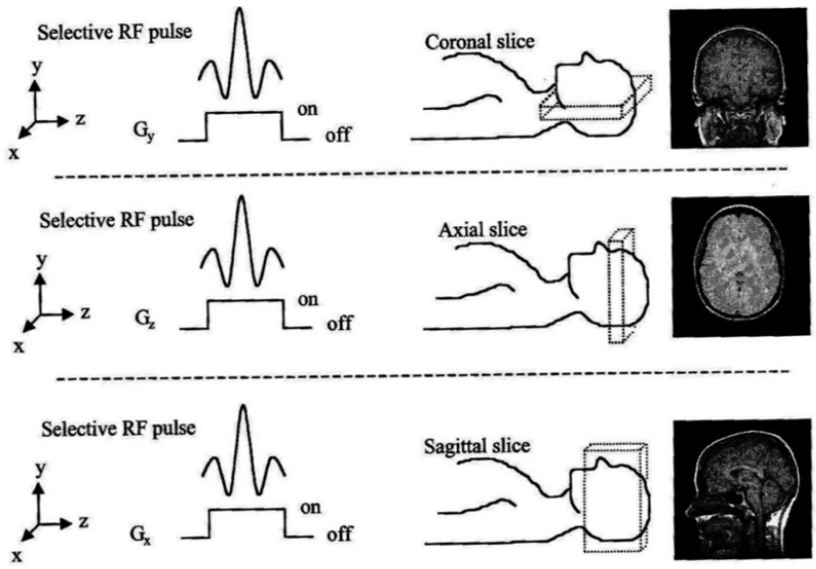

Figure 3.8 *A schematic slice selection in MRI. By using a frequency-selective pulse in combination with the y, z, or x gradient, a coronal, axial or sagittal slice, respectively, can be chosen* (From Sahayaraj, 2015)

The RF signal from each individual voxel must be separated from all of the other voxels and its intensity is displayed in the corresponding image pixel, as shown in ***Figure 3.9*** (Sahayaraj, 2015).

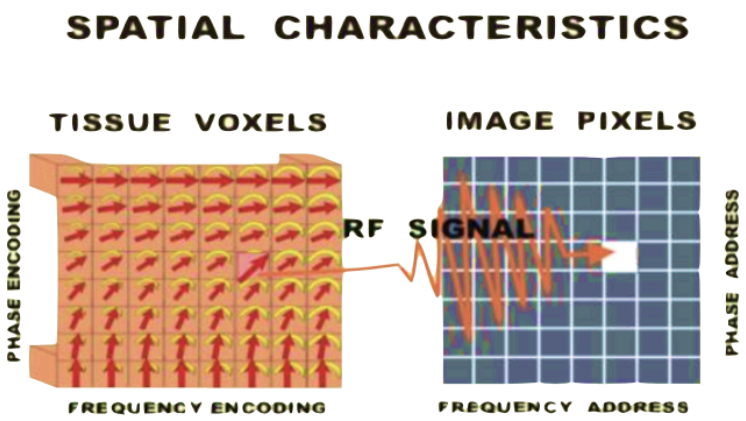

Figure 3.9 *The relationship of tissue voxels to image pixels* (From Sahayaraj, 2015)

This is achieved by encoding or addressing the signals during the acquisition phase and then delivering the signal intensities to the appropriate pixels which have addresses within the image during the reconstruction phase (Sahayaraj, 2015).

3.1.2.2 Signal Acquisition and Image Reconstruction

During the acquisition phase the RF signals are emitted by the tissue and received by the RF coils of the equipment. During this process the signals from the different slices and voxels are given distinctive frequency and phase characteristics so that they can be separated from the other signals during image reconstruction. The acquisition phase consists of several repeated shooting cycles. The time required for image acquisition depends on the time repetition, which is the duration of one cycle, and the number of cycle repetitions. The number of imaging cycles is determined by image quality requirements. In general, image quality can be improved by increasing the number of imaging cycles. The result of the image acquisition process is a large amount of data collected and stored in computer memory. At this point, the data are not yet in the form of an image but are located in k space. The data will later be transformed into image space by the reconstruction process (Sahayaraj, 2015).

Image reconstruction is a mathematical process performed by the computer. It transforms the data collected during the acquisition phase into an image. The mathematical process used is known as Fourier transformation. Image reconstruction is typically much faster than image acquisition and requires very little, if any, control by the user (***Figure 3.10***) (Sahayaraj, 2015).

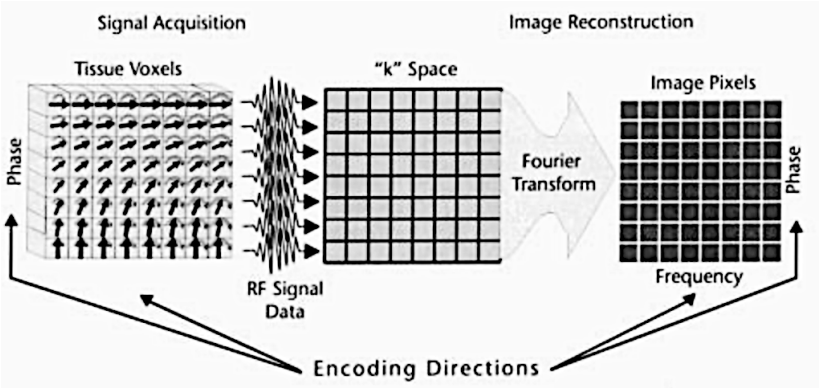

Figure 3.10 *Two phases: signal acquisition and image reconstruction, that are acquired to produce an FMR image* (From Sahayaraj, 2015)

3.2 Functional Magnetic Resonance Imaging

In the first years of 1990, the neurophysicists Seiji Ogawa and Kenneth Kwong discovered a new non-invasive technique to study brain activity by measuring changes in blood flow and they call it Functional MRI (fMRI). Today, it is one of the most widely used methods for functional brain imaging and is increasingly used to probe the functional integrity of brain networks (Bandettini, 2012). Functional MRI is utilized in the clinical setting, for example in neurosurgery for pre-surgical planning and intraoperative monitoring of brain areas. It allows to plan the surgical strategy to minimize the risks of postoperative deficit. However, fMRI is mainly used as a research tool and is widely used in the field of neurological and cognitive neuroscience to study the different cognitive processes (language, attention, memory) in normal and pathological subjects (Poldrack et al., 2011). The goal of the fMRI studies is to identify the areas of the brain activated during predefined stimulation tasks, in an easily interpretable and reproducible way. It has excellent spatial resolution, and the experiment can be repeated any number of times, but fMRI lacks temporal resolution (Sahayaraj, 2015).

3.3 Functional MRI Basic Principles

The brain needs nutrients such as oxygen and glucose to perform its functions. Most of the body's energy is consumed by the brain, which however does not have a stored energy reservoir. During the execution of a certain task, be it motor, cognitive or sensory, the neurons involved are activated more, by sending more signals than in the resting

condition. The brain areas involved in the task are more active, and here there is an increase in blood flow. This means that an increase in neural activity leads to a greater demand for energy.

Functional MRI measures the small changes in blood flow that occur with brain activity using BOLD contrast. This contrast is based on two fundamental principles (Ogawa et al, 1990):

1) the hemoglobin has different properties depending on its level of oxygenation (oxyhemoglobin is diamagnetic, while deoxyhemoglobin is paramagnetic);

2) the regional blood oxygenation varies according to the levels of neural activity.

These properties can be used to indirectly evaluate brain activity (***Figure 3.11***) (Amaro et al, 2006): the activation of a cortical area causes an increase in the flow of oxygenated blood, higher than the strict metabolic consumption.

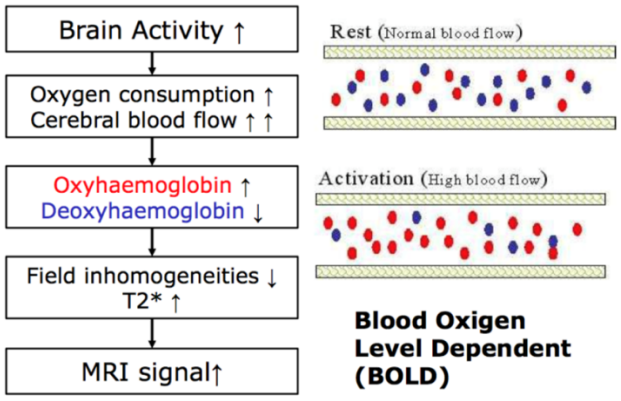

Figure 3.11 *Brain activity and BOLD signal principles* (From Amaro et al., 2006)

3.3.1 BOLD effect

It is known that metabolic activity uses oxygen, in fact, the oxidation processes transform the chemical energy contained in food into thermal energy and mechanical energy essential for the performance of vital functions and human activities. Therefore, blood in the vicinity of metabolically active tissues will have a different proportion of oxygenated to deoxygenated hemoglobin (Hb) than that surrounding quiescent tissue (Amaro et al., 2006). The hemoglobin has different magnetic properties depending on the O_2 saturation: when it is completely saturated with oxygen (oxyhemoglobin) it behaves like a diamagnetic substance (i.e. acquires an induced magnetization opposite to the

magnetizing field), while when some oxygen atoms have been removed (deoxyhemoglobin) it becomes paramagnetic (i.e., it acquires an induced magnetization opposite to the magnetizing field); when some oxygen atoms have been removed (deoxyhemoglobin), hemoglobin becomes paramagnetic (i.e., it assumes a magnetization intensity proportional to that of the inducing field and with the same direction) (***Figure 3.12***) (Amaro et al, 2006):

- the hemoglobin can distort the magnetic field of MRI scanner in a region of the cortex according to its level of oxygenation;
- the regional blood oxygenation varies according to the levels of neural activity

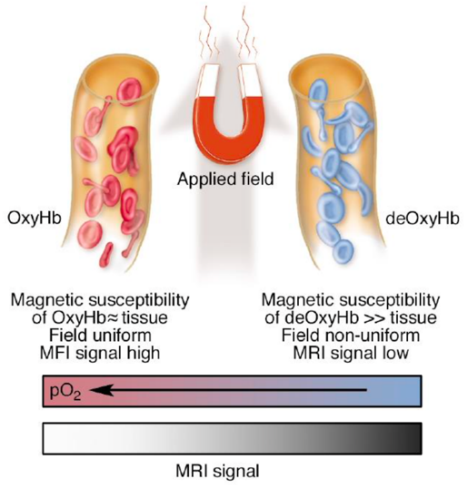

Figure 3.12 *Schematic representation of the origin of the BOLD effect in fMRI* (From Gore, 2006)

The moments of *stimulus* processing in a given brain region are accompanied by a transient increase in the concentration of deoxyhemoglobin, resulting in an *initial drop*. This effect serves to increase the spatial specificity of the BOLD effect, although the initial decline is not consistently detected. However, after this initial component, the fMR signal evolves and there is an increase in the oxy/deoxy-hemoglobin ratio leading to an elevated fMR signal. This increase in signal (the positive BOLD effect) is proportional to the neural activity under consideration. Eventually a *plateau* is reached if the stimulus is maintained for a sufficient time (approximately more than 3 seconds). After the stimulus ceases, the fMR signal returns to the baseline, but there is a negative overshoot of the line, called the *undershoot effect*. This effect is believed to result from venous bed capacity, which tends to normalize regional blood volume at a slower rate than changes in blood flow, thus leading to a relatively high deoxyhemoglobin concentration (***Figure 3.13***) (Amaro et al., 2006).

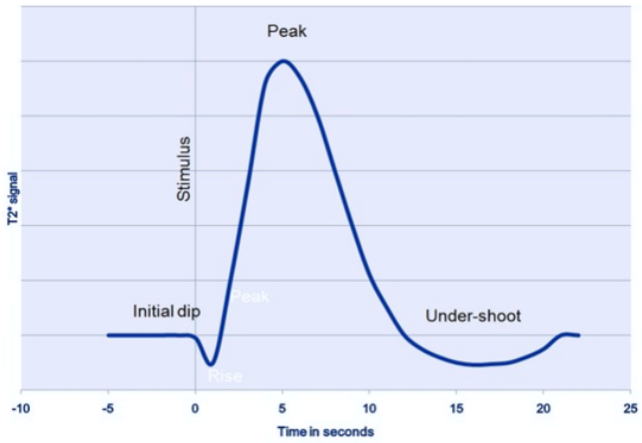

Figure 3.13 *Theoretical representation of BOLD signal response* (From Gore, 2006)

The practical implication is that, by using BOLD images, one can indirectly detect the increase in neuronal activity at the moment that a subject performs a particular task, compared to another moment when that task is not executed (Amaro et al., 2006).

3.3.1.1 BOLD effect to produce images

The standard fMR imaging method used to produce information related to brain function and to observe different areas of the brain is the BOLD imaging technique. This method is based on fMR images made sensitive to changes in the oxygenation state of hemoglobin, having as a basis for acquiring anatomical MRI images of the subject, which allow to reconstruct the entire structure brain base. Functional MRI does not produce direct images of what is happening in the brain, since these images are an indirect effect, resulting from the hemodynamic response, of neuronal activity.

Within a particular imaging voxel (which represents a small part of the brain) the proportion of deoxyhemoglobin to oxyhemoglobin determines how the fMR signal will behave in a BOLD image: areas with a high concentration of oxyhemoglobin give a higher signal (a brighter image) than areas with low concentration. It is, therefore, statistical distribution maps, derived from average effects, of the activation of an area in the performance of a specific task (***Figure 3.14***) (Amaro et al., 2006).

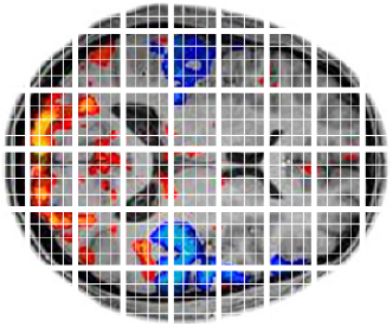

Figure 3.14 *fMRI data with several voxels* (From Gore, 2006)

The BOLD effect is also influenced by blood flow and brain volume, and as such it is not a simple measurement parameter (Amaro et al., 2006). In addition, there is a contribution from water molecules in blood and from water molecules in the tissue space around the vessels. The observed signal is a volume weighted average of signal changes both from intravascular water in local capillaries and veins and water in the immediate extravascular compartment. BOLD signal change increases linearly with the static field strength of the MRI scanner for blood vessels that are of greater radius than approximately 8 μm and quadratically when considering blood vessels that are smaller than this value (Matthews et al., 2004).

3.3.2 Hemodynamic Response

To map brain activity based on the transient fMRI signal, it is important to understand the basic nature of the BOLD contrast hemodynamic response (Buckner, 1998).

The mathematical model of the neurovascular coupling transfer function between local neural activity and the corresponding BOLD fMRI signal, is called the hemodynamic response function (HRF). HRF represents the transfer function that links neural activity with the fMRI signal, modeling neurovascular coupling (Rangaprakash et al., 2021). It is used as an indirect measure of neuronal activity. HRF characterizes changes in BOLD signal over time, typically peaking around three to five seconds after stimulus presentation (West et al., 2019).

The shape of the HRF is controlled by both neural and non-neural factors. The shape of the HRF can be characterized by three parameters: response height, time-to-peak and full-width at half-max (***Figure 3.15***) (Rangaprakash et al., 2017).

HRF has very limited temporal resolution compared to methods that directly measure neuronal electrical activity, such as electroencephalogram-based techniques and magnetoencephalography. Furthermore, the effect of HRF is equivalent to that of a low-pass filter, further attenuating the temporal variances of neuroelectric activity (Palmer et al, 2010).

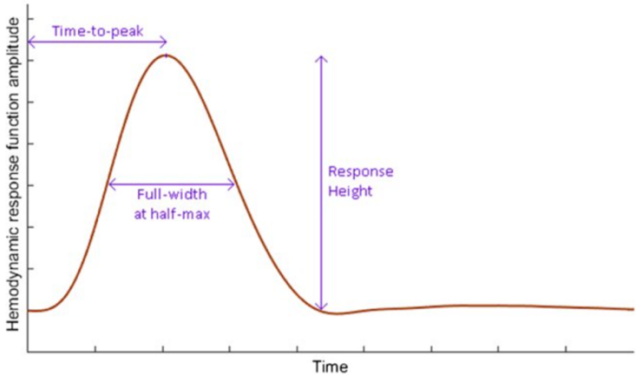

Figure 3.15 *The HRF with its three parameters: response height, time-to-peak and full-width at half maximum* (From Rangaprakash et al., 2021).

3.4 Resting State fMRI

The resting state brain activity refers to spontaneous activity without deliberately given stimuli. Such activity shows relatively consistent distributed patterns and can be used to characterize network dynamics without needing an explicit task to drive brain activity (Uddin, 2013).

Biswal and colleagues were the first to demonstrate that during rest the left and right hemispheric regions of the primary motor network are not silent but show a high correlation between their fMRI BOLD time-series suggesting ongoing information processing and ongoing functional connectivity between these regions during rest (van den Heuvel et al., 2010).

In their study (schematically shown in ***Figure 3.16***, the resting-state time-series of a voxel in the motor network was correlated with the resting-state time-series of all other brain voxels, revealing a high correlation between the spontaneous neuronal activation patterns of these regions. This leads to the intuition that the brain is mainly driven by its intrinsic activity and that external stimulations can modulate rather than determine its

activity. Proving that the brain is always active, even in the absence of a specific task being performed (van den Heuvel et al., 2010).

It was showed a high level of functional connectivity between the left and right hemispheric motor cortex, but also between regions of other known functional networks, like the primary visual network, auditory network, and higher order cognitive networks. Furthermore, to map out all functional connections of the selected region (seed voxel), the time-series of the seed voxel can be correlated with the time-series of all other voxels in the brain, resulting in a functional connectivity map evidencing the regions showing a high level of functional connectivity with the selected seed region.

Several studies were replicated, and they mark that during rest the brain network is not inactive, but rather shows a vast amount of spontaneous activity that is highly correlated between multiple brain regions (van den Heuvel et al, 2010).

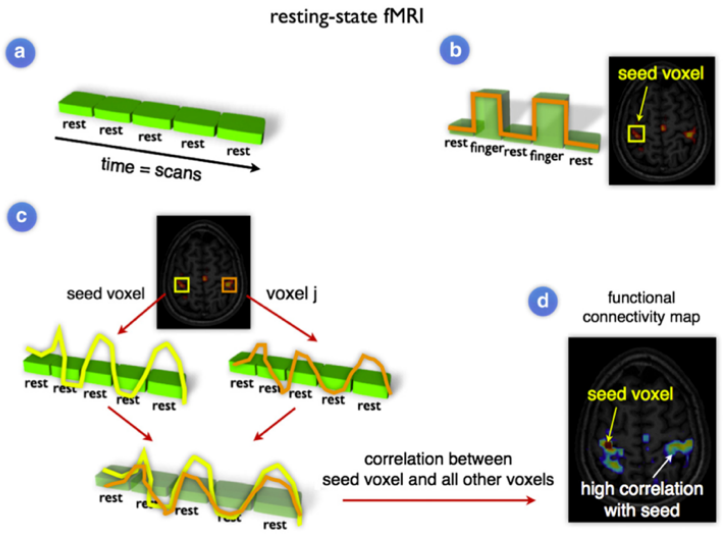

Figure 3.16 *Panel a, shows the BOLD fMRI signal measured throughout the experiment. The panel b shows the selection of a seed region of interest. In the panel c is shown the correlation between the resting-state time-series of the seed voxel is correlated with the resting-state time-series of region j, to examine the level of functional connectivity between the selected seed voxel i and a second brain region j. In panel d is shown the functional connectivity map* (From van den Heuvel et al., 2010).

The fMRI allows recording temporal correlations of spatially distinct brain regions, thus highlighting neuronal networks known as Resting State Networks (RSNs).

Resting-state fMRI (RS-fMRI) measures spontaneous low-frequency fluctuations in the BOLD signal to investigate the functional architecture of the brain. It investigates

synchronous activations between regions that are spatially distinct, occurring in the absence of a task or stimulus, to identify the RSNs, and in addition the Functional Connectivity (FC) is evaluated, defined as the temporal correlation of the activated voxels between spatially distinct brain regions. Clinical applications of resting-state fMRI are still under development. Its use in presurgical planning for patients with brain tumor and epilepsy demonstrates a good promise, and the technique may have a future role in providing diagnostic and prognostic information for neurologic and psychiatric diseases. (Lee et al., 2013).

3.4.1 Resting State Networks

The RSNs consist of anatomically separated, but functionally linked brain regions that show a high level of ongoing functional connectivity during rest. RSNs are always present in the human brain, both in the waking state, during sleep or under anesthesia, highlighting the fact that the spontaneous neuronal activity of the brain plays a fundamental role in brain functions. The most often reported RSNs, i.e., networks of anatomically separated brain regions showing a high level of functional connectivity during rest, include the motor network, the visual network, two lateralized networks consisting of superior parietal and superior frontal regions, the so-called default mode network, consisting of functionally linked posterior cingulate cortex, medial frontal and inferior parietal and temporal regions, the network consisting of bilateral temporal/insular and anterior cingulate cortex regions (***Figure 3.16***). Most of these resting-state networks tend to represent known functional networks, overlapping regions that are known to share a common function, supporting the functional relevance of these networks. They overlap the primary motor regions, the primary visual regions and parietal–frontal networks involved in attention processing. The most common RSNs identified are discovered by Beckmann and its collaborators, and Smith with his coworkers (van den Heuvel et al., 2010).

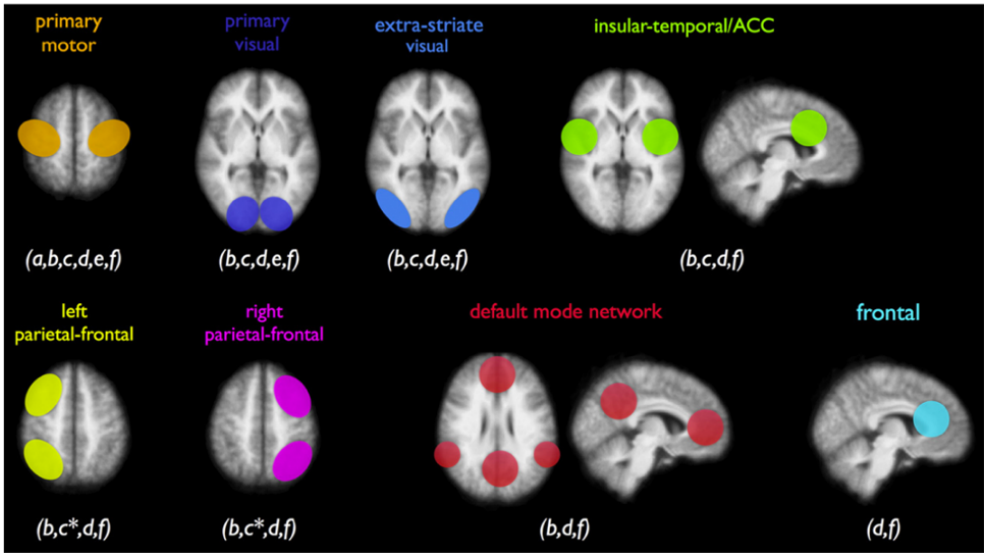

Figure 3.16 *Resting-state networks. This figure shows the most consistent resting-state networks, including the primary sensorimotor network, the primary visual and extra-striate visual network, a network consisting of bilateral temporal/insular and anterior cingulate cortex regions, left and right lateralized networks consisting of superior parietal and superior frontal regions and the so-called default mode network consisting of precuneus, medial frontal, inferior parietal cortical regions and medial temporal lobe* (From van den Heuvel et al, 2010).

Studies on brain connectivity in the absence of stimuli allowed Beckmann and his collaborators to highlight 8 resting state networks, which carried out the analysis on a group of 10 subjects. In ***Figure 3.17*** it is possible to distinguish the components in (Beckmann et al., 2005):

a) *medial visual cortical areas*

b) *lateral visual cortical areas*

c) *auditory system*

d) *sensorimotor system*

e) *visuospatial system*

f) *executive control*

g) *dorsal visual stream right*

h) *dorsal visual stream left*

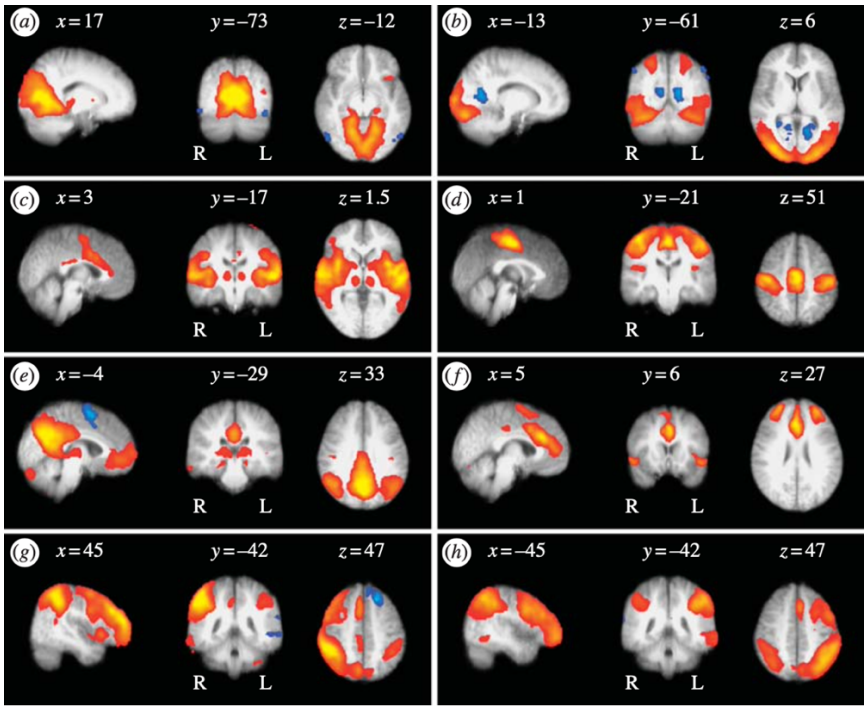

Figure 3.17 *Sagittal, coronal and axial views of different spatial maps associated with low-frequency resting patterns estimated from a group of 10 subjects* (From Beckmann et al., 2005)

Few years later, Smith and his collaborators, identified 10 networks of the state of rest studying 36 healthy patients during resting state. They compared the networks activated during rest and the networks activated during task to check whether or not there was a correlation between the networks activated at rest and those activated during a task. The networks activated are shown in ***Figure 3.18.*** They are Ten well-matched pairs of networks from the 20-component analysis of the 29,671-subject BrainMap activation database and (a completely separate analysis of) the 36-subject resting FMRI dataset (Smith et al., 2009).

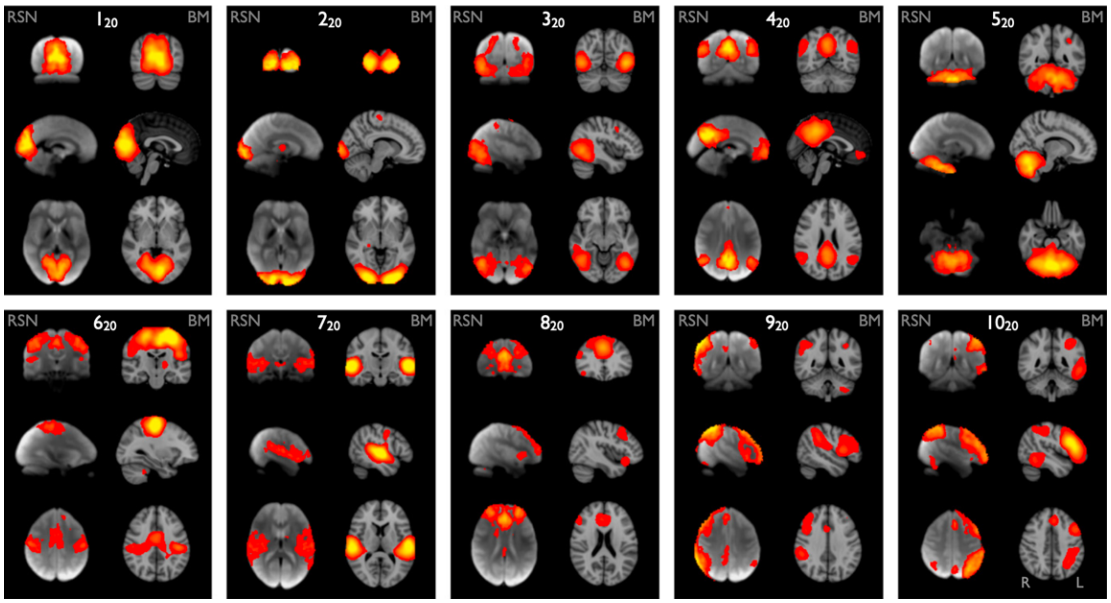

Figure 3.18 *The 10 Resting State Networks discovered by Smith et al. The left column of each pair shows the 3 most informative orthogonal slices, while the right shows an average of all subjects. They are represented in the three planes: sagittal, coronal and horizontal* (From S.M. Smith, et al., 2009)

- Maps 1_{20}, 2_{20} and 3_{20}: they correspond to medial, occipital pole, and lateral visual areas.
- Map 4_{20}: default mode network.
- Map 5_{20}: it covers the cerebellum. This corresponds most strongly to action–execution and perception–somesthesis– pain domains.
- Map 6_{20}: it includes supplementary motor area, sensorimotor cortex, and secondary somatosensory cortex.
- Map 7_{20}: It includes primary and association *auditory cortices*. This corresponds most strongly to action–execution–speech, cognition–language–speech, and perception–audition paradigms.
- Map 8_{20}: "executive control" and it covers several medial–frontal areas. This corresponds to action–inhibition, emotion, and perception–somesthesis–pain.
- Maps 9_{20} and 10_{20}: they cover several frontoparietal areas, right and left respectively. They correspond to several cognition/language paradigms.

Chapter 4 "fMRI Tools for Data Analysis"

4.1 Independent Component Analysis

Independent component analysis (ICA) is a method for automatically separating data into underlying informational components, where such data can take for of images, sounds, telecommunication channels, and this technique rapidly finds applications in analysis of biomedical signals. ICA belongs to a class of Blind Source Separation (BSS) methods for separating the data into underlying informational components, in that it is essentially a method for extracting useful information from data. A large set of signals are measured, and it is known that each measured signal depends on several distinct underlying factors, which provide the driving forces behind the changes in the measured signals.

ICA is based on the simple and physically realistic assumption that if different signals are produced by different physical processes, then those signals are statistically independent. ICA separates signal mixtures into statistically independent signals.

ICA has proven very useful for the identification of artifacts in fMRI data. The fMRI brain image collected at each time point is treated as a mixture of spatial independent components (sICs), which are extracted by spatial ICA (sICA) (Stone, 2002).

The BOLD signal (4-D data) reflects hemodynamic events within the brain, which in turn are driven by metabolic changes and neural activity. However, the link between BOLD changes and neural activity is indirect and can be influenced by several non-neuronal processes. For this reason, the BOLD signal is a multivariate signal, resulting from a set of noise and signal of interest. Therefore, to identify which signal represents noise and which ones represent neural activity, it is necessary to unpack the observed BOLD signal (Bijsterbosch, et al., 2017).

ICA model is a linear model, and it is defined as:

$$x = As \qquad [3]$$

where **x** is the signal that we are trying to decompose (BOLD signal), **s** is a set of unknown sources (or *components*), and **A** is the unknown *mixing matrix* that combines the components to obtain the observed signal (Poldrack, 2011). ICA relies upon the assumption that the components in **s** are *statistically independent*.

At the end, the entire 4-dimensional data set is rearranged into a 2-dimensional matrix by organizing all voxels for each time-point into a single row (i.e., one row per 3D functional image). This data set is then decomposed into two new matrices, the first one containing a time course of an underlying signal in each column and the second matrix containing a spatial component's map in each row (***Figure 4.1***) (Beckmann, 2012).

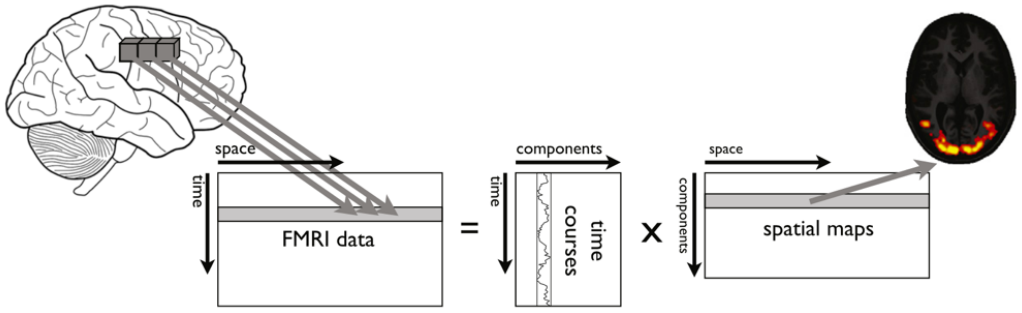

Figure 4.1 *Schematic illustration of the data representation and the spatial decomposition performed by spatial ICA on FMRI data* (From Beckmann, 2012)

The final result of the ICA is described by a spatial map, indicating the area of the brain where activity is detected, and a time series, describes the signal time course measured at each voxel (Beckmann, 2012).

4.1.2 Probabilistic ICA

The probabilistic ICA (PICA) model for fMRI, models the observations as mixtures of spatially non-Gaussian signals and artefacts in the presence of Gaussian noise (Smith et al., 2004). It is suited to automatically estimate the number of relevant noise and signal sources in the data. The data is decomposed into a set of spatially independent maps, each with an internally consistent temporal dynamic characterized by a time course. Probabilistic ICA provides intensity values (z scores) and thus a measure of the contribution of the time course of a component to the signal in a given voxel. The PICA approach estimates components, including artefacts, based on the Laplace approximation of the Bayesian model evidence. Hence, this approach makes it feasible to separate uninteresting physiological noise from other effects such as resting-state maps even in cases where the physiological noise fluctuations become aliased in the temporal domain. The components relating to artefacts were removed and only the

artefact not related components were included for further analysis (Mingoia, et al., 2012).

Beckmann and Smith proposed a PICA model for fMRI data. This new methodology is implemented in his MELODIC software for FSL (Beckmann and Smith, 2004).

The PICA model includes a noise term (e):

$$x = As + e \qquad [4]$$

where $e \sim N(0, \sigma)$.

The model was improved by adding other processes as the use of voxel-wise temporal pre-whitening, of variance normalization of the time series, and prior information about the spatiotemporal nature of the source process. Next, the resulting spatial map will be converted to Z-scores, so it is needed to determine an appropriate threshold (usually $|Z|>2.0$). Above this, values of Z correspond to statistically significant activations with respect to background noise. To perform inference and evaluate maps in relation to voxels activated in a significant way, the PICA algorithm uses a probabilistic mixture modeling model applied to the probability densities of the Z-score spatial map. The distribution of the statistical data of interest was split into her two components: un-activated voxels and activated voxels *(**Figure 4.2**)* (Beckmann and Smith, 2004).

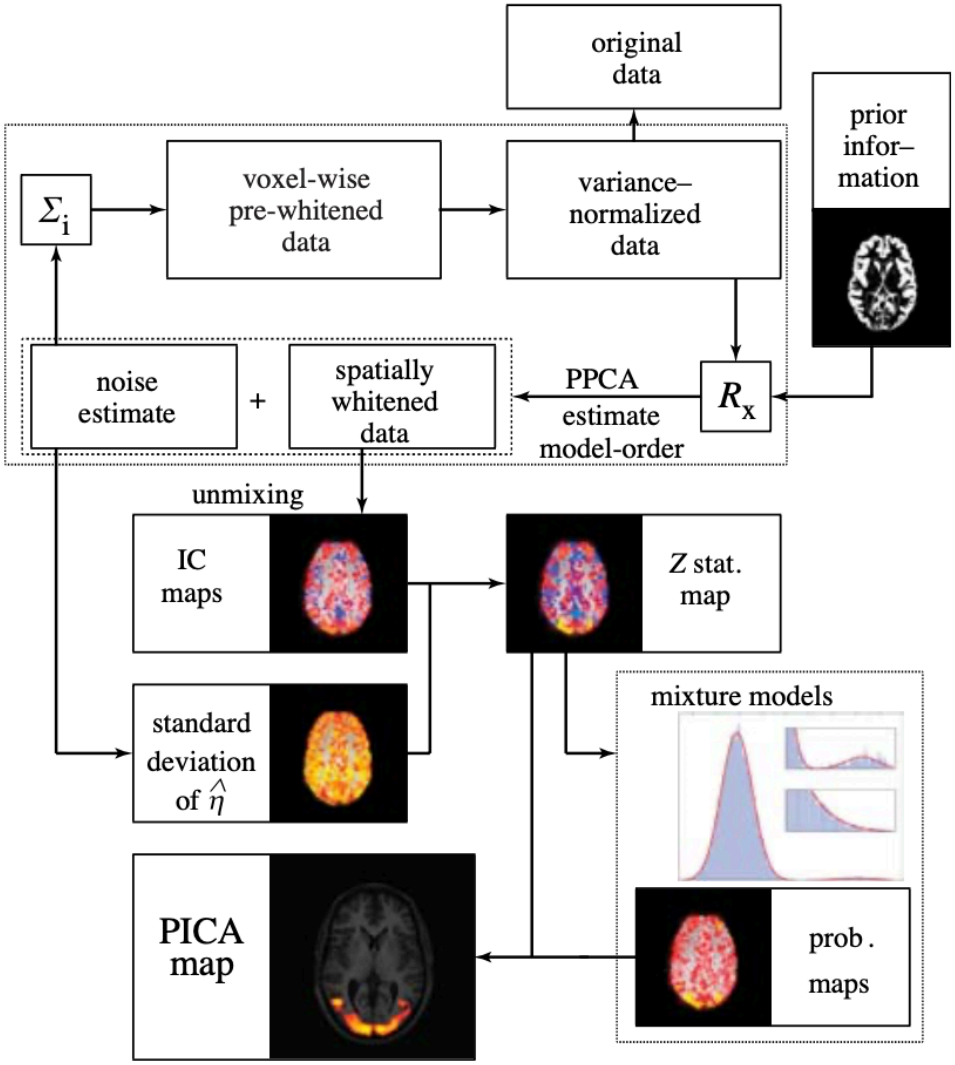

Figure 4.2 *Schematic illustration of PICA model* (From Beckmann & Smith, 2004).

Chapter 5 "Materials & Methods"

5.1 Partecipants

The data used in this study were acquired from two right-handed patients, P1, P2, P3, P4, P5 (age: 42-60 years; M/F=4/1) who had severe epilepsy episodes in their history, and four healthy subjects S1, S2, S3, S4 (age: 31-64 years; M/F=1/4). Four patients underwent callosotomy different years ago, except for P2. More in detail, P1 underwent posterior callosotomy, P3, P4, P5 complete callosotomy. The data acquisitions with the MRI were performed between May 2018- June 2019, and the clinical patient's details are reported in ***Table 2***.

Table 2 *Clinical details of patients*

CASE	*GENDER*	*AGE TESTING*	*HANDEDNESS (OLDFIELD SCORE)*	*CALLOSOTOMY*	*YEARS AFTER SURGERY 2ND SURGERY*
P1	M	60	RIGHT (10)	PARTIAL POSTERIOR	19
P2	M	52	RIGHT (10)	NO SURGERY	
P3	M	42	RIGHT (21)	TOTAL	23
P4	F	46	RIGHT (10)	TOTAL	19
P5	M	52	RIGHT (10)	TOTAL	24

5.2 MRI Data Acquisition

The subjects instructed in this study during the fMRI acquisition in the resting state, were warned in advanced to lie down and remain still as much as possible, to keep their eyes open, and to relax without falling asleep and without focusing on anything.

Resting-state BOLD fMRI data and T1-weighted structural images were acquired using a 1.5 Signal HDxt GE Medical System MRI scanner.

It was used an echo planar image (EPI) gradient-echo sequence to acquire the functional images with parameters echo time (TE)= 50 ms, repetition time (TR)= 3000 ms, flip angle=

90°, Field of View (FOV) of 192 × 192 mm, matrix size of 64 × 64, number of volumes= 300, number of axial slices= 35, slice thickness= 4 mm with no gap between slice acquisition and voxel resolution is 3×3×4 mm. The duration of resting state fMRI was 900 s (15 minutes). The T1-weighted structural image (high-resolution whole-brain images, also called structural image) was acquired using a MPRAGE sequence with parameters TE= 6.7 ms, TR= 14.7 ms, FOV of 256×256 mm, matrix size of 512×512 mm, number of sagittal slices= 158 (166 in the RM data acquisition), slice thickness is 1 mm with no gap between slice acquisition and the voxel resolution is 0.5664×0.5664×1 mm, for co-registration with 3D data set and anatomical localization.

5.3 FMRIB Software Library

FMRIB (Functional Magnetic Resonance Imaging of the Brain) Software Library (FSL) is a software created by the Analysis Group, Oxford (UK) and is a comprehensive and open-source library, that contains tools for image analysis and statistical programs for the analysis of data from functional, structural and diffusion tensor magnetic resonance images. It works on Apple and Linux and also on Windows 10 via a virtual machine. It can be downloaded for free from the dedicated link. In order that the program works properly, there are some system requirements that must be observed, and which can be checked on the official website. Once the program is started via the terminal, it appears as in ***Figure 5.1***, equipped with a very intuitive Graphical User Interface (GUI) that shows all the tools made available for image analysis.

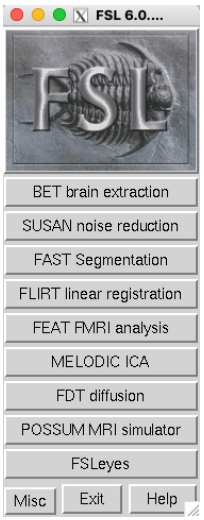

Figure 5.1 *FSL graphical interface* (From FSL User Guide 2020)

5.4 Pre-Processing

Once the data have been acquired, the structural and functional MRI images were processed to obtain the information necessary to continue the study with FSL software. The MRI images acquired were in DICOM format; since by default FSL uses the NifTI.gz image format, i.e. the compressed NIfTI file (.nii or .nii.gz). Therefore, it was necessary to convert them to the NIfTI format, considered the new standard format for medical and brain images. NIfTI file is a modern incarnation of the Analyze format but includes important information like the orientation of the image. For this purpose, in addition to FSL software, MRIcron software was also used to convert the DICOM file into a NifTI file (*https://www.nitrc.org/projects/mricron*).

MRIcron software was downloaded from the official website, extracted the folder in zip format, opened and finally launched as MRIcron application. Then, a screen will appear (***Figure 5.2***) with an options bar allowing to Import and then Convert DICOM to NIfTi.

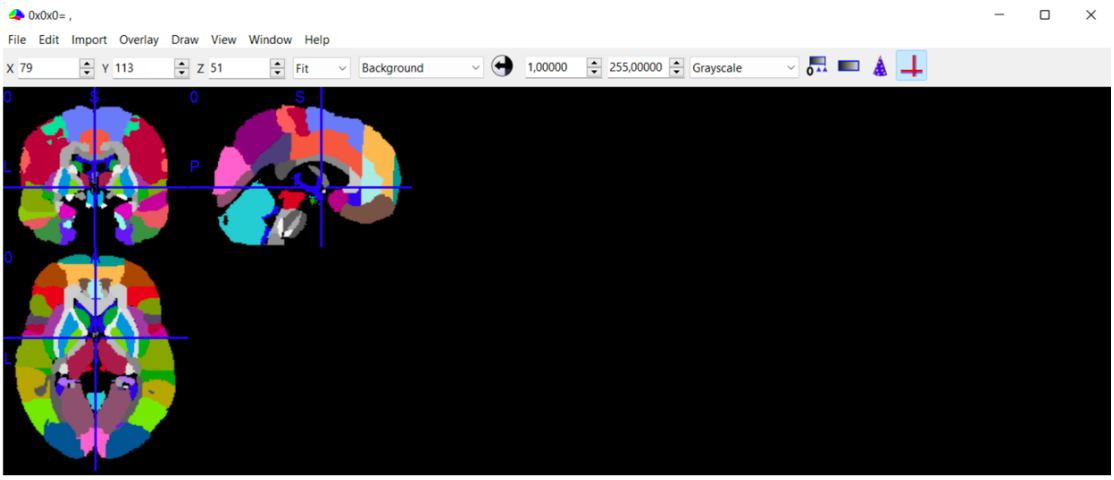

Figure 5.2 *MRIcron screen*

Before the statistical fMRI analysis, it was necessary to perform some steps to eliminate artifacts and noise components in fMRI. A series of preprocessing pipeline were used on the raw data and the standard operations to follow are shown in ***Figure 5.3***.

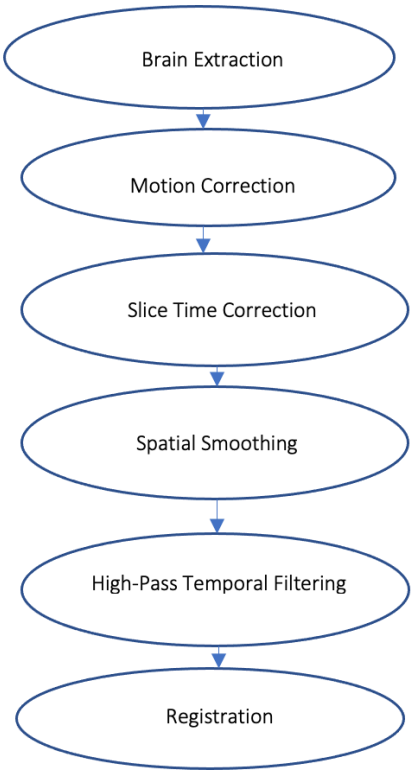

Figure 5.3 *Common fMRI pre-processing steps*

Quality control must be ensured for each phase in order to verify the effectiveness of the pre-process technique and prevent the propagation of the error. FSL uses MELODIC tool (see below, section 5.4.2) to do the pre-processing steps, by selecting MELODIC ICA GUI or by typing Melodic_gui on the shell (Poldrack et al., 2011).

5.4.1 Brain Extraction Tool- BET

After the conversion of data in NifTI files, the Brain Extraction Tool (BET) was used to remove, for example, skull and meninges from an anatomical dataset that will be used in the FEAT analysis. The BET deletes non-brain tissue from an image of the whole head. It can also estimate the inner and outer skull surfaces, and outer scalp surface, if good quality T1 and T2 input images are available (Smith et al., 2004). This is the first pre-processing step to differentiate brain from non-brain tissue, and it is performed on T1-weighted structural images. In particular, the BET is applied on the *ISO images* that represent the structural images. The output is an image that according to default settings will have the same name as the input file with the addition of "_brain", added by default (***Figure 5.4***).

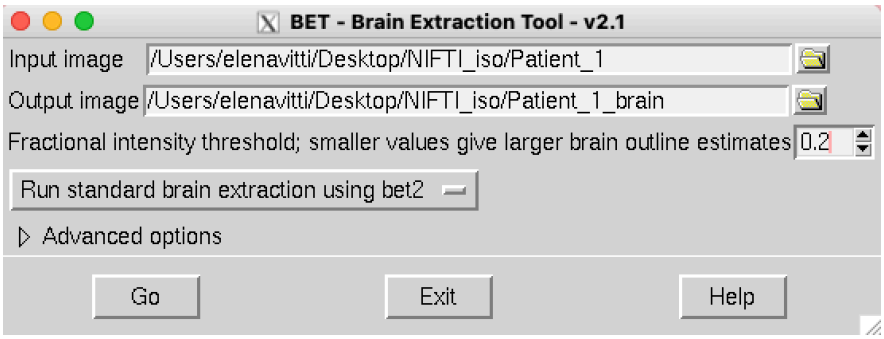

Figure 5.4 *FSL- Brain Extraction Tool* (From FSL User Guide 2020)

With BET all the non-brain tissues are removed from the structural image, and it is a completely automated algorithm. Furthermore, since each image of the brain is different, some parameters must be adjusted to obtain a better result, such as the fractional intensity threshold parameter. This parameter controls the threshold that distinguishes brain from non-brain tissue, and it represents the smoothness constraint, that is the constraint that allows to have a solution adequately clean from the effects of the image distortion field; and if a suitably clean solution is not arrived at then the whole process is rerun by the tool with a higher smoothness constraint (Smith et al., 2004).

Different threshold parameters were set, to choose the best one that represented the best portion of the brain extracted with BET. As shown in ***Figure 5.5*** the different thresholds were highlighted with different colors, to qualitative appreciate the difference between them in terms of having a clear image of the brain without other components that could cause distortions and artifacts during the study. In particular, for 0.2 threshold was set the yellow color, for 0.22 the red color, for 0.28 the blue color, and for the 0.3 threshold was set the green color.

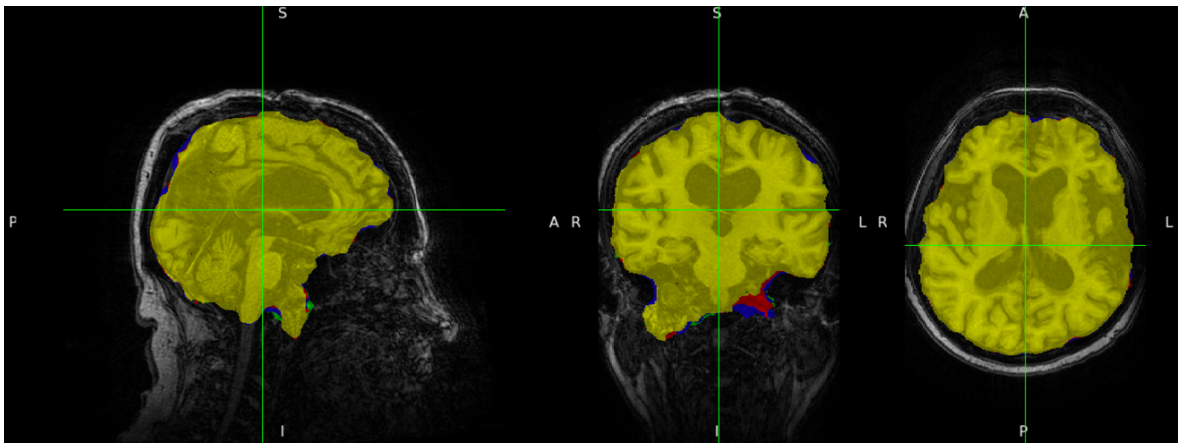

Figure 5.5 *Different representation of the use of BET fractional intensity threshold*

Finally, in this study case, the fractional intensity threshold parameter is selected to 0.2, resulting the best one in the extraction of brain's portion.

As a general rule, it is better exceed leaving too much skull, rather than removing too much cortex - bits of skull here and there won't cause future preprocessing steps to fail (such as normalization), but once cortex is removed, it is impossible to recover it (University of Michigan, 2022).

5.4.2 MELODIC

Before the pre-processing steps, such as motion correction, slice time correction, spatial smoothing and temporal filtering, it is necessary to select the fMRI data previously converted into NIfTi file. In MELODIC (Multivariate Exploratory Linear Optimized Decomposition into Independent Components) section, the independent component analysis (ICA) is used to carry out temporal model-free exploratory analysis. This approach can identify signal and structured noise in fMRI data without needing to be given a temporal model (Smith et al., 2004). The ICA attempts to split the 4D functional data into a set of spatial maps, each with an associated time course (***Figure 5.6***) (FSL User Guide 2020).

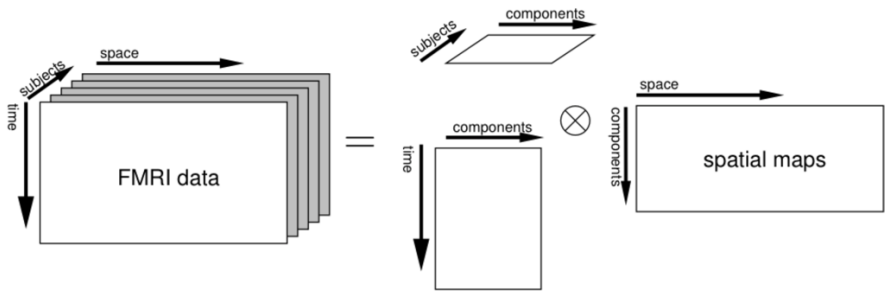

Figure 5.6 *Representation of MELODIC analysis* (From FSL User Guide 2020)

MELODIC is used to filter out unwanted components from the original data; the number of components is calculated using Bayesian dimensionality estimation techniques. It allows us to extract probabilistic information from the data, and to probabilistically combine information from multiple modalities (Woolrich et al., 2008). The ICA is a technique that allows to decompose a set of data into different components independent from each other. It is also possible to distinguish connectivity maps from non-neural signals, in such a way as to separate the components from noise, artifacts, due to

movement or other physiological activities (for example heartbeat or breathing, etc.) independent that are obtained from the analysis, are related either to the activation of areas of the brain, or to other physiological processes or to artifacts such as movement (FSL User Guide 2020).

5.4.2.1 Data Selection

In the "Data" section, the 4D data option (fMRI file in -nii.gz format) is selected from the Resting-State image folder that contains all the functional images in NIfTI format, and the first 5 volumes have been deleted before any further processing (***Figure 5.7***). It is also selected the output directory where to save the output file.

The deleted volumes are referred to the slices of the 4D image; considering that the time for stabilization should be more than 3 seconds, the number of scans to delete is dependent on the relaxation time. Therefore, if the relaxation time is more than 3 seconds, just one volume can be deleted, f the time is equal or less than 3 seconds, from 2 to 5 or more volumes can be deleted.

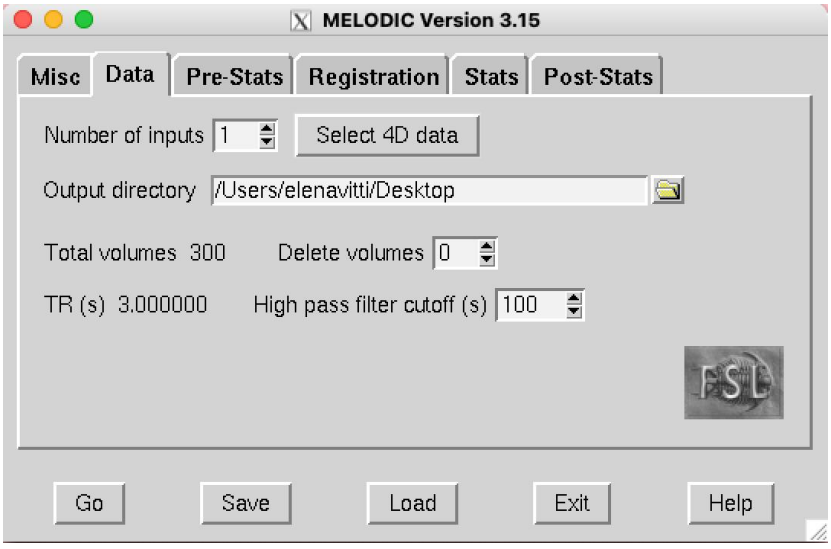

Figure 5.7 *MELODIC window after been selected "Data" section* (From FSL User Guide 2020)

5.4.2.2 Pre-statistical Analysis

As shown in ***Figure 5.3***, there are several key steps before co-registration: pre-processing the fMRI data, correcting for head motion, filtering noise, and smoothing the fMRI image.

After having selected the data to analyze, the section *Pre-Stats* (***Figure 5.8***) includes the *Motion Correction*, also known as realignment, since the head movement correction is the main pre- processing procedure to obtain better results in the data analysis. The *Motion Correction* is an important issue in the analysis of fMRI data because even slight movements of the patient can induce large artifacts and some signals can be with greater intensity than the BOLD signal.

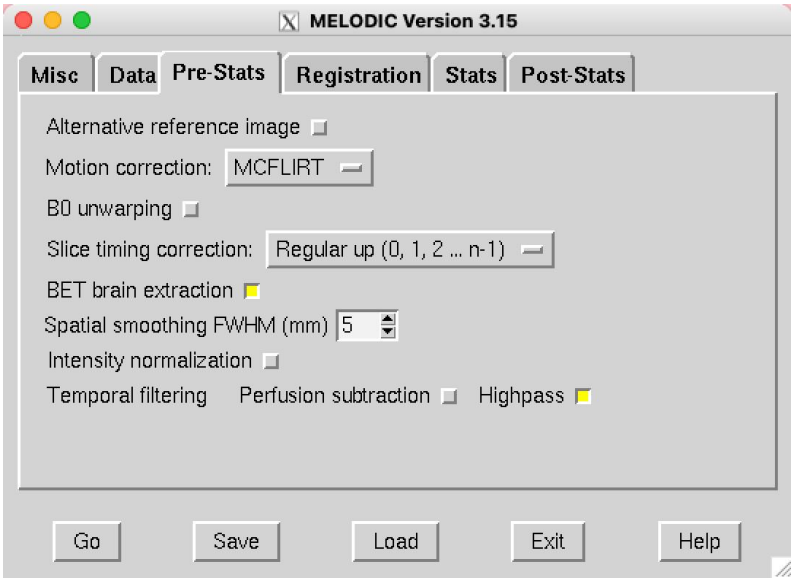

Figure 5.8 *MELODIC window after selecting the Pre-Stats option* (From FSL User Guide 2020)

MCFLIRT is selected for *Motion Correction*, and it is a fully automated robust and accurate tool for linear (affine) inter- and intermodal brain image registration, designed for fMRI time series intramodal motion compensation based on the optimization and registration techniques used in FLIRT. It is a fully automated robust and accurate tool for linear (affine) inter- and intermodal brain image registration.

Motion Correction is needed because if the subject's head moves during fMRI scan, successive slices may be misaligned, resulting in incorrect anatomical positioning between voxels in subsequent images. Hence, the images need to be aligned to a common standard, because the time series corresponding to a particular voxel at each time point is assumed to belong to the same brain region during data analysis. In this algorithm, translation and rotation are calculated at any time using six parameters, three each for translation and rotation, to represent the head motion. Thus, each volume is

translated and rotated to match the position of the reference volume (FSL User Guide 2020).

The *Slice Time Correction* is a temporal correction procedure, since not all acquired volumes are obtained at the same instant. The slices can be acquired sequentially, in ascending or descending order, or interleaved. *Sequential slice acquisition* acquires each adjacent slice in succession from bottom to top or top to bottom. Interleaved acquisition acquires one slice at a time and fills the gaps in a second pass, i.e., the tool repeats the passage, filling the time space between one acquisition and another, making sure that all the voxel slices have a continuous TR and not at intervals.
Since fMRI analysis is based on the time course of the signal, slice timing problem scan seriously affect the analysis. Thus, the slice timing correction method attempts to adapt to the problem of delayed slice acquisition. This time delay is corrected by aligning each acquired slice at the same instant that the reference slice was acquired (FSL User Guide 2020).
Using FSL it is necessary to know in what order the slices were acquired and set the appropriate options here. If the slices were acquired from the bottom of the brain to the top, select *Regular up*. If slices were acquired from the top of the brain to the bottom, select *Regular down*. If the slices were acquired with interleaved order (0, 2, 4, ... 1, 3, 5 ...) then choose the *Interleaved option*. If slices were not acquired in regular order, it will be necessary to use a slice order file or a slice timings file *(*FSL User Guide 2020).
For the present analysis, the subjects' fMRI sequences were acquired sequentially in ascending order (from bottom to top), therefore *Regular up* button was selected.

The *Spatial Smoothing* is commonly applied in most fMRI studies and consists of averaging adjacent voxels. This has the effect of a low-pass filter. This filter is applied to remove the high frequencies of the signal from the image, prevailing the low frequencies information typical of resting neural activity. As a result, sharp "edges" in the image are blurred and spatial correlations in the data become more pronounced (Figure 5.9), because the signal-to-noise ratio is improved losing the spatial resolution (the higher is the spatial smoothing, the blurrier is the image).

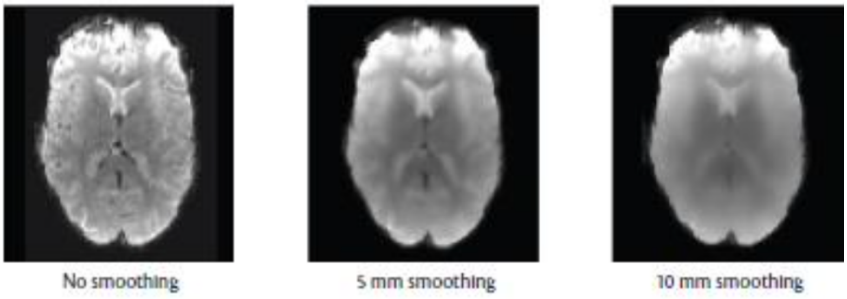

Figure 5.9 *Example of Spatial Smoothing application with different values* (From Poldrack et al., 2011)

During smoothing, the fMRI image is convolved with a 3D Gaussian kernel, or filter. This is determined by the parameter's full width at half maximum (FWHM), or standard deviation in statistical terms. FWHM is the half-height diameter of the smoothing kernel. Higher FWHM values represent more data being smoothed and the smoothness correspond to (FSL User Guide 2020):

$$FWHM = \sqrt{FWHM_{intrinsinc}^2 + FWHM_{applied}^2} \qquad [7]$$

In conclusion, the Spatial Smoothing is performed separately for each volume of the fMRI dataset. This is intended to reduce noise without reducing effective activations. This will succeed as long as the underlying activation area is larger than the smoothing range. If a very small activation area is searched, it would be better to reduce the smoothing from the default 5 mm. If a larger area is the target of the study, the smoothing could be up to 10 or 15 mm (FSL User Guide 2020), (***Figure 5.10***). In the study was selected the smoothing of 5 mm.

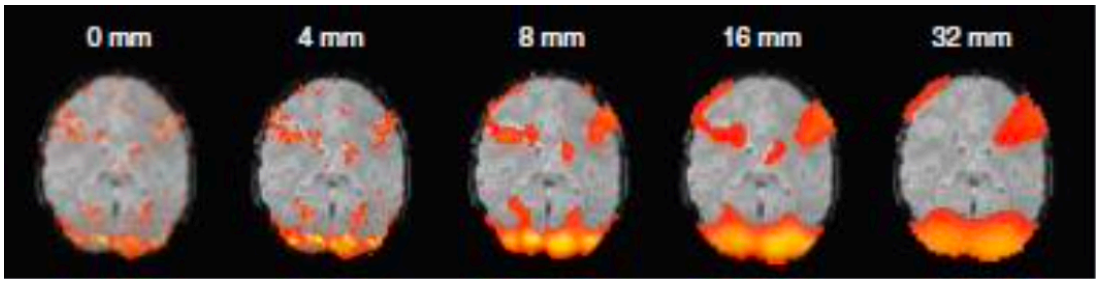

Figure 5.10 *Larger FWHM values show activity in more voxels, thus detecting more large clusters but fewer small clusters* (From Poldrack et al., 2011)

The *Temporal Filtering* is the last pre-processing step of MELODIC tool, and it is used to remove the unwanted signal from the times series of each voxel without removing the

desired signal. The applied filter is a high-pass filter because the fMRI data are high-pass filtered and this means that from the data are removed the lowest frequencies. The amount of temporal filtering applied is expressed using a cutoff frequency (in Hertz) or a cutoff period (in seconds) and depends on the quality of the data. For high quality datasets it is possible to set higher cutoff frequency (0.001 Hz) to remove less data and retain more data, while for lower quality datasets, lower cutoff frequency (0.01 Hz) is often used to remove much noise (Bijsterbosch et al., 2017). In this study, a high-pass filter was used, with a cutoff frequency of 0.01 Hz, to remove (completely or partially) signal variations that change more slowly than the cutoff frequency value.

The alignment between the functional and anatomical images is called *Registration* phase. In this case, the Main Structural Image and the Standard Space are selected, as shown in ***Figure 5.11.***

The Main structural image, also called T1-weighted structural image, is the main high resolution structural image which the low-resolution functional data will be registered with (optionally via the initial structural image), and this in turn will be registered to the standard brain. It is highly recommended that this image has non-brain structures already removed, for example by using BET. The functional image is aligned with T1-weighted structural image for each subject, to interpret the results and to accurately recognize the regions of interest in functional image to and understand in which brain region the voxels were active (FSL User Guide 2020).

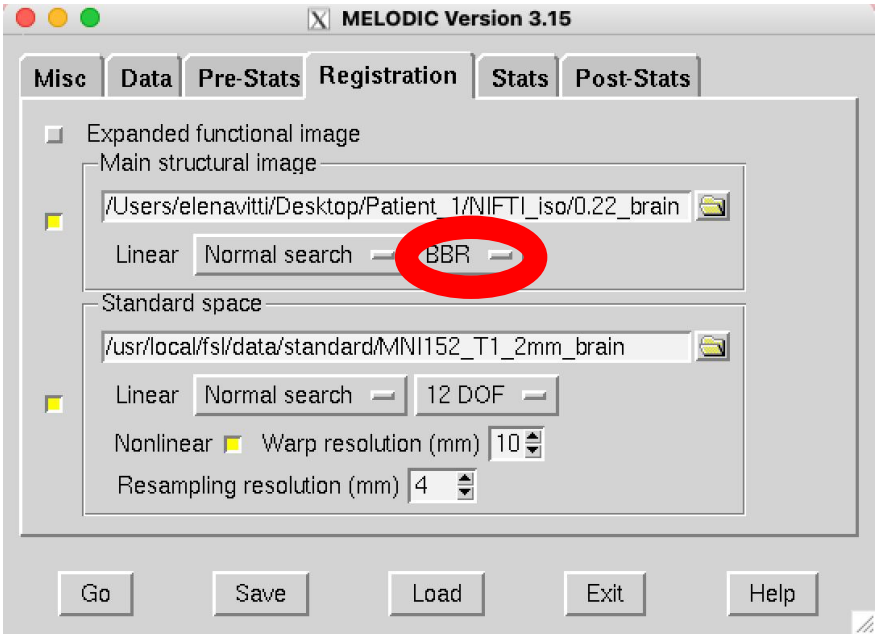

Figure 5.11 *MELODIC window after selecting the Registration option* (From FSL User Guide 2020)

Since the human brain varies from subject to subject in both size and shape, functional and anatomical images of the subject were aligned with standard space to perform comparisons between different subjects to have the results more comparable and integrated. (***Figure 5.12***)

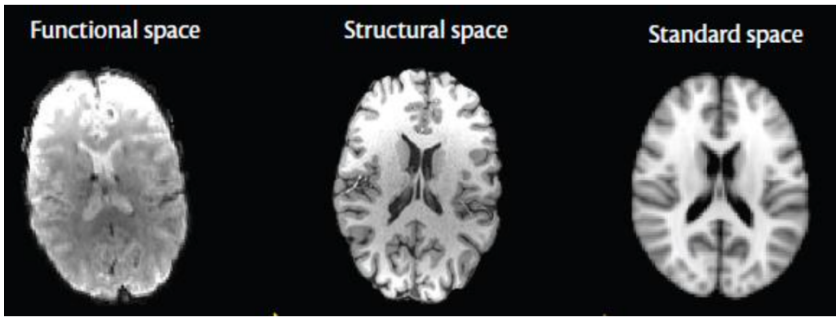

Figure 5.12 *Registration methods are used to align the subject's functional and structural image (both in native space) into the same standard space* (Bijsterbosch et al., 2017).

Every acquisition can be aligned to a specific template, an image representing an atlas (a guide for localizing activations and interpreting results) and provides targets against which individual images can be positioned (Poldrack et al., 2011).

Two different approaches are used in fMRI:

• *Talairach* approach, developed in 1967 by Jean Talairach and Gabor Szikla as a standardized grid (Talairach & Szikla, 1967), which is based on the observations of the brain of a 60-year-old woman, and which uses Brodmann's areas to label areas of the brain.

• *Montreal Neurological Institute (MNI)* approach, slightly larger and obtained thanks to the images acquired from 152 right-handed subjects.

In this study, the MNI approach was used reference system, called MNI152 in FSL (***Figure 5.13***).

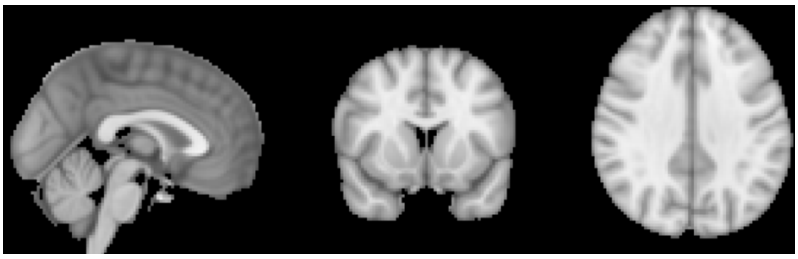

Figure 5.13 *An example of a commonly used template in FSL, the MNI152 brain* (From FSL User Guide 2020)

The registration consists in two-steps:

1. The *co-registration* aligns the preprocessed functional images to their corresponding T1-weighted anatomical image. The goal is to overlay the information contained in the functional image onto an image in which anatomical regions can be distinguished. The registration algorithm moves through the images to test different overlays of anatomical and functional images, matching bright voxels in one image to dark voxels in another image, and dark voxels to bright images, until a match that cannot be improved, is found (FSL User Guide 2020).
2. The second step, called *normalization*, consists of registering the images of interest (functional and anatomical) into the atlas. The main advantage comes from the possibility to generalize the results to a larger population of subjects, to improve comparisons between different studies, and to perform averaging processes between different subjects (FSL User Guide 2020). The linear registration to register the high-resolution structural brain image to a standard space (MNI152, T1-weighted, 2x2x2 mm) is used, with resampling resolution of 2 mm. FMRIB's Linear Image Registration Tool (FLIRT) is used for linear brain image registration (FSL User Guide 2020).

The co-registration is different for healthy subjects and patients. In case of patients, it is done through the *boundary-based registration* (BBR) method, based on white-matter boundaries and the fact that it is expected to see reliable changes in intensity across this boundary in the functional MR images, whereas the exterior grey-matter boundaries tend to be less reliable (FSL User Guide 2020) (Figure 4.11).

For healthy subjects, as shown in ***Figure 5.14***, the Linear Normal Search for 12 Degree of Freedom (DOF) was used to realign the different images. The reason of this is that the BBR uses intensities near the white-matter boundary, generally more robust in pathologies (atherosclerosis, multiple sclerosis, excess of alcohol, head trauma, memory problems and cognitive impairment).

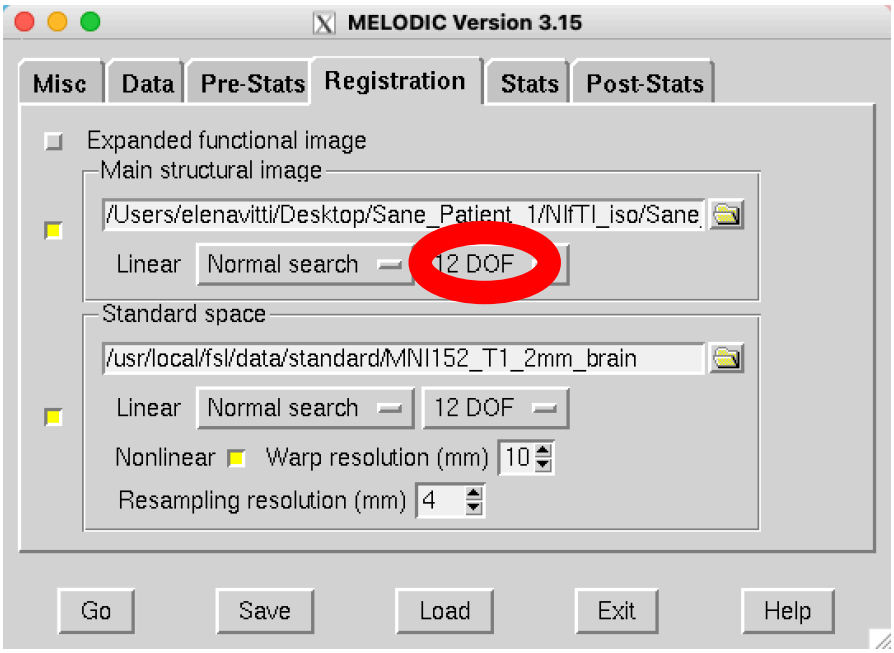

Figure 5.14 *Registration phase for healthy subject* (From FSL User Guide 2020)

The second step is the normalization. The linear registration is used to align the multiple images of a single subject, e.g., to register high-resolution brain structural images in standard space (MNI152, T1-weighted, 2×2×2 mm) with a resampling resolution of 2 mm. FLIRT is the FSL tool for linear registration: it is used 12 degrees-of-freedom (3 translations, 3 rotations, 3 zooms, and 3 shears) (Jenkinson et al., 2002).

The linear registration is used to initialize non-linear registration performed by using FSL's tool FNIRT. This allows to obtain a better alignment of internal structures (FSL User Guide 2020). Non-linear registration is used when registering multiple subjects to one another, or to a standard template, after the linear registration to have an optimal accuracy. The warp resolution was set to 10 mm.

In *Stats* and *Post-Stasts* (***Figure 5.15 A, B***) the two options are already selected by default.

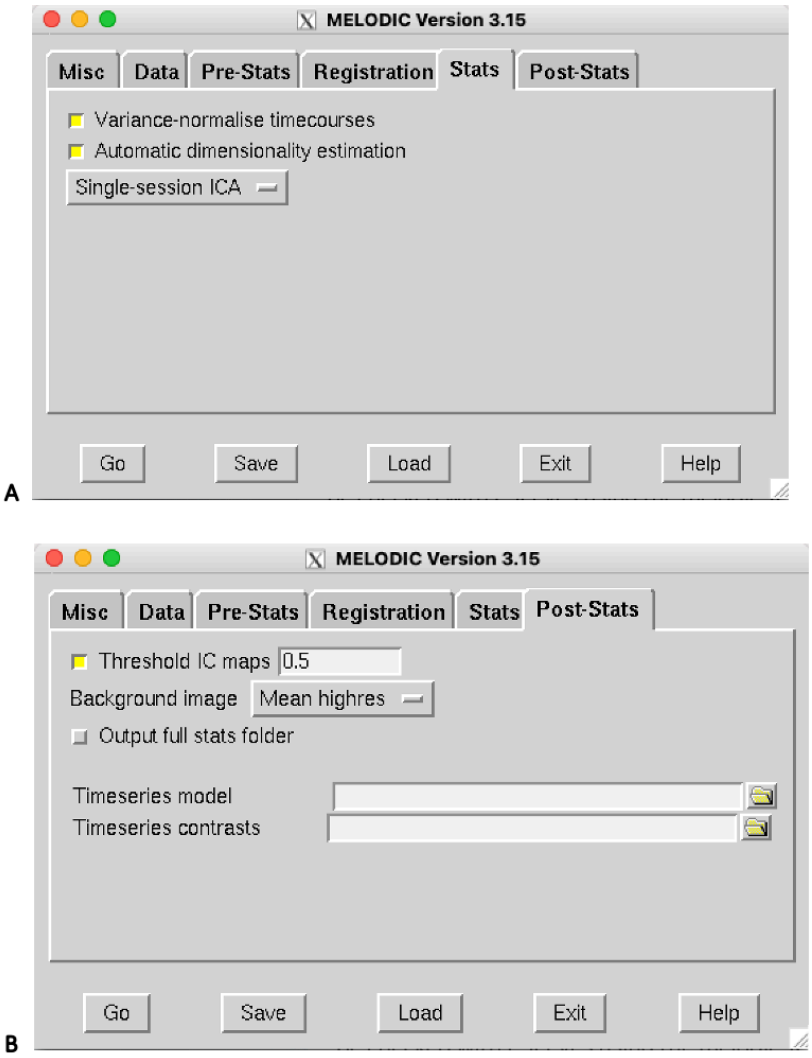

Figure 5.14 *Registration phase Stats (A) and Post-Stats options (B)* (From FSL User Guide 2020)

In the *Stats* section, the "multi-session temporal concatenation" option allows to perform a single 2D ICA run on functional images concatenated in a data matrix. When analyzing multiple subjects (or sessions) all datasets are temporally concatenated to form a matrix whose dimension is 2D Space multiplied by Concatenated Time data. Multiple fMRI data sets are temporally concatenated, and ICA is applied in order to identify large-scale patterns of functional connectivity in the population (***Figure 5.15***). This approach is recommended to be used when looking for common spatial patterns (FSL User Guide, 2020). In this study, the "multi-session temporal concatenation" option is selected for the analysis of the 4 healthy subjects in order to obtain common activation patterns.

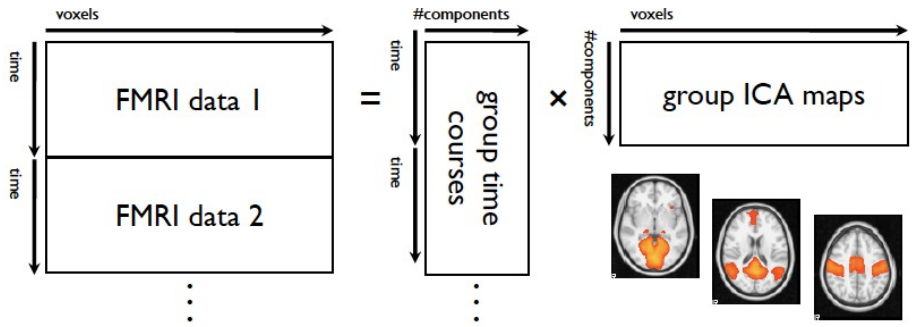

Figure 5.15 *Concatenation representation used by the ICA in MELODIC tool*

Pressing the "Go" button, it will initiate the procedure and the results will be placed in the output folder shown earlier in the *Data* section.

Within this folder are several files with .html extensions that create a summary of all the operations performed, essential to understand whether the co-registration process was successful. These results can also be checked with FSLeyes using the melodic_IC file in the folder in the folder "filtered_func_data.ica" and the image of the 10 resting state networks (rsn10), which can be downloaded from fmrib library (https://www.fmrib.ox.ac.uk/datasets/brainmap+rsns/).

During the *Post-Stats*, the PICA is implemented in MELODIC using the Gaussian/Gamma Mixture Model (GGM). This approach allows us to model the histogram of the inactive voxels (Gaussian background noise) with a Gaussian distribution (which primarily models the intensity histogram), where the histogram of the Z-map of the non-Gaussian source (activated voxels) can be modeled using a gamma distribution (both negative and positive gamma) (***Figure 5.16***) (Beckmann and Smith, 2004)

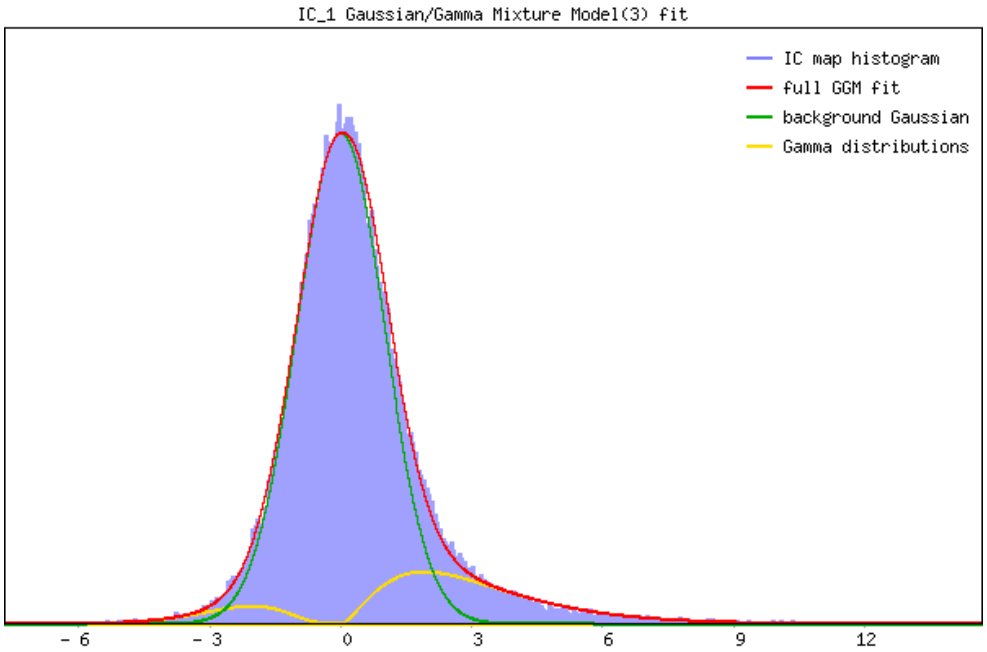

Figure 5.16 *Gaussian/Gamma Mixture Model implemented within FSL used to model the histogram of inactive voxel with the Gaussian distribution (green curve) and the active voxel with Gamma distribution (yellow curve) (From Beckmann, 2012)*

The number of ICs was automatically estimated, and the value chosen as the threshold for identifying activated voxels was p>0.5 (***Figure 5.14, B***)

5.5 Hand Classification of Independent Components

ICA gives different spatiotemporal components, and the information defined in the ICA decomposition is employed to recognize the noise independent components (N-ICs), that is the components characterized by a noise/artefact signal, and the neural signals independent components (S-ICs), that is the signals of interest. These two components differ in terms of spatial, temporal, and spectral characteristics, and this exploiting to reduce the negative effect of noise on the analysis of fMRI data. There are different approaches to label the components, most of which are completely automated, that are useful when dealing with a large population of healthy subjects. In case of a small population size with unusual characteristics, for example epileptic disorders, it is preferable to use a visual inspection of the components, that corresponds to the gold standard technique, although it is time-consuming and it requires expertise (Griffanti et al., 2017).

The goal of ICA-based data cleanup is to preserve as much signal as possible, removing artifacts from the fMRI data. Its success depends on the accuracy of ICs' labelling (Robert et al., 2010).

To classify the components, each component must be inspected looking at:

- the *spatial map*, is the representation of the slices on FSLeyes. It observes the number and size of clusters in the active area, if the clusters overlap with gray matter or with blood vessels, cerebrospinal fluid, white matter, or edges of the brain. It is the key information for distinguishing the signal of interest from noise (Griffanti et al., 2017).
- *the time series*, represents the signal that is measured at each voxel across the entire run. It checks the overall aspect of whether there are one or more sudden peaks, or it exhibits a saw-tooth pattern (regular top and bottom alternation) (Robert et al., 2010).
- *the power spectrum*, is the description of the power into frequency components composing the signal. It checks for low or high frequency where the distribution of power in the frequency domain occurs (Robert et al., 2010; Griffanti et al., 2017).

The features of signal- and noise-related independent components are shown in ***Table 3*** (Griffanti et al., 2017).

Table 3 *Features of signal and noise independent components* (From Griffanti et al., 2017)

Features	S-IC characteristic	N-IC characteristic
Spatial Number and dimension of clusters Overlap with GM	Low number of large clusters Clusters' peaks in GM and overall good overlap of the clusters with GM.	Large number of small clusters Indiscriminate overlap with non-GM tissues, or clusters' peaks in WM/CSF High overlap with one or more of WM, CSF, blood vessels Ring-like or crescent shape or stripes near the edges of the field-of- view
Overlap with WM, CSF, blood vessels Overlap with brain boundaries or areas close to the edges of the FOV.	Very low or absent overlap with WM, CSF, blood vessels Very low or absent overlap with brain boundaries. Clusters follow known anatomical (e.g. structural/histological) boundaries.	Located within the region of signal loss (e.g. areas of air-tissue interface)
Location near area of susceptibility induced signal loss (e.g. orbitofrontal) Non-biological, acquisition-related patterns	Generally located away from these areas Patterns have no relation to acquisition parameters	Often show banding patterns in slice direction or streaks along the phase encoding direction, accelerated sequences may have centrally located artefacts
Temporal (and spectral) features Overall aspect of the time series Distribution of power in frequency domain	Fairly regular/oscillatory time course Predominantly low frequency (at least one strong peak within 0.01 – 0.1 Hz)	Large jumps and/or sudden change of oscillation pattern. Predominantly high frequency, very low frequency, or pan frequency

Legend: GM = grey matter; WM = white matter; CSF = cerebrospinal fluid

Consequently, the main features can be visually evaluated, and the spatial maps of signal components should contain a low number of relatively large clusters, while the presence of small and scattered clusters suggests the presence of a noise component. The main characteristic to look for the time series is the presence of sudden jumps in the signal, likely suggesting rapid motion. Also, the oscillation pattern should not change significantly across the time course. The signal components are identified by the presence of predominantly low-frequency power (<0.01 Hz), visible in the power spectrum as a low-frequency peak, but also in the time series as regular low frequency oscillations. (Griffanti et al., 2017).

An example of signal reported by the study of Griffanti and co-workers is shown in ***Figure 5.17***

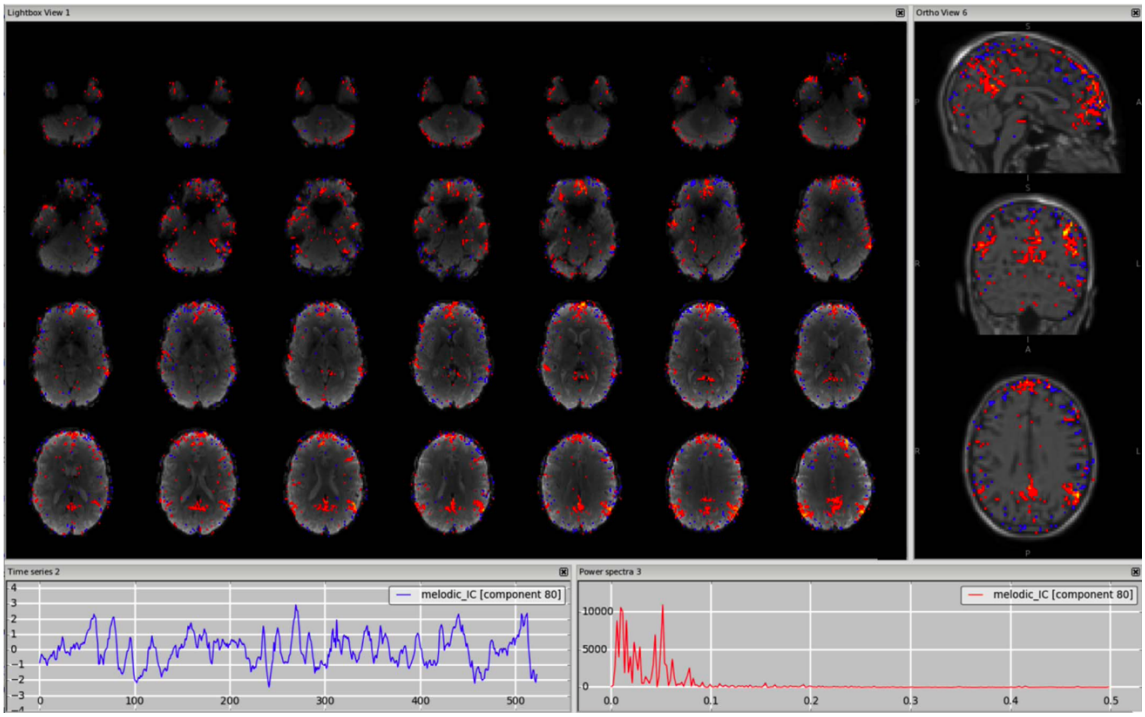

Figure 5.17. *An example signal component showing the Default Mode Network (DMN), in the two panels below are reported the time series in blue and the power spectrum in red, while in the left are reported the slices of the brain in the horizontal plane, while in the right part represents the three different plane-view of the brain (sagittal, coronal and horizontal) (From Griffanti et al., 2017)*

Some examples of commonly seen noise components identified in the study of Griffanti and co-workers are (Griffanti et al., 2017):

- *Motion:* this type of artefact is mostly seen well as a ring around the edge of the brain and in the time series plot as a sudden spike (in correspondence to sudden peak in the motion correction graphic derived from the pre-processing). The cause of this artefact is the movement of head during the acquisition (Griffanti et al., 2017) (***Figure 5.18***). The voxels in these areas are inside or outside the brain depending on the subject's head motion, therefore the time series might follow the trend of the realignment parameters and sudden jumps, or gradual drifts should be visible in both in the time series and the head motion profile.

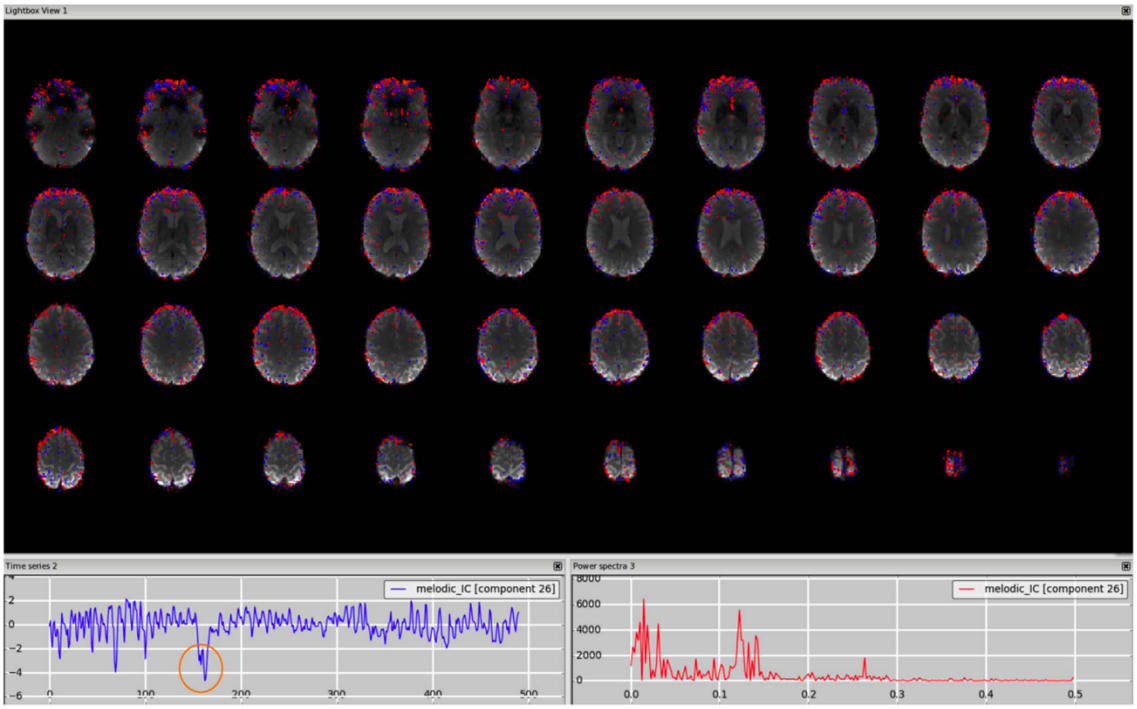

Figure 5.18 *Motion artefact. The spatial map presents the typical ring at the edge of the brain and the time series contains a sudden jump in correspondence to sudden head movement (From Griffanti et al., 2017)*

- *MRI-related artefacts*. Some artefacts can be related to MRI hardware or acquisition (Jezzard and Clare, 1999). Because of the complex nature of the imaging process, they can be quite hard to identify and understand fully.

- *Cerebrospinal Fluid pulsation.* The CSF pulsation is mainly due to cardiac and respiratory cycles. Frequencies of the cardiac and respiratory cycles are around 1 Hz and 0.3 Hz respectively; therefore, also in this case, the corresponding signal is aliased into lower frequency (Griffanti et al., 2017) (**Figure 5.19**).

- *Arteries*. The components containing BOLD signal coming from the arteries also have a distinctive high frequency spectrum. How distinct this peak will appear from the rest of the spectrum depends on the RT. This artefact is mainly detectable in the power spectrum plot for the peak a frequency higher than 0.1 Hz and for the high-frequency pattern in the time series plot. Also, in the spatial maps, the active areas run close to the arteries (Griffanti et al., 2017) (***Figure 5.20***).

- *Unclassified noise*. If that component that is evaluating has one or more features typical of a noise component (see ***Figure 5.16***). The unclassified noise, counts as N-IC, will be removed from the data (***Figure 5.21***) (Griffanti et al., 2017).

- *Susceptibility artefacts*. They are acquisition-related artifacts that are usually best detected from the spatial map as the associated time course can be predominantly low frequency (***Figure 5.22***) (Griffanti et al., 2017)

- *Veins.* The signal coming from the veins is usually low frequency, so the time series and the power spectrum can sometimes be very similar to those from a signal component (***Figure 5.23***) (Griffanti et al., 2017).

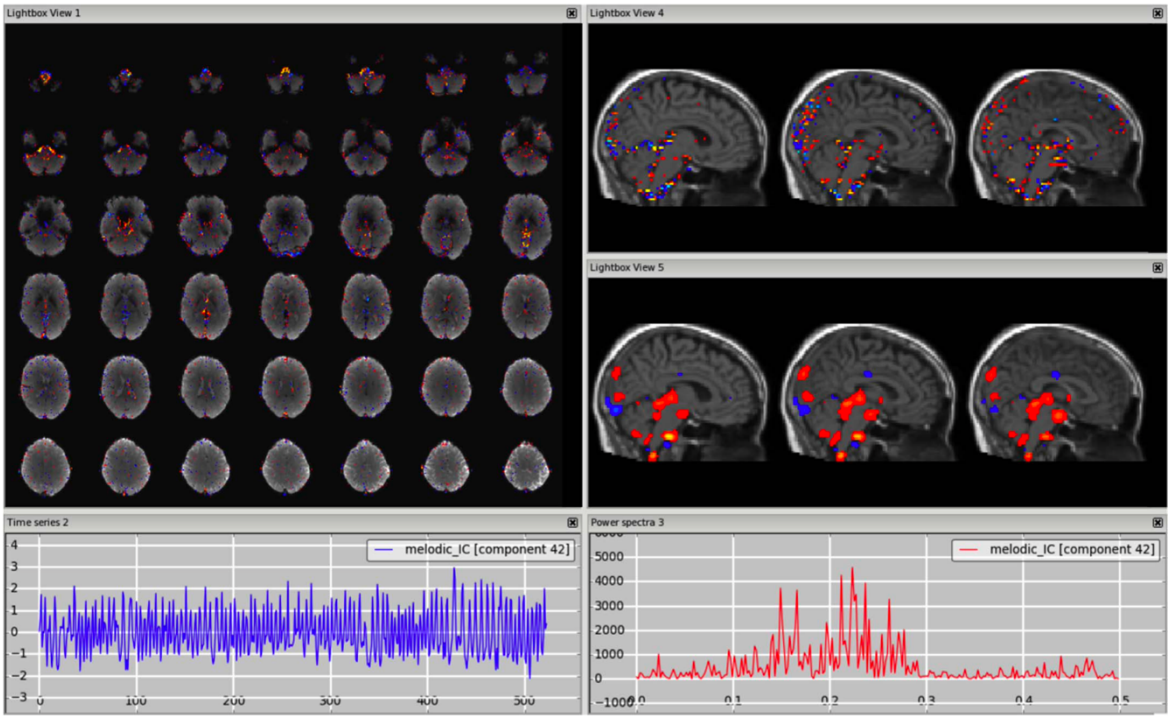

Figure 5.19 *Cerebrospinal fluid pulsation. The spatial pattern overlaps the third and fourth ventricle* (From Griffanti et al., 2017)

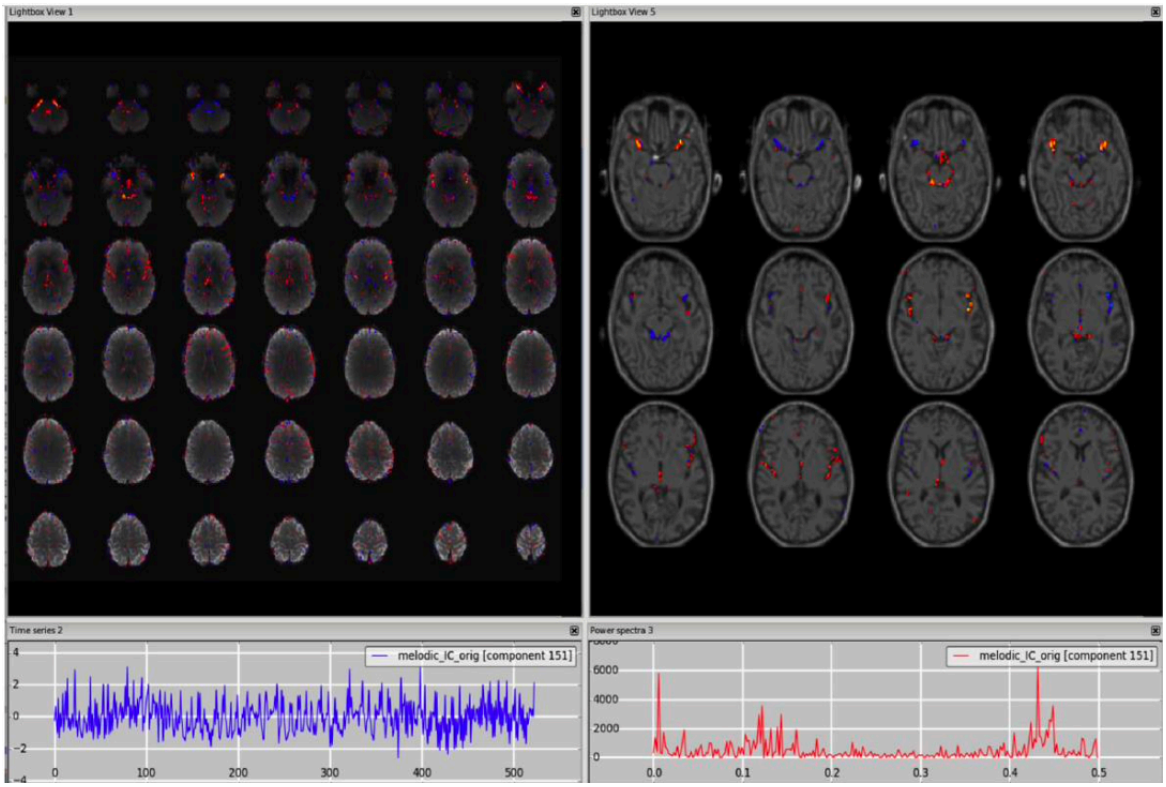

Figure 5.20 *Arteries. The time series shows a pattern with high oscillations (bottom-left panel) and the power spectra shows a high peak at high frequency, typical of the cardiac* signal (From Griffanti et al., 2017).

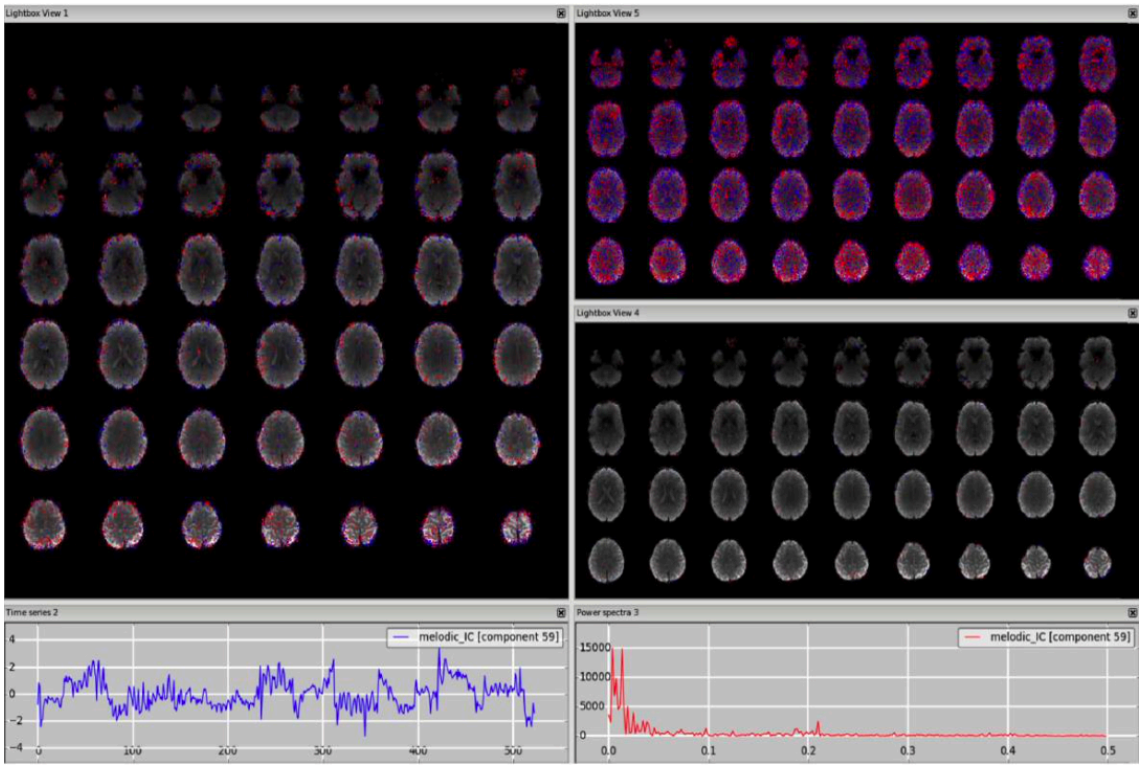

Figure 5.21 *Unclassified noise. The time series (bottom-left panel) show non-uniform pattern, with several temporal discontinuities and the power spectra has a low-frequency pattern* (From Griffanti et al., 2017).

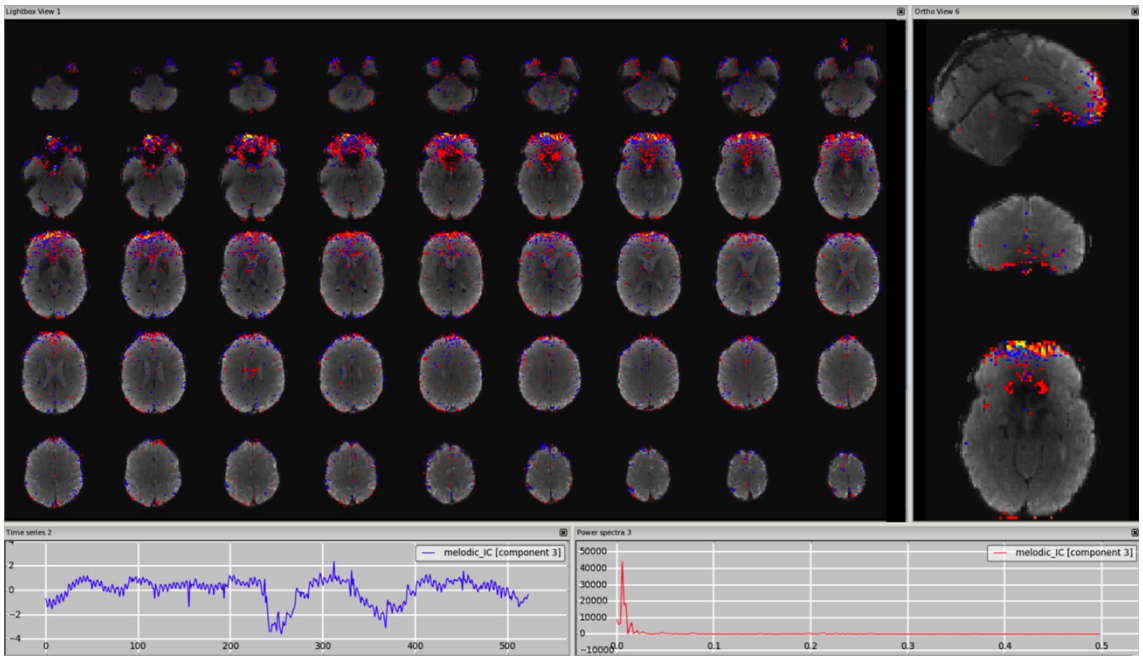

Figure 5.22 *Susceptibility artefacts. Localized on the EPI in areas of signal drop, due mainly to air-tissue interfaces.* (From Griffanti et al., 2017).

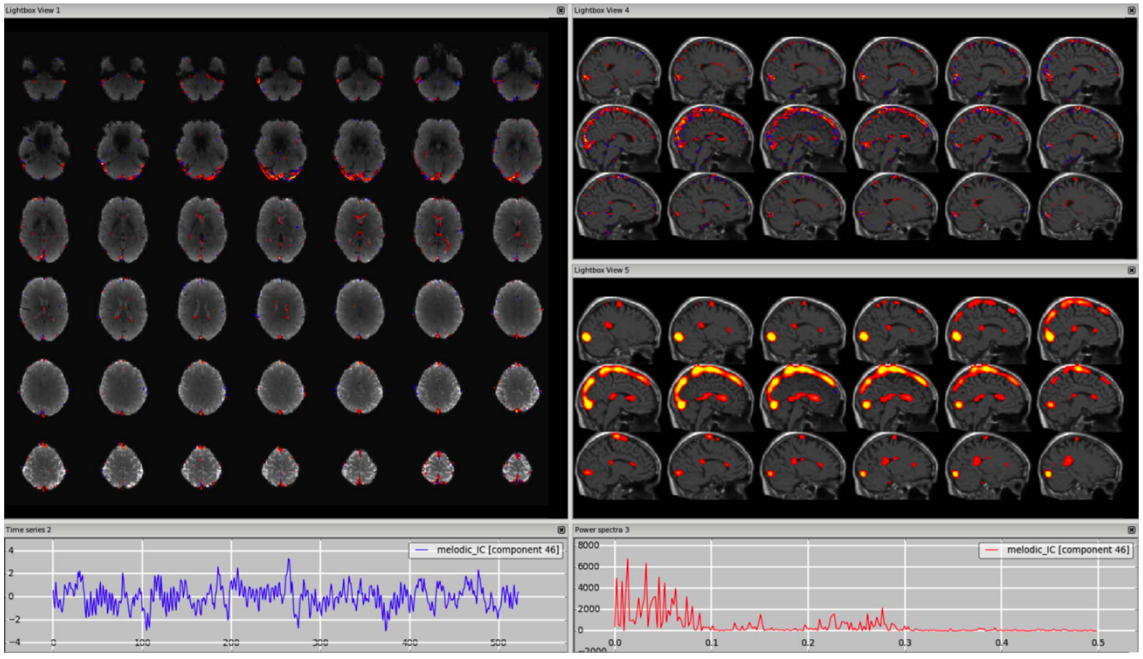

Figure 5.23 *Veins artifacts. The vessel is most visible in the sagittal plane, with a structural image as underlay (top-right panel)* (From Griffanti et al., 2017).

At the end of the signal and noise selection and recognition process, the signal images of the patients were compared with the signal images of the healthy subjects.

Chapter 6 "Results"

This chapter reports the results obtained from the analysis performed as described in Chapter 5. Firstly, motion compensation and registration are inspected and, if they meet the requirements, the IC inspection is performed. After recognition of the artifact, the RSNs was detected by comparison with RSNs identified by Smith and colleagues (Smith et al., 2009) and Beckmann and colleagues (Beckmann et al., 2005).

6.1 Pre-processing Results

As shown in ***Figure 6.1***, in patient P2 there is significant displacement around volume 230, principally around the x-axis and along the x- and y-axes, as obtained from the MCFLIRT within the FSL. The x-axis indicates the volumes while the y-axis the time expressed in seconds. For this reason, the patient P2 is excluded from the study.

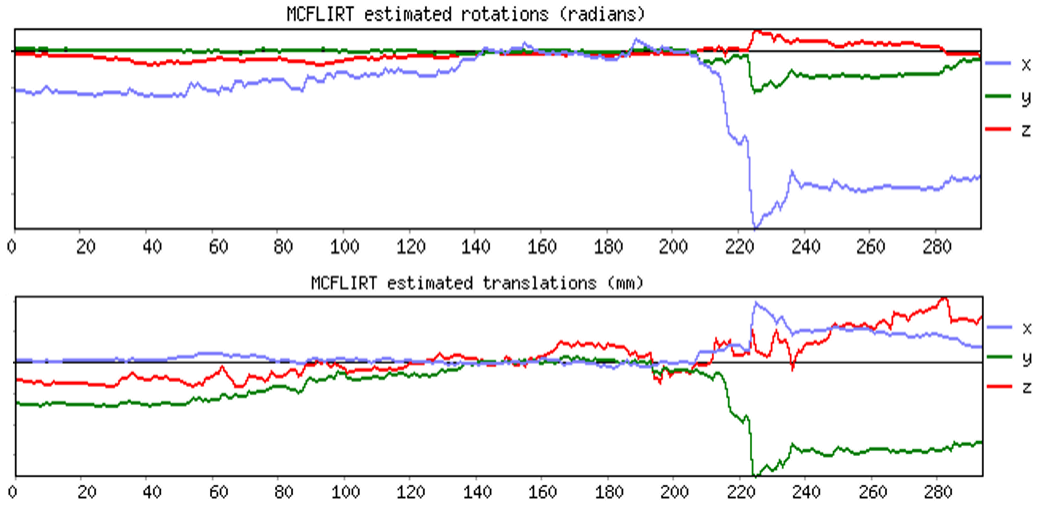

Figure 6.1 *Displacement detected in the subject P2. The upper panel indicates the rotation movement along the axes. The lower panel indicates the translation movement around the axes*

All the control healthy subjects (S1-S4) and the remaining four patients (P1, P3- P5) display an acceptable head movement, therefore their data are suitable to be analyzed.

In the ***Figure 6.2*** and ***Figure 6.3*** the displacements of the healthy subjects S1 and S2 are shown, respectively, evidencing an initial displacement that tends to zero.

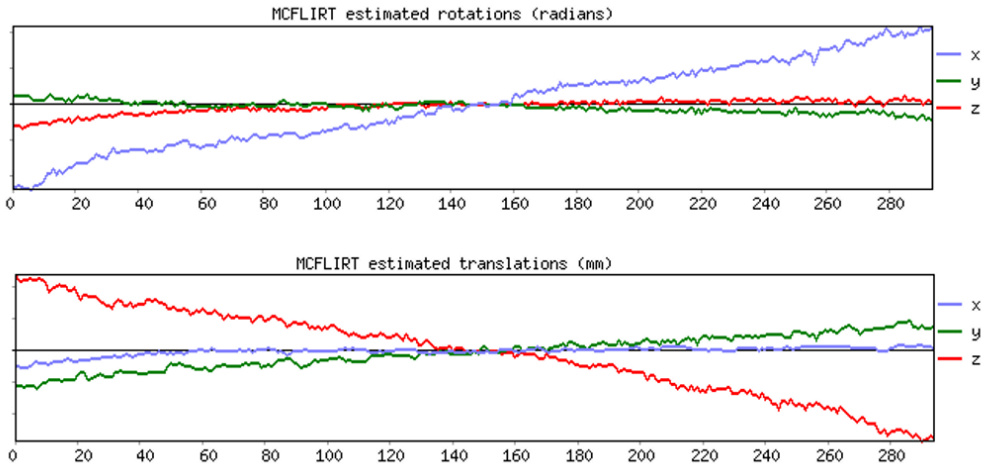

Figure 6.2 *Displacement detected in the subject S1. The upper panel indicates the rotation movement along the axes. The lower panel indicates the translation movement around the axes*

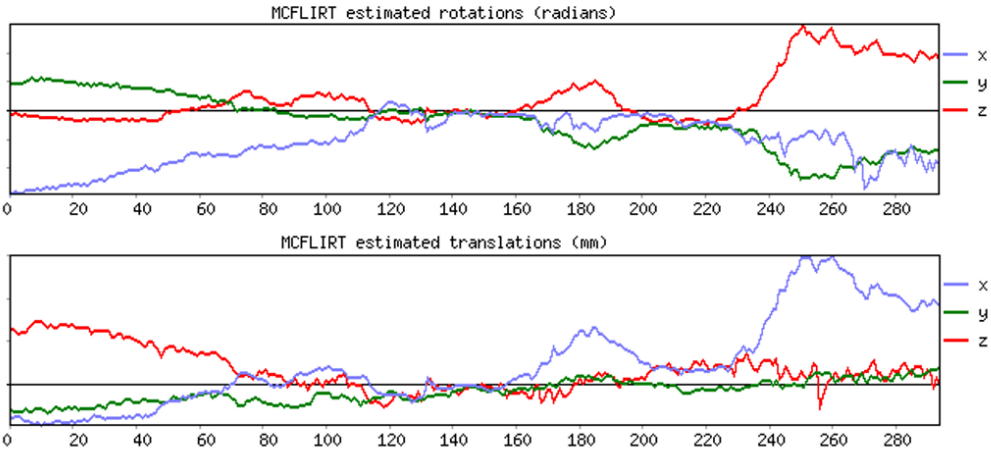

Figure 6.3 *Displacement detected in the subject S2. The upper panel indicates the rotation movement along the axes. The lower panel indicates the translation movement around the axes*

In the subjects S3 and S4 the displacement is low, in a range around zero, as shown in ***Figure 6.4*** and ***Figure 6.5***, respectively.

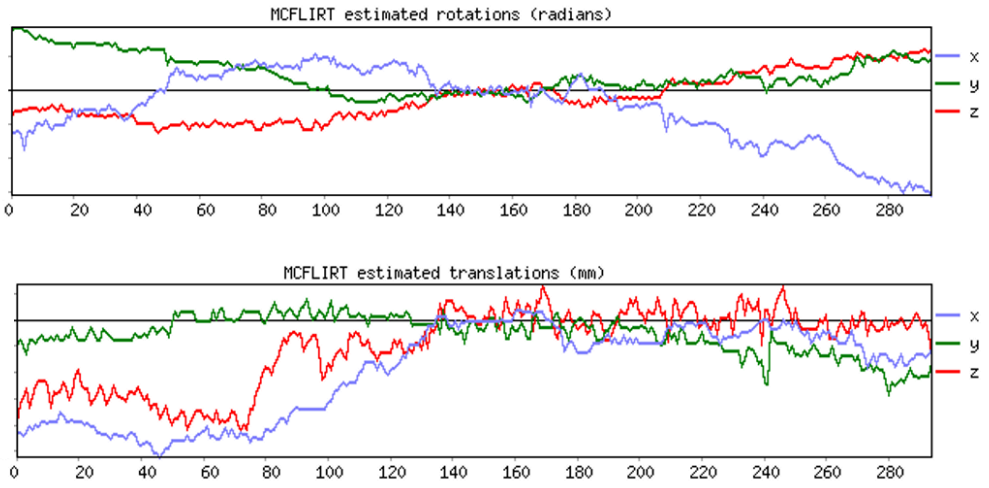

Figure 6.4 *Displacement detected in the subject S3. The upper panel indicates the rotation movement along the axes. The lower panel indicates the translation movement around the axes*

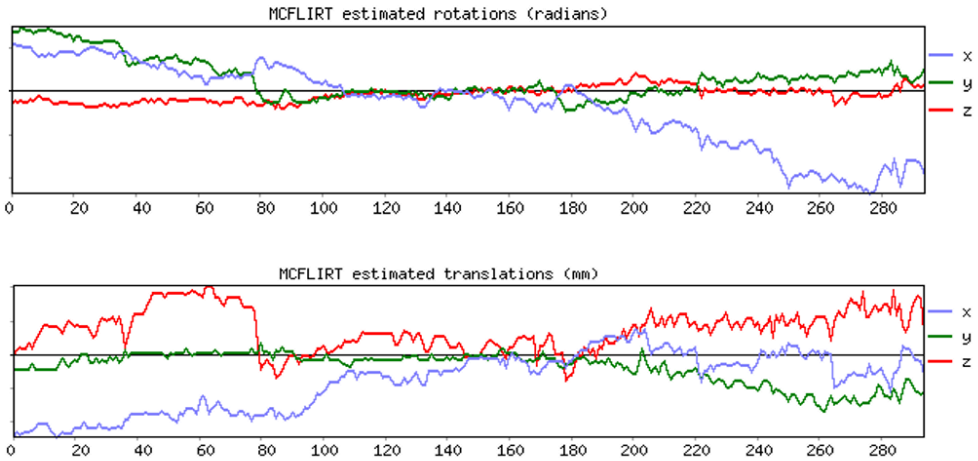

Figure 6.5 *Displacement detected in the subject S4. The upper panel indicates the rotation movement along the axes. The lower panel indicates the translation movement around the axes*

In *Figure 6.6* is shown the displacement of patient P1, that is low in a range of zero as for patient P4 (*Figure 6.8*).

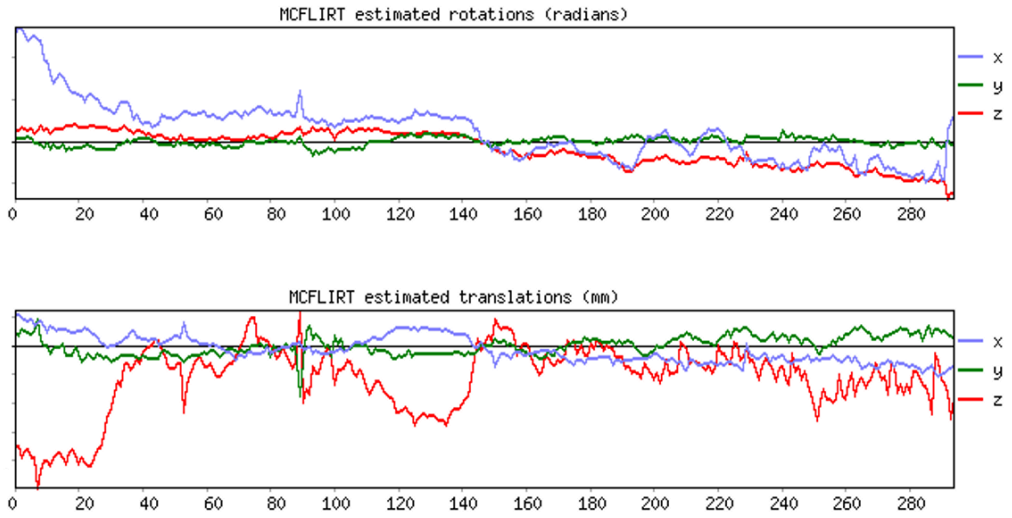

Figure 6.6 *Displacement detected in the subject P1. The upper panel indicates the rotation movement along the axes. The lower panel indicates the translation movement around the axes.*

Figure 6.7 shows the displacement of patient P3: around the volume 290 there is a peak of movement, and is possible to notice, also, an initial displacement in rotation around x and y axes; but the entity of this movement can be considered an acceptable. All the peak results in the IC as motion artefact.

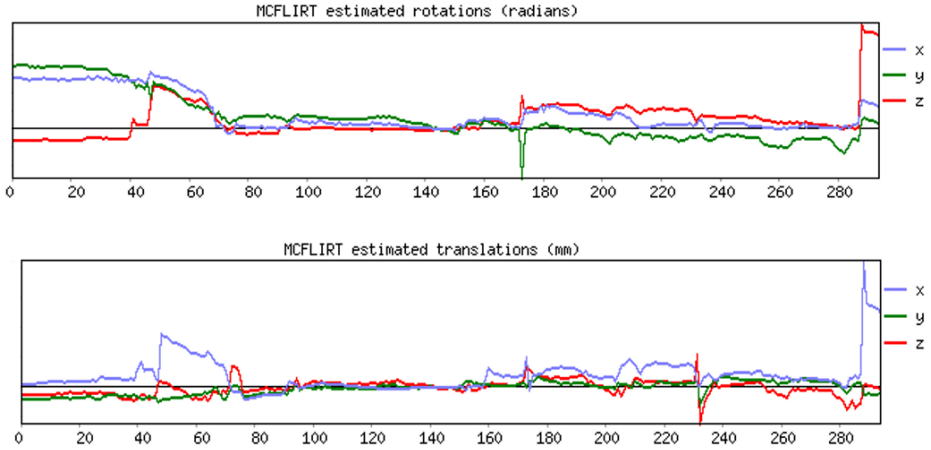

Figure 6.7 *Displacement detected in the subject P3. The upper panel indicates the rotation movement along the axes. The lower panel indicates the translation movement around the axes.*

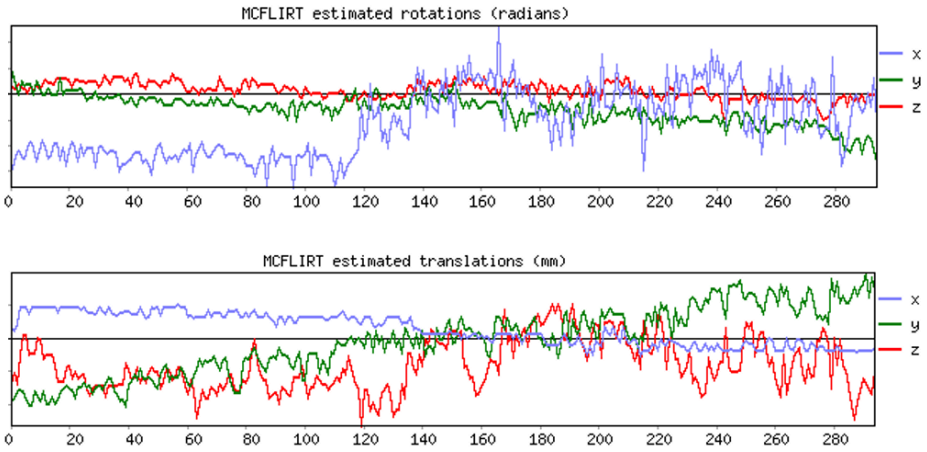

Figure 6.8 *Displacement detected in the subject P4. The upper panel indicates the rotation movement along the axes. The lower panel indicates the translation movement around the axes.*

Figure 6.9 represents the movement of patient P5, showing an initial displacement that tends to zero.

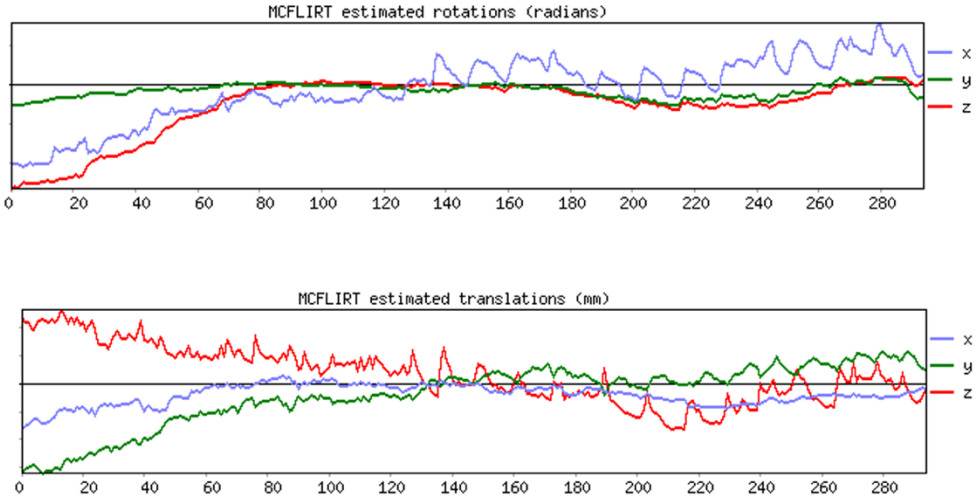

Figure 6.9 *Displacement detected in the subject P5. The upper panel indicates the rotation movement along the axes. The lower panel indicates the translation movement around the axes*

After the registration step, that was successful for all the subjects analyzed, an example of the results obtained from the co-registration of the patient P1, within FSL is shown in ***Figure 6.10***

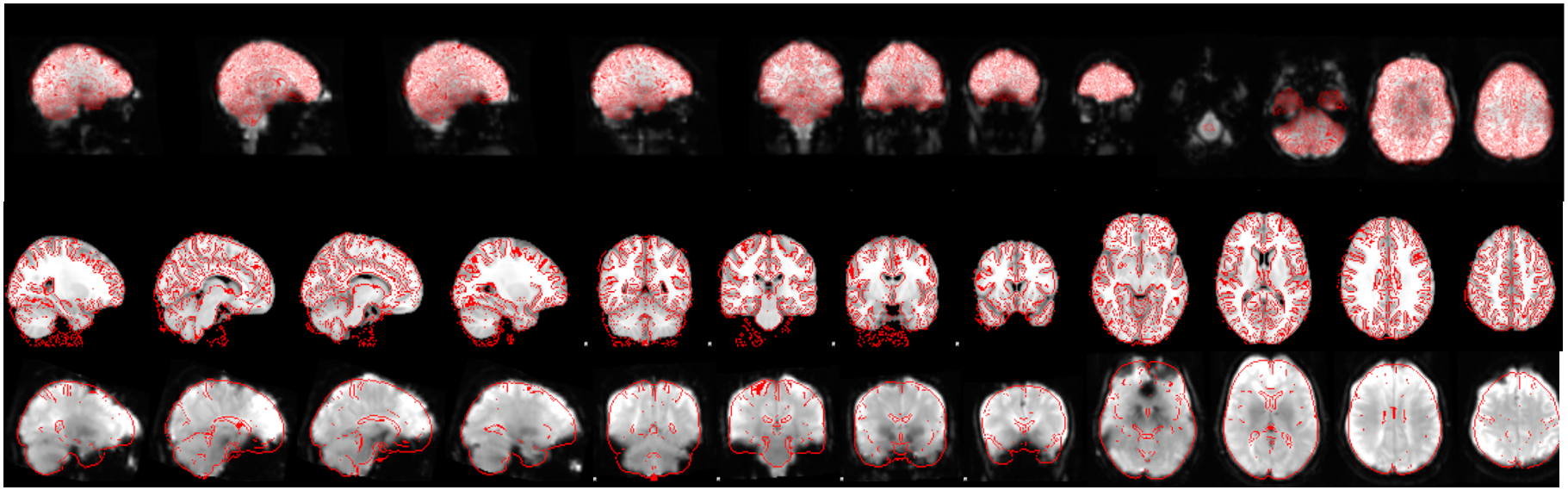

Figure 6.10 In the top panel is represented the co-registration of functional image (in grey) with structural BET image (red line). The middle panel shows the alignment of the MNI152 template (in grey) and the structural BET image (red line). The bottom panel represents the normalization of functional image (in grey) with the MNI152 template (red line).

6.2 Independent Component Analysis Results

The number of estimated ICs using FSL software differ for each subject: specifically, 69 ICs were obtained from the analysis on patient P1, 70 ICs from P3, 41 ICs were obtained from patient P4 and 94 ICs from patient P5. In the healthy subjects, 53 ICs were obtained from ICA on subject S1, 65 ICs estimated on subject S2, 52 ICs from subject S3 and 57 for S4. A total of 501 components were identified: 372 (74%) were labelled noise IC (N-IC) (160 ICs were unclassified noise, 135 motion artifacts and 77 cardiac), 129 (27%) were labelled signal-ICs (S-IC) (79 ICs were signal of interest (15%), 50 unknown (10%)).

Comparison between the resting state networks and components was performed manually for all the subjects. In ***Figure 6.11***, in yellow/red are reported the networks obtained from the subject S1 superimposed on the Smith's standard ones, shown in cyan/blue.

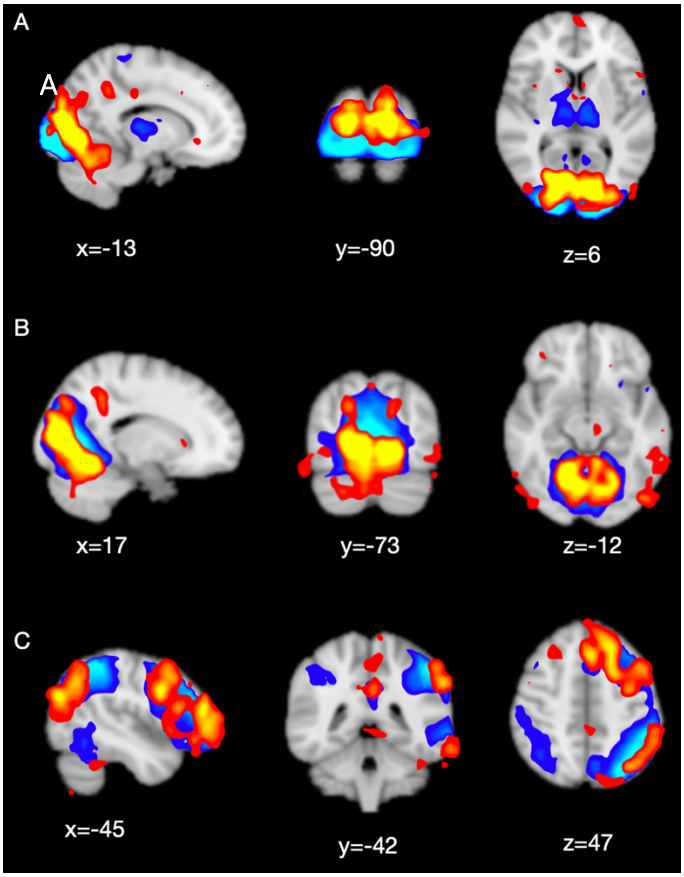

Figure 6.11 *Example of comparison between S1 activations (yellow/red) and Smith (cyan/blue) RSN10. Panel A and B represent the occipital and medial visual areas. Panel C shows the frontoparietal (left) area that correspond to cognition/language paradigms*

The classification of component in *Signal, Cardiac Artifacts, Movements, Unclassified Noise,* and *Unknown* is performed by examining slice, time courses and frequency spectra, and applying the labelling rules states by Griffanti and co-workers (Griffanti et al., 2017). An example of signal component is shown in ***Figure 6.12***, examples of noise component are shown in ***Figure 6.13*** *and* ***6.14***, and examples of motion artifacts component are shown in ***Figure 6.15*** and ***6.16***.

All the figures show the Time series (bottom-left panel), the Power spectra (bottom-right panel), and the axial slices in top-left panel (can be moved to coronal and sagittal plane). The red/yellow activation are overlayed onto the high-resolution image obtained from the ICA.

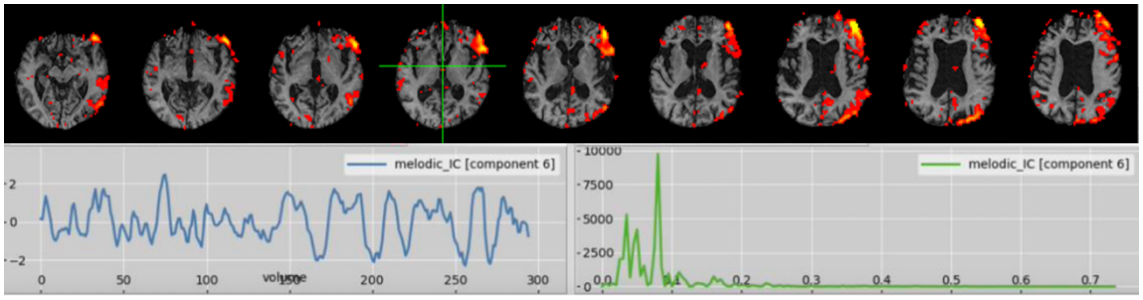

Figure 6.12 *Example of patient P1 of signal component analyzed using FSLeyes. The signal component is characterized by a regular oscillatory time and a frequency low than 0.1 Hz. The spatial maps show activated area across the slices and on the grey matter*

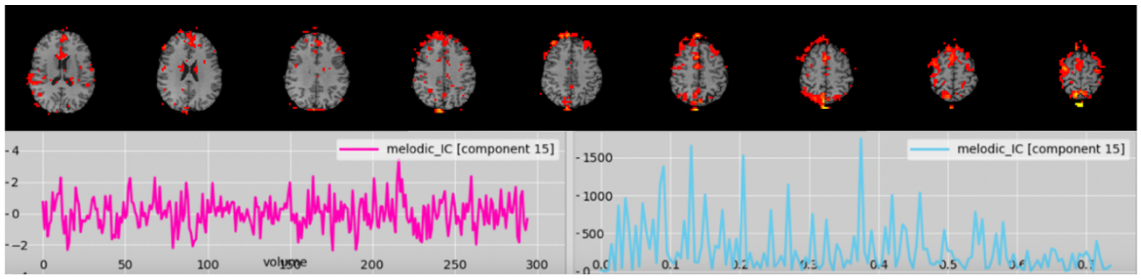

Figure 6.13 *Example of patient P1 of cardiac noise (arteries and veins) component analyzed using FSLeyes. The cardiac component is characterized by a high frequencies power spectra and a time series with fast oscillations*

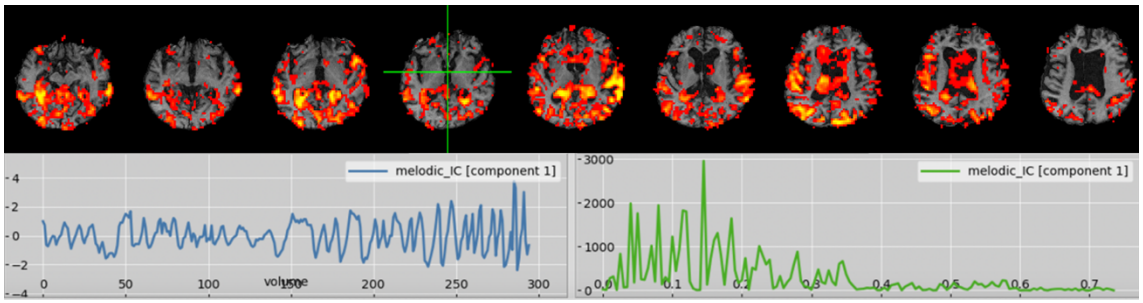

Figure 6.14 *Example of patient P1 of unclassified noise analyzed by using FSLeyes. The frequency is higher than 0.1 Hz and the activated area are localized mostly around the brain. The time series is not very smooth with a few temporal jumps/discontinuities*

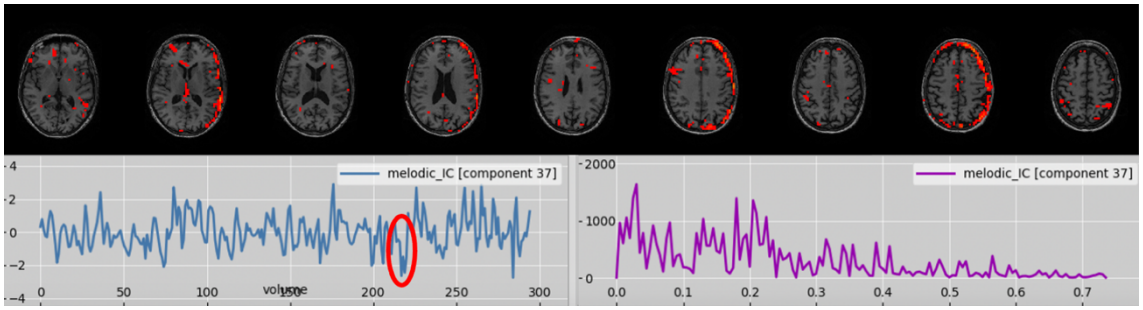

Figure 6.15 *Example of motion artifacts: The spatial map has the typical ring at the edge of the brain and the time series presents a sudden jump in correspondence to sudden head movement (red circle)*

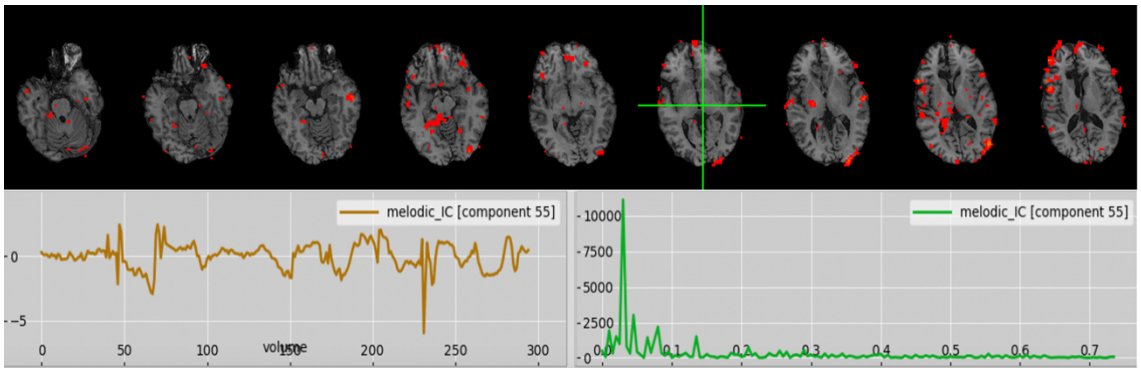

Figure 6.16 *Example of susceptibility motion artifacts: the time series presents big jumps in correspondence of the head motion, and the power spectra has low frequencies range but in the spatial map is possible to see small points in the upper and lateral part of the brain*

The different identified signals were classified in the different activation areas of the brain following the Smith and co-workers' indications (Smith et al., 2009).

In *Figure 6.17* are reported the 10 resting state networks identified in healthy subjects, following the Beckmann's coordinates (Beckmann et al., 2005).

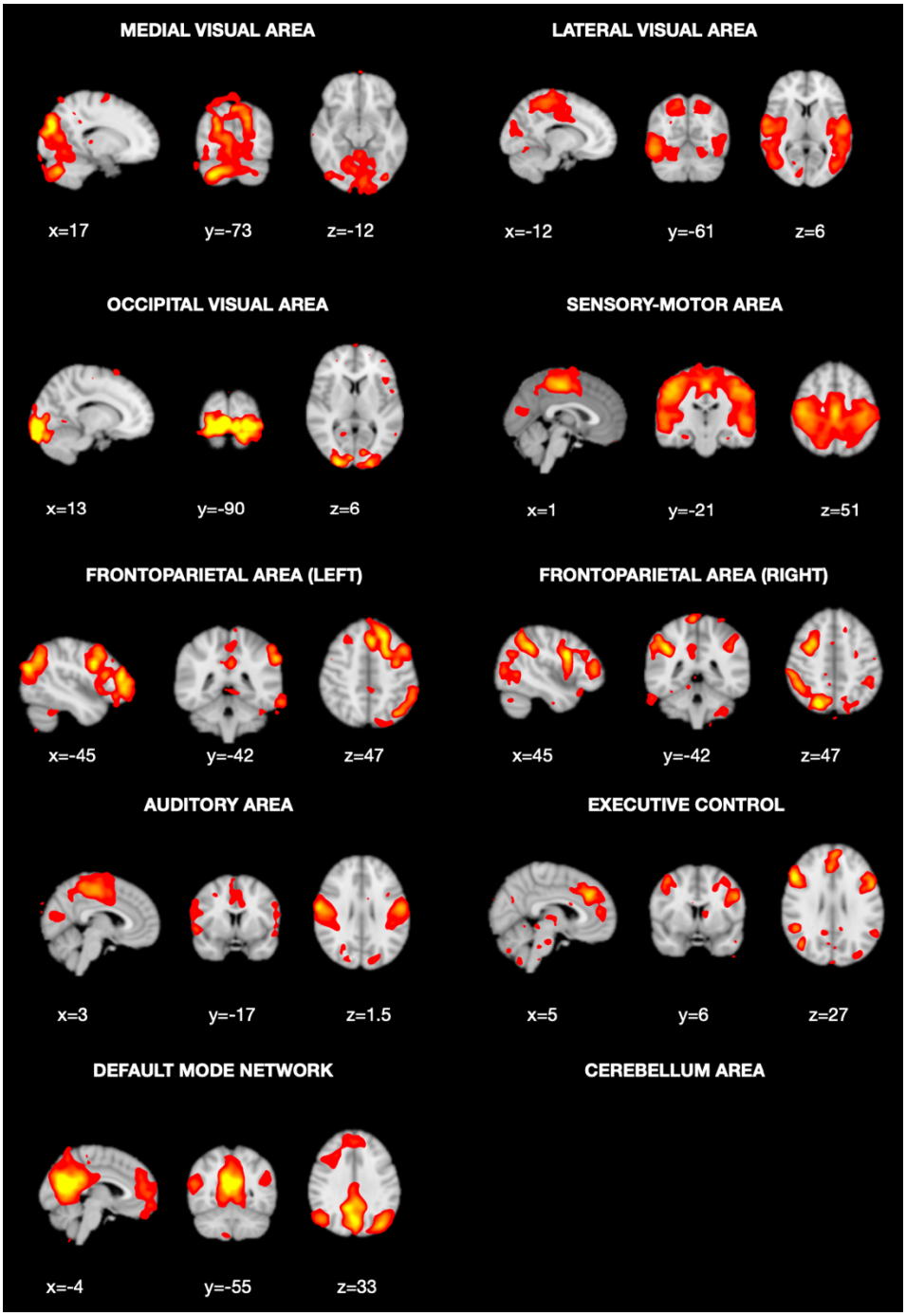

Figure 6.17 *In the figure are shown the identified networks in healthy subjects using FSLeyes-BrainMaps representation. In particular, the medial and lateral visual areas, the default mode network, the auditory area, and executive control network are identified in all subjects; the occipital visual area and the frontoparietal area (left) in subjects S1-S3; the sensory motor areas in subjects S3 and S4; the frontoparietal area (right) in subject S1; none of the subjects had activation of the cerebellum*

The ***Figure 6.18*** shows the activations obtained from the patient P2, and it is possible to see that they are affected by motion artifacts and noise, due to the high rotation and translation of the head during the acquisition with the MR.

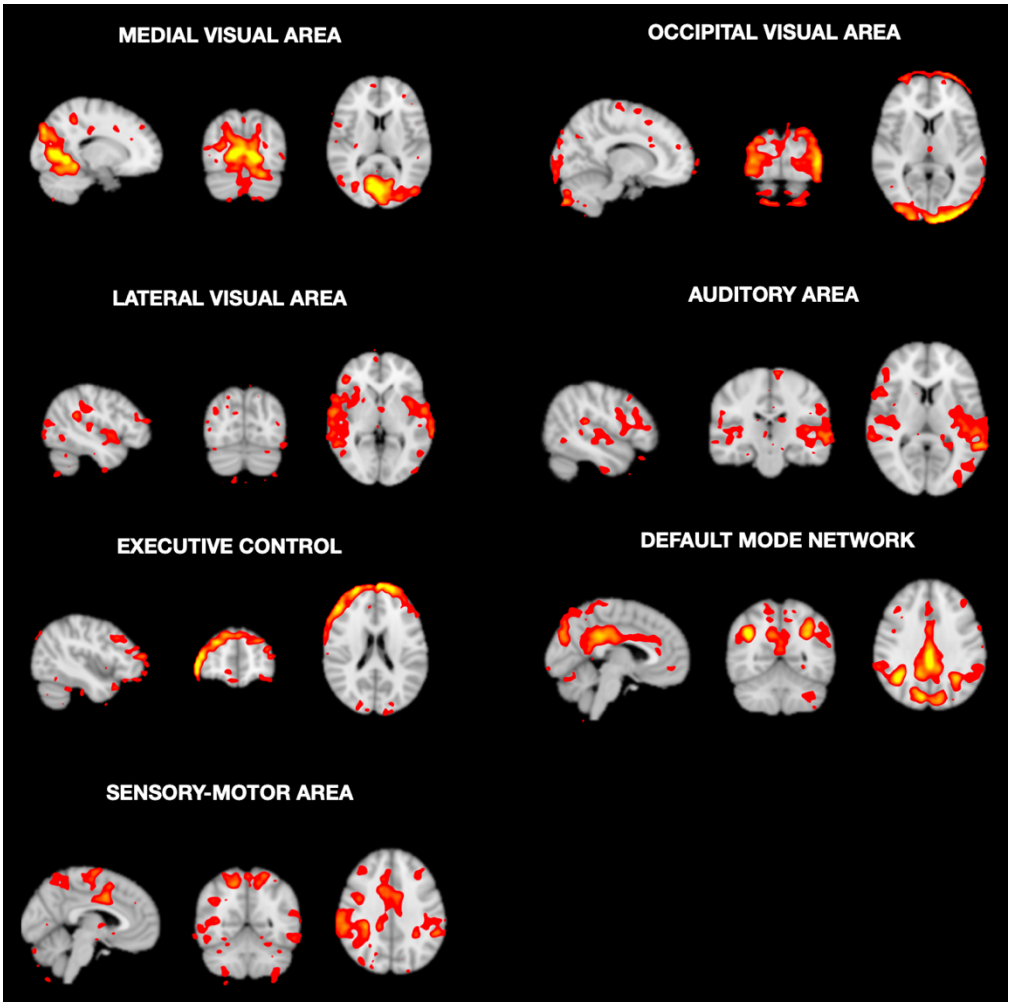

Figure 6.18 *The MNI coordinates are: Medial Visual Area (left) (17, -73, 10), Occipital Pole Visual Area (right) (-17, -88, 0), Lateral Visual Area (left) (39, -71, -12), Auditory (right) (50, -22, 8), Executive control (left) (-43, 50, 20), Default mode network (right) (-4, -55, 33), identified in the patients using FSLeyes-BrainMaps representation. The annulus at the top represents motion artifact, while the different dots scattered across the brain represent noise*

The ***Figure 6.19 - 6.23*** show the areas activates in some networks in patients, following the Smith's coordinates (Smith et al., 2009).

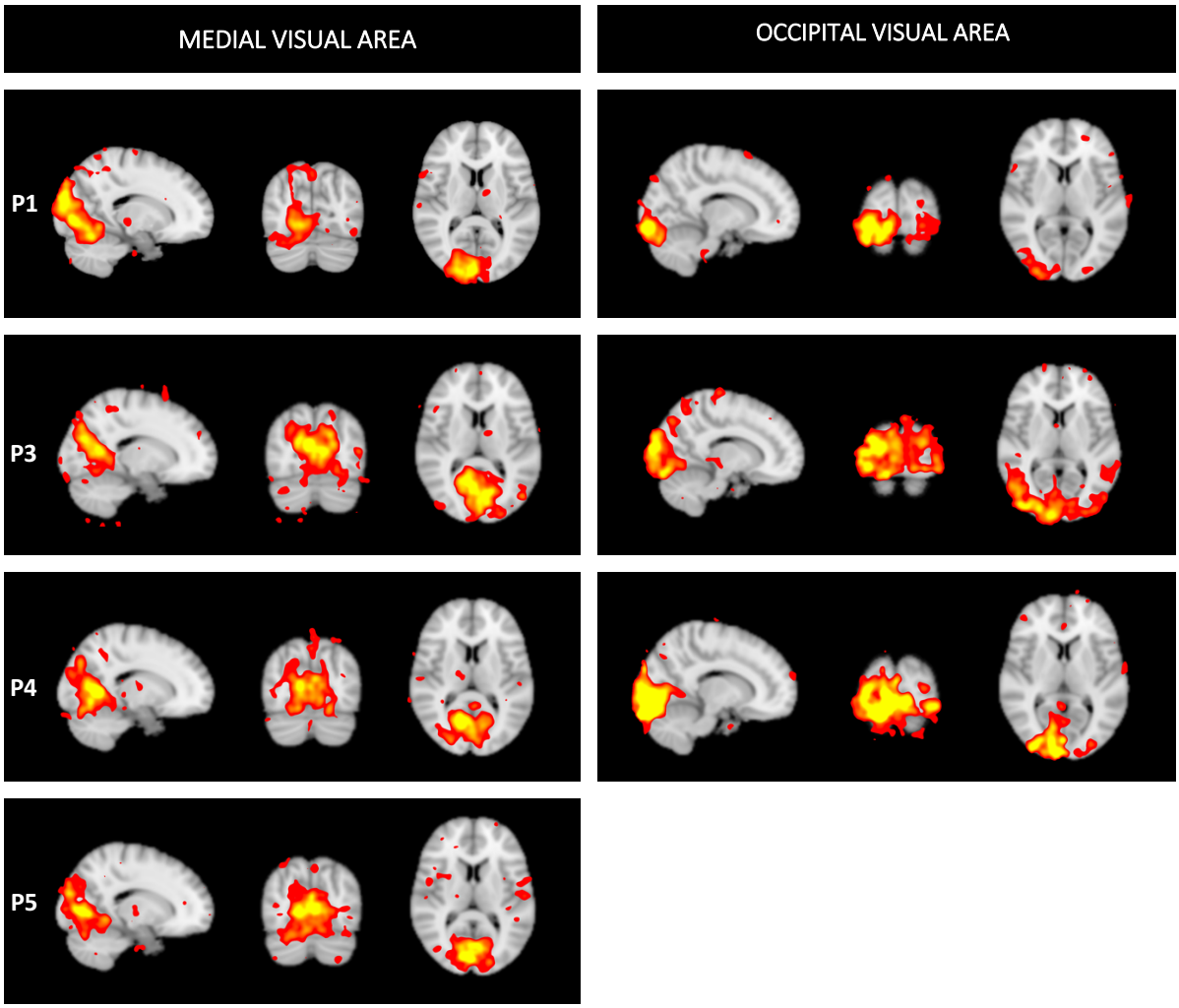

Figure 6.19 *The MNI coordinates are: Medial Visual Area (left) (17, -73, 10), Occipital Pole Visual Area (right) (-17, -88, 0), identified in the patients using FSLeyes-BrainMaps representation*

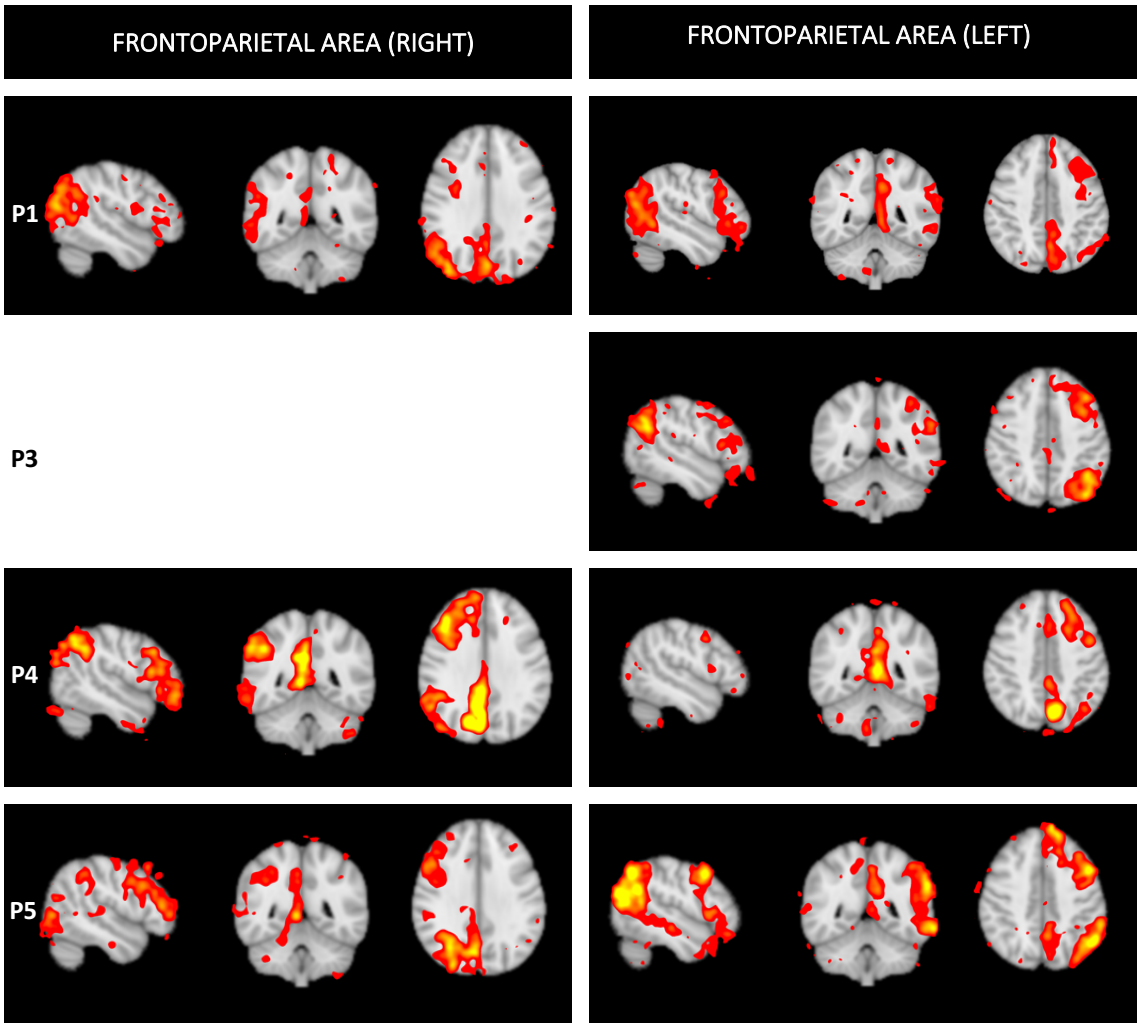

Figure 6.20 *The MNI coordinates are: Frontoparietal right (left) (49, -48, 32), Frontoparietal left (right) (-43, -48, 42), identified in the patients using FSLeyes-BrainMaps representation*

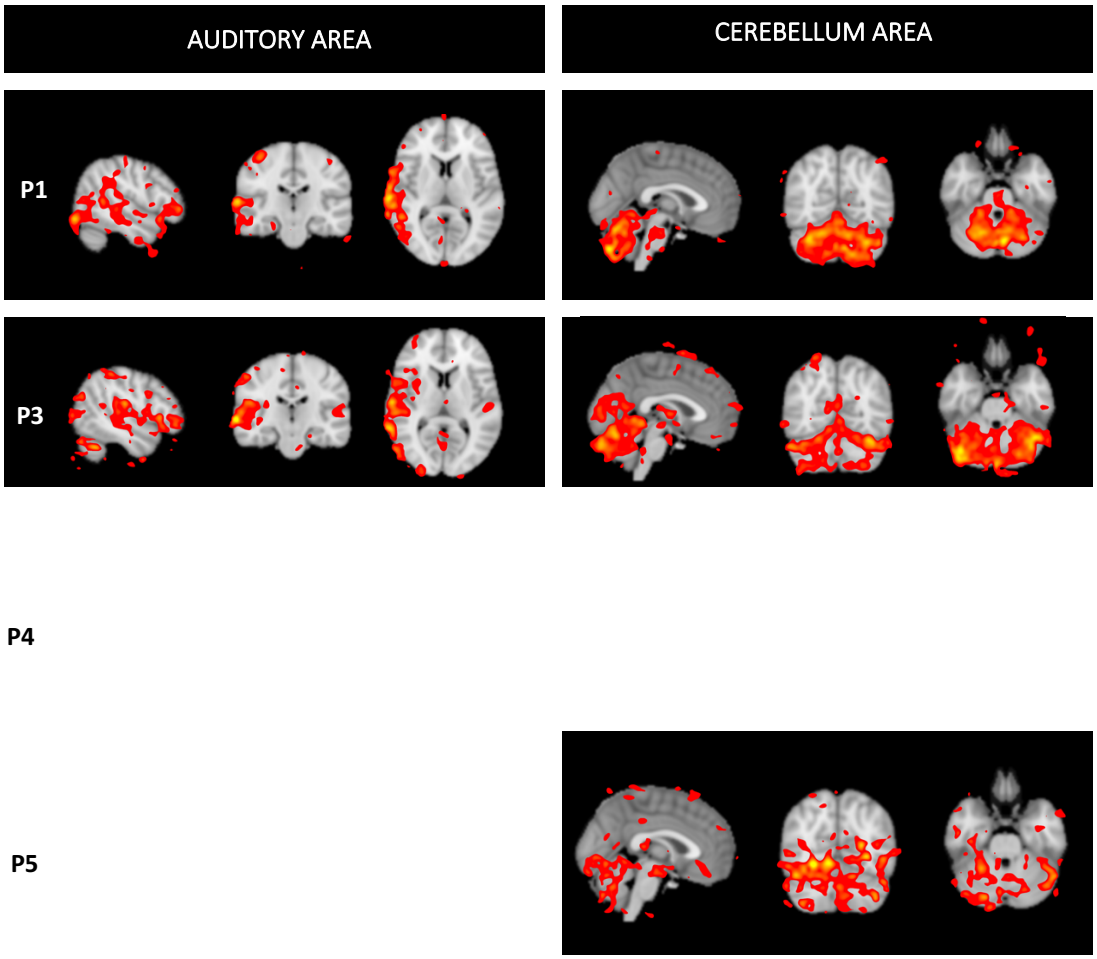

Figure 6.21 *The MNI coordinates are: Auditory (left) (50, -22, 8), Cerebellum area (right) (0, -62, -28), identified in the patients using FSLeyes-BrainMaps representation*

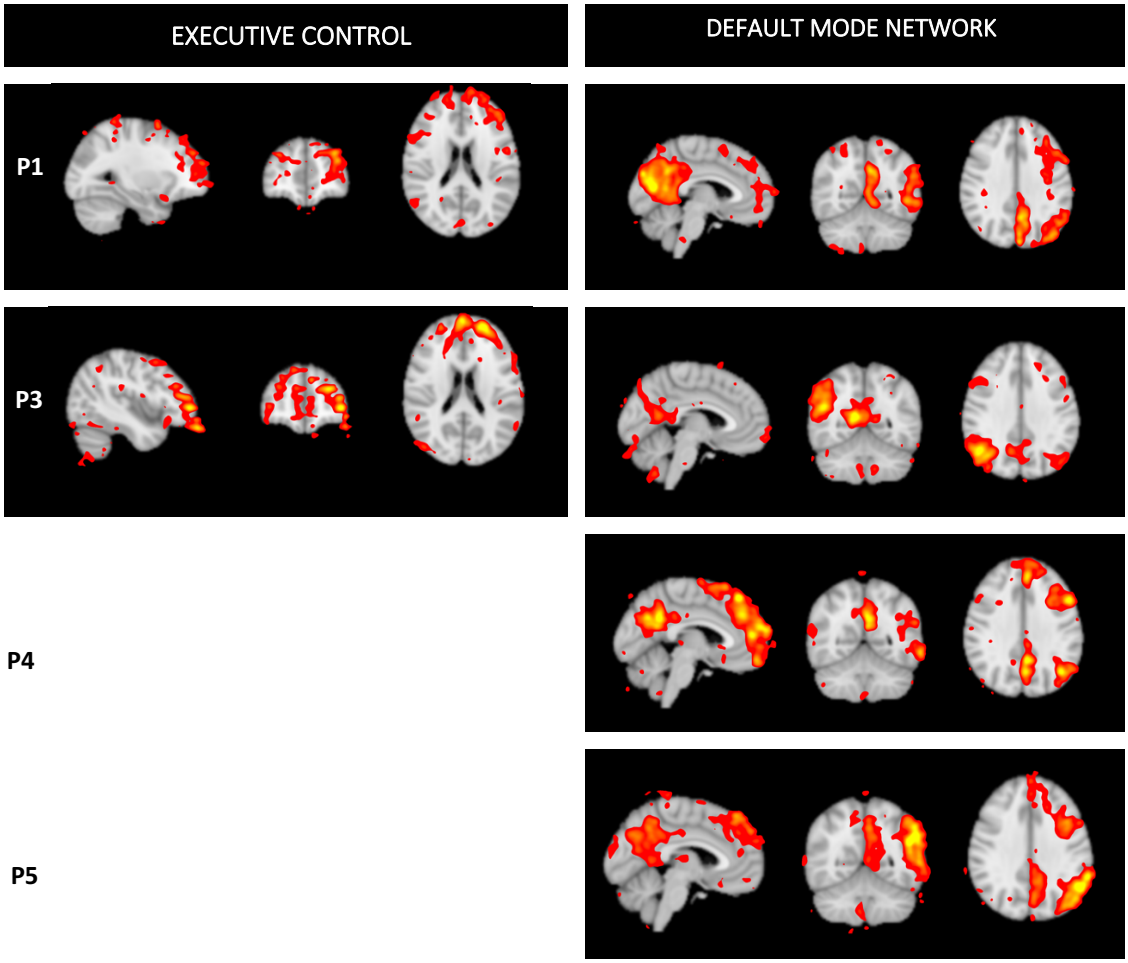

Figure 6.22 *The MNI coordinates are: Executive control (left) (-43, 50, 20), Default mode network (right) (-4, -55, 33), identified in the patients using FSLeyes-BrainMaps representation*

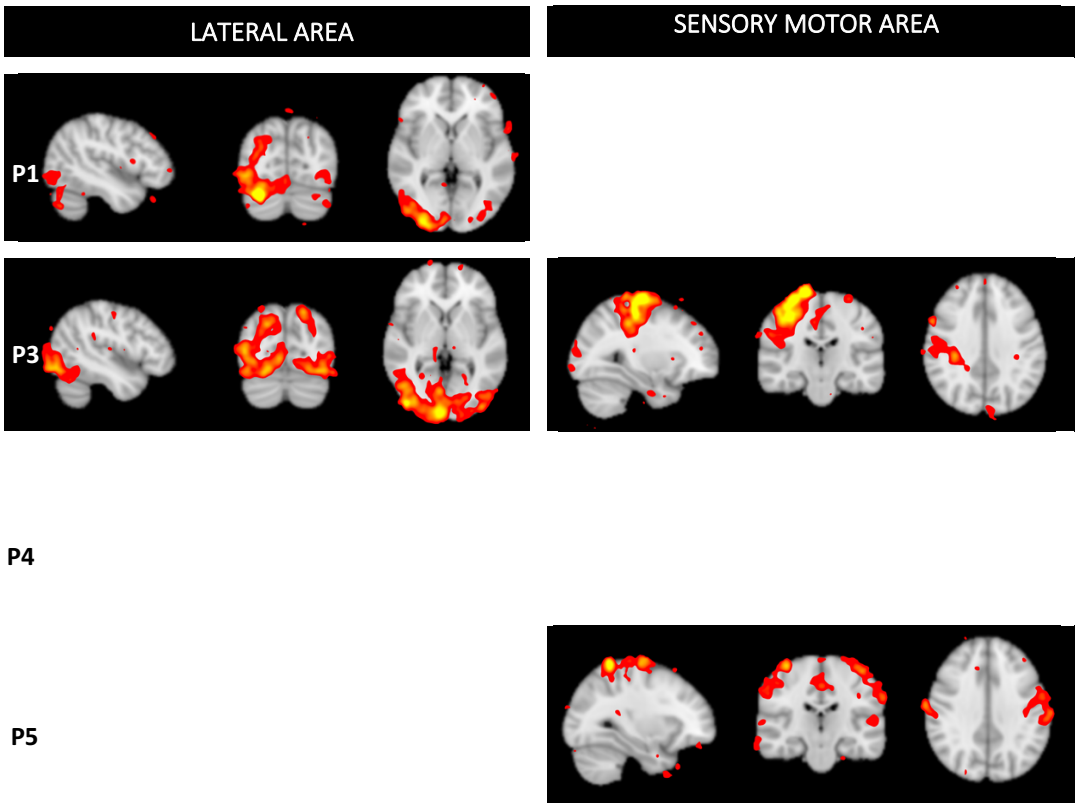

Figure 6.23 *The MNI coordinates are: Lateral visual area (left) (-45, -75, 1), Sensory motor area (right) (30, -22, 34; for patient P5 -30, -22, 34), identified in the patients using FSLeyes-BrainMaps representation*

Table 4 summarizes the RSNs identified among all the S-ICs of each subject, distinguishing between activations with some degree of bilaterality and activations that occur in patients with callosotomy with unilaterality.

Table 4 *RSNs identified in all subjects by using FSL analysis: blue symbol identified the presence of the activation while the green one represents some degree of bilaterality in the activations of the RSNs*

	P1	P3	P4	P5
MEDIAL VISUAL AREA	✓	✓	✓	✓
OCCIPITAL VISUAL AREA	✓	✓	✓	
LATERAL VISUAL AREA	✓	✓		
DEFAULT MODE NETWORK	✓	✓	✓	✓
SENSORYMOTOR SYSTEM		✓		✓
AUDITORY SYSTEM	✓	✓		
EXECUTIVE CONTROL	✓	✓		
FRONTOPARIETAL RIGHT	✓	✓	✓	✓
FRONTOPARIETAL LEFT	✓	✓	✓	✓
CEREBELLUM AREA	✓	✓		✓

Multisubject analysis highlights two activation patterns common to the 4 healthy subjects analyzed in the study: visual medial area and default mode network.

Figure 6.23 shows a comparison between the activation of the medial visual area, obtained from the multi-subject's analysis, and the same activation obtained from the split-brain patients' analysis. ***Figure 6.24*** represents the default mode network obtained from the multi-subject's analysis, and the same activation obtained from the split-brain patients' analysis. ***Figure 6.25*** represents the sensory motor area obtained from the multi-subject's analysis, and the same activation obtained from the split-brain patients' analysis.

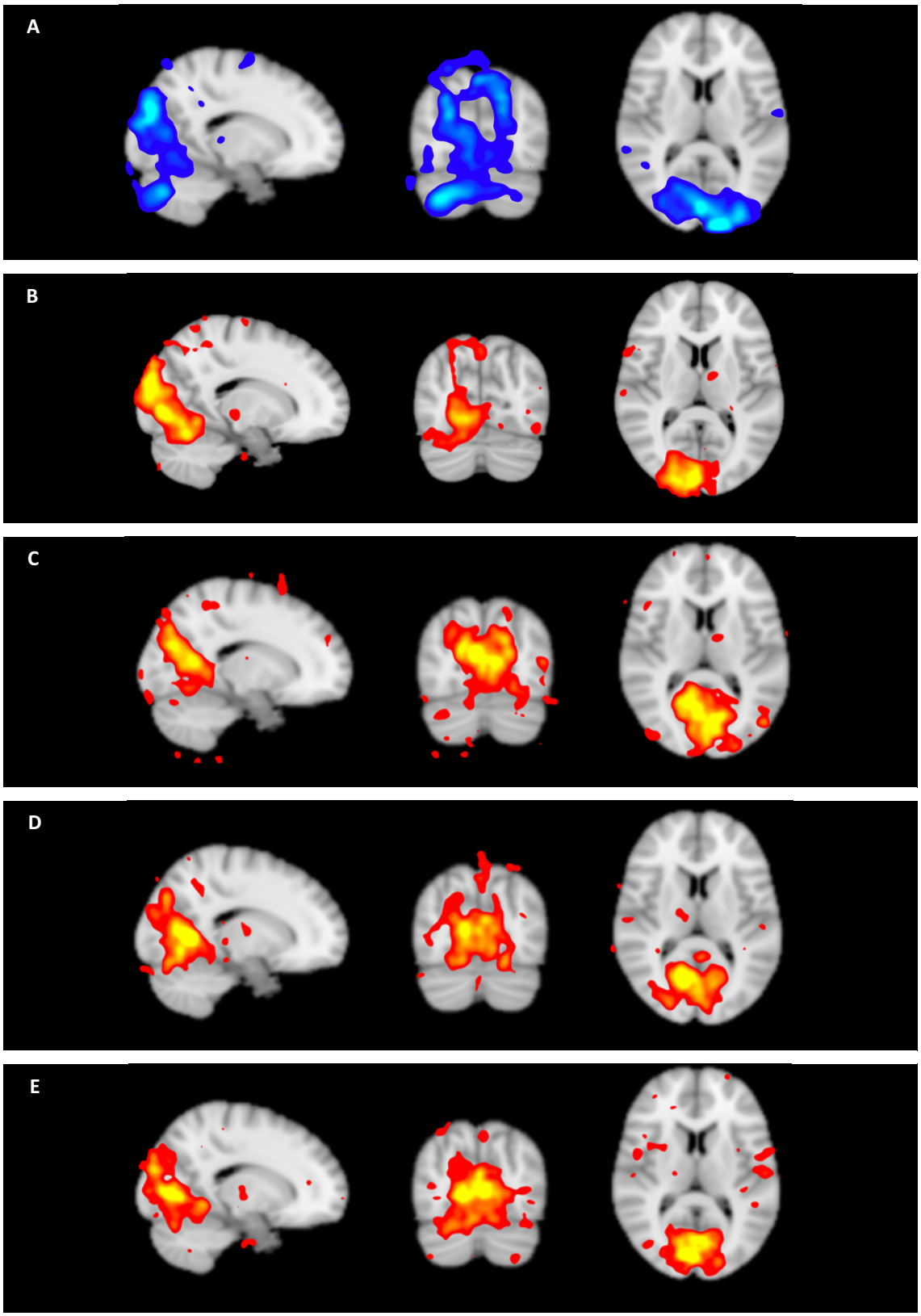

Figure 6.23 *Panel A identifies the medial visual area for the healthy template obtained from an average of 4 healthy subjects, while Panel B, C, D and E show the medial visual area of the patients P1, P3, P4 and P5 respectively, with a degree of bilaterality in all the patients*

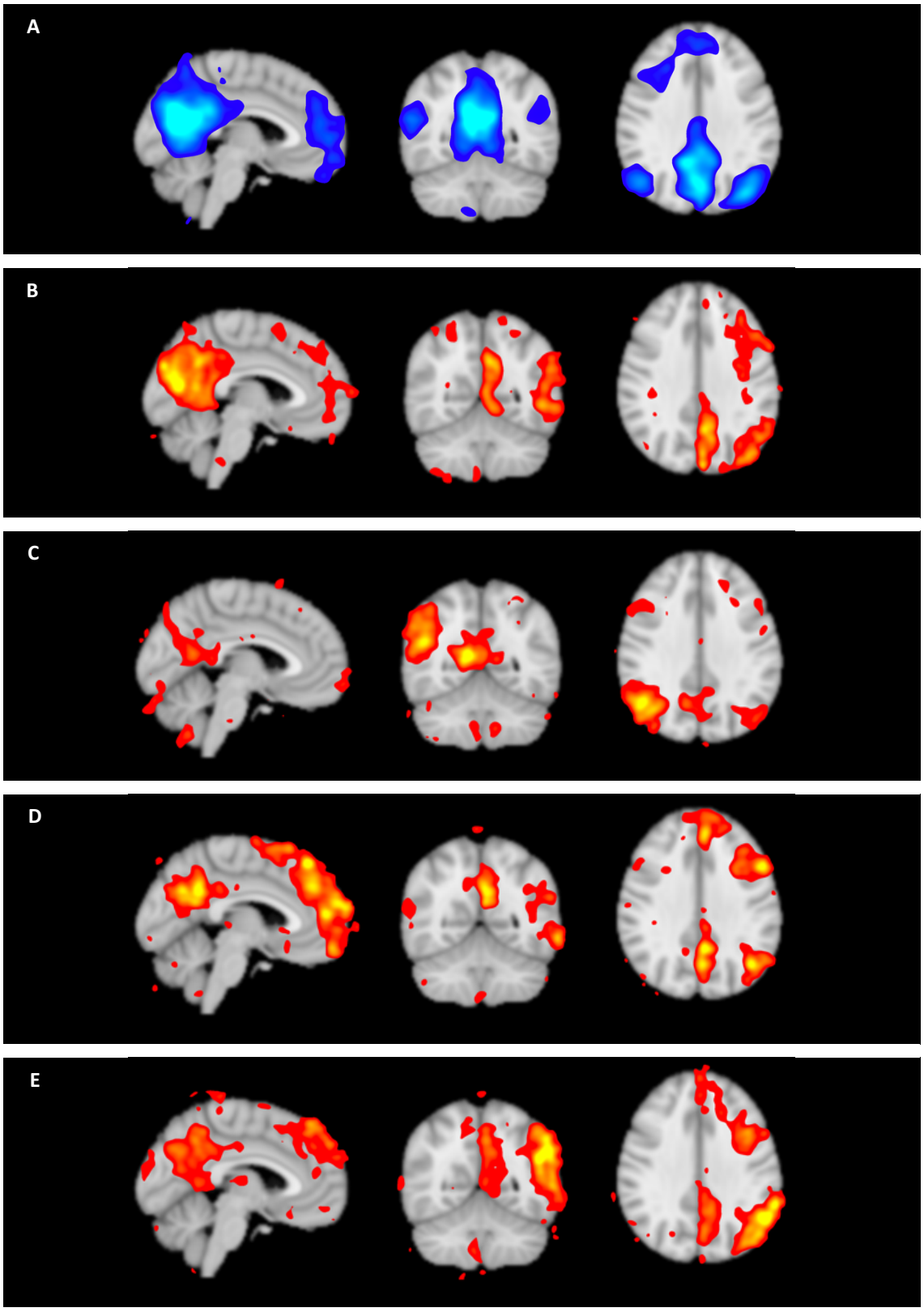

Figure 6.24 *Panel A identifies the default mode network for the healthy template obtained from an average of 4 healthy subjects, while Panel B, C, D and E show the default mode networks of the patients P1, P3, P4 and P5 respectively, with some degree of lateralization in the patients except for the patient P4*

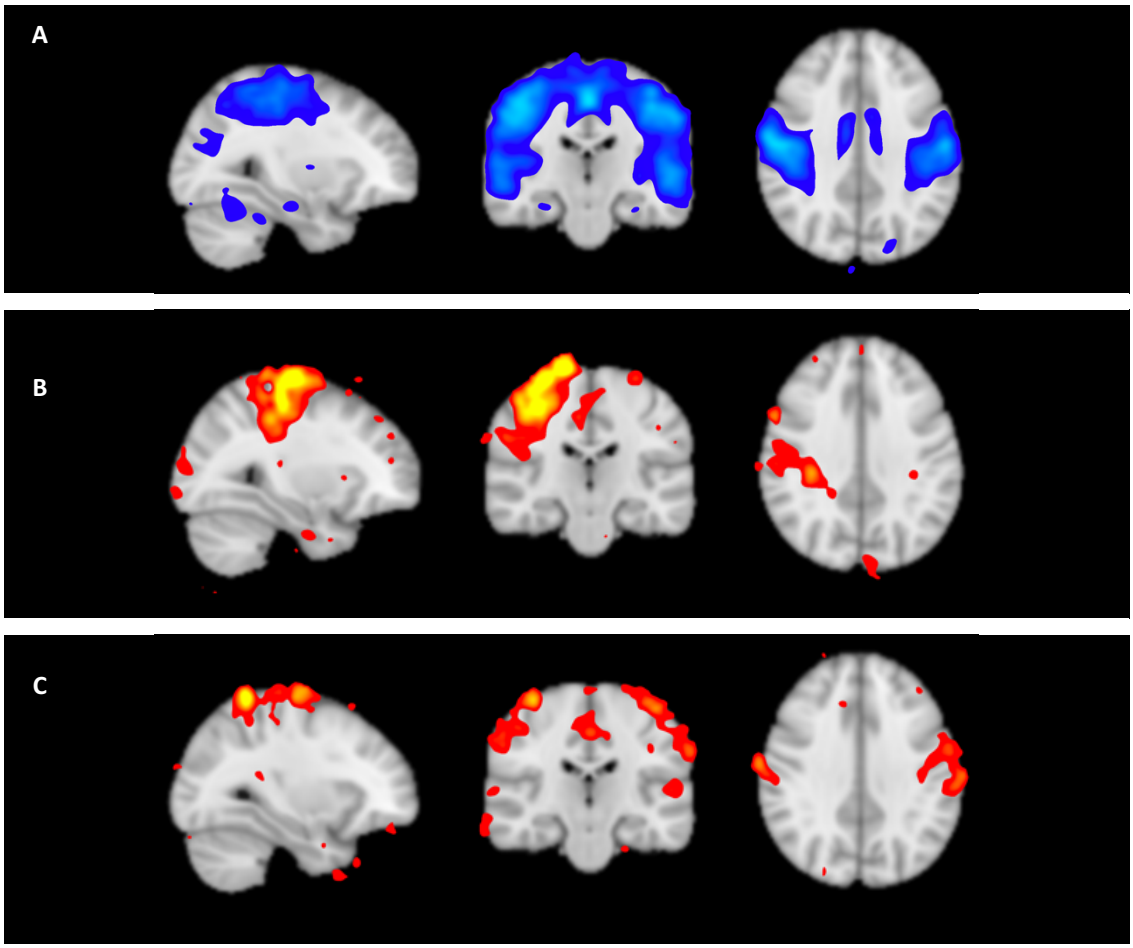

Figure 6.25 *Panel A identifies the sensory motor area for the healthy template obtained from an average of 4 healthy subjects, while Panel B and C show the sensory motor area of the patients P3 and P5 respectively, demonstrating a low degree of bilaterality in patient P5*

Chapter 7 "Discussion & Conclusions"

The aim of this thesis was to investigate the functional connectivity and the bilaterality activations in the brain in patients undergone callosal surgical resection. The results are based on the analysis of resting-state fMRI data using the ICA method, a tool made available by FSL; a library developed by members of the Analysis Group of the Oxford Center for Functional MRI of the Brain (FMRIB) for the purpose to analyze fMRI images.

Patients undergoing split-brain surgery to alleviate severe intractable epilepsy offer a unique opportunity for neuroscientists to examine the mechanisms of interhemispheric interactions, neuroplasticity, and compensatory reorganization (Uddin et al., 2008).

The analysis was performed on 4 healthy subjects and 5 epileptic patients, 4 of whom undergone surgical callosotomy about 20 years ago. The original dataset consisted of 5 epileptic patients renamed P1-P5. P2 was rejected for too high rotational and translational movements of the head during the acquisition of functional and structural images with MR, resulting in too much noise during FSL analysis.

The more neuronal activity is shown in the right hemisphere of the brain respect to the left, this because, based on the theory of the lateralization the right hemisphere is more involved in spatial awareness, spatial visualization, and visual perception of the motion and shape of objects around us. This result is also perceptible from the study of patients who appear to have the right hemisphere with more neuronal activation than the left.

Across all the subjects, the networks more lateralized are the default mode network and the auditory area. The frontoparietal area left is identified in all the patients, resulting a good result since the left hemisphere is mainly involved in the comprehension and speech production. In all patients is also identified the default mode network, that results to be unilateral respect to healthy subjects in which it is strongly bilateral. It is associated with cognitive processes such as introspection, imagery of the future, and memory of the past. It is active only during the rest phase when the person is relaxing.

While some studies of typical interhemispheric coordination in neurologically intact participants suggest entirely cortical-cortical connections, others involve subcortical contributions (Uddin et al., 2008). Therefore, one could consider the fact that the brain, during its maturation over the years, has built new subcortical communication pathways, alternatives to the corpus callosum, which were then reorganized once the callosotomy

occurs. Through these alternative pathways the right hemisphere would be able to communicate with the left one, and therefore maintain a possible interhemispheric communication even with callosotomy.

Results from patients' analysis show a low degree of bilaterality in most resting state networks, probably due to callosotomy or pharmacological treatment of epilepsy. For these reasons, the functional connectivity of the networks is slightly altered. However, high degree of bilaterality is shown mainly in visual areas. In the comparison between patients and healthy template, the results show that patients P1, P3, P4 and P5 have bilaterality for the visual medial area and P5 also for the sensory-motor area.

The brain reaches its maturity around 20 years of age, once this maturity is reached, the communication routes between the two hemispheres alternative to the corpus callosum are fully developed. Thus, it is possible that in patients P1, P3, P4 and P5 alternative neural pathways to the corpus callosum for interhemispheric connections, prior to total callosotomy, have developed.

As shown in the study of Uddin and co-workers (Uddin et al. 2018), it is generally accepted that some interhemispheric transfer exists in the split-brain patients, because it is possible that specific resting state networks maintain bilateral presence after complete commissurotomy, suggesting that their coordination is subcortical in origin, post-surgery. In consequence, the comparison with intact brains suggests that in healthy patients' brain a possible dual mechanism exists meaning that cortical and sub-cortical mechanisms work together to coordinate networks. The persistence of some bilateral networks in patients demonstrates that the corpus callosum is not the only pathway involved in the connections between the two hemispheres.

Limitations

One limitation of this study is the manual classification of ICA components as signal of interest or noise/artifacts, which can be incorrectly interpreted due to the presence of noise that distorts the signal and which can be confused with signal if not carefully visualized and classified. Therefore, this procedure is preferred over automatic classification because the data set analyzed in this study corresponds to a group of

subjects with altered neural activity. Thus, some components corresponding to valid resting-state networks, may not be recognized, and classified as noise.

Another limitation of the study is the small number of patients, which however can be justified by the fact that the subjects who have undergone callosotomy are not a very large population, this type of operation being a solution that was performed in the past to correct epilepsy.

The multi-subject analysis allows the identification of only three activations attributable to Smith's 10 resting state networks. The small number of subjects (4) used for the analysis constitute a limit in the identification of the different areas of activation. Considering a greater number of subjects in the study would allow to recognize a greater number of ICA components corresponding to Smith's resting state networks.

Conclusions

The persistence of interhemispheric coordination in split-brain patients, can be justified by the possible presence of subcortical pathways. These pathways seem to be sufficient to transmit simple visual information, being the visual network bilateral in all considered split-brain patients. Moreover, the results demonstrate that the sensory-motor activation area shows a certain degree of bilaterality in patient P5, suggesting the existence, also in this case, of possible alternative networks to the corpus callosum.

Furthermore, in the comparison between intact brain and split-brain, it was found that the callosal connections may have a role when present, but in case of callosal resection, a subcortical route for information transferring to both hemispheres may be involved.

An improvement of this study could be targeted to the analysis of the Diffusion Tensor Imaging (DTI), acquiring the diffusion-weighted magnetic resonance images along two scanning directions (normally Antero-Posterior and Posterior-Anterior). Diffusion of water molecules plays a crucial role in understanding the local microstructure of the brain. DTI is a promising method to characterize microstructural changes providing image contrast based on differences in the amount of diffusion of water molecules in the brain. Thus, through DTI analysis it would be possible to obtain reliable images in which to identify the maximum diffusivity of molecules along the white matter, allowing to

highlight interhemispheric structural connections. DTI analysis applied to split-brain patients could demonstrate whether alternative interhemispheric pathways exist, despite callous resection, by controlling the diffusion intensity of fibers in different directions.

The present study has been able to highlight patterns of activation in split-brain patients comparable to those of healthy subjects that demonstrate functional interhemispheric connectivity following resection of the corpus callosum. The presence of bilateral activations in split-brain patients suggests that alternative sub-cortical connections to the corpus callosum have developed, allowing a structural connection between the two cerebral hemispheres. This study can be considered a milestone for future studies that target structural analysis, via diffusion tensor analysis, on split-brain patients.

Bibliography

Andy's Brain Book, 2019 GitHub

Amaro E. Jr., G.J. Barker, *"Study design in fMRI: Basic principles."* Brain and Cognition Volume:60(3), Pages:220-232. 19 January 2006, ELSEVIER

Ambrosi G., Cantino D., Castano P., et al., *"Anatomia dell'uomo"*, Chapter 14-Sistema Nervoso Centrale, Pages 313-401, Edi-Ermes, Milano 2010

Anastasi G., Capitani S., Carnazza M.L., et al., "Trattato di anatomia umana", Chapter:14, Pages: 10-15, edi-ermes, 2012, Google Scholar

Arnold S.T., Dodson W.E., *"Epilepsy in children"*, Baillieres Clin Neurol, Chapter 4, Pages:783-802, 1996 December 5, Scopus

Asadi-Pooya A.A.; Sharan A.; Nei M. ; et al*., "Corpus Callosotomy",* Epilepsy Behav, Chapter: 13, Pages: 271–278, 2008, CrossRef

Baynes K., Corpus Callosum, in *"Encyclopedia of the Human Brain"*, 2002, Chapter: I Anatomy. From: The Neuroscience of Autism Spectrum Disorders, 2013, PubMed

Bandettini P. A., *"Twenty years of functional MRI: The science and the stories."* Volume: 62(2), Pages:575-588, Neuroimage, 2012.

Beckmann C.F., "*Modelling with independent components",* Volume: 62, Pages: 891–901, 2012, NeuroImage

Beckmann C.F., DeLuca M., Devlin J.T., "*Investigations into resting-state connectivity using independent component analysis"*, Volume: 360(1457), Pages:1001-13, 2005, The Royal Society

Beckmann CF, Smith SM. *"Probabilistic Independent Component Analysis for Functional Magnetic Resonance Imaging"*. Transactions on Medical Imaging, Chapter:23 (2), Pages:137-152, 2004.

Beghi E., Carpio A., Forsgren L., et al., *"Recommendation for a definition of acute symptomatic seizure"*, Epilepsia, 51(4) Pages:671–675, 2010, PubMed

E. Beghi, G. Giussani, J. W. Sander. "*The natural history and prognosis of epilepsy*", March 25, 2015, PubMed

Berkovic S., Mulley J. C., Scheffer I. E., et al., *"Human epilepsies: interaction of genetic and acquired factors",* Vol. 29 No.7 July 2006, Elsevier Ltd. Pages:391-397, Scopus

Binder J.R., Frost J.A., Hammeke T.A., et al. *"Human brain language areas identified by functional magnetic resonance imaging"*, 1997 January, Chapter 17, Pages: 353-362. PubMed

Bijsterbosch J., Smith S.M., Beckmann C. *"Introduction to Resting State fMRI Functional Connectivity",* Oxford University Press, 2017.

Brodal P., "The central nervous system", Chapter 2, Pages:19-20, Oxford University Press, 2010

Buckner R. L., "*Event-Related fMRI and the Hemodynamic Response",* Human Brain Mapping Volume:6, Pages:373–377, 1998, PubMed

Chan R. W., Lau Justin Y.C., Wilfred W. Lam, et al., Encyclopedia of Biomedical Engineering, Pages 574-587, 2019, Magnetic Resonance Imaging

Chaplin T.A., Rosa M.G.P., Yu H., Chapter 22 – *"Scaling Up the Simian Primate Cortex: A Conserved Pattern of Expansion Across Brain Sizes",* 2020, Pages 533-545, Evolutionary Neuroscience (Second Edition), PubMed

Chen I.; Lui F.*, "Neuron Action Potential",* Neuroanatomy, National Library of Medicine, August 11, 2021, Google Scholar

Cleary J.O.S.H., Guimarães A.R., *"Pathobiology of Human Disease",* A Dynamic Encyclopedia of Disease Mechanisms, Pages 3987-4004, 2014, Magnetic Resonance Imaging

Eccher M., in "*Encyclopedia of the Neurological Sciences"* (Second Edition), 2014, Corpus callosum, Introduction. From: The Neuroscience of Autism Spectrum Disorders, 2013, Google Scholar

Farlex Partner Medical Dictionary, Farlex 2012.

Finger S., *"Origins of Neuroscience: A History of Explorations Into Brain Function"*. Oxford University pp. 42. Retrieved 26 January 2013, Scopus

Fiore F. *"L'area di Wernicke: la sede della comprensione del linguaggio*" – Introduzione alla Psicologia, 06 dicembre 2018, Sigmund Freud University, Milano

Fisher R.S., Acevedo C., Arzimanoglou A., et al. *"ILAE official report: a practical clinical definition of epilepsy"*. Epilepsia. 2014; Volume: 55(4) Pages:475-482, PubMed

FSL-GUI, FMRIB Software Library version 6.0, Created by the Analysis Group, FMRIB, Oxford, UK,2020

Gore J.C. ,*"Principles and practice of functional MRI of the human brain."* The Journal of Clinical Investigation, Volume: 112, Pages: 4-9, 2003, ResearchGate

Griffanti L, Douaud D, Bijsterbosch J, et al., *"Hand classification of fMRI ICA noise components"*, Chapter:154 Pages: 188-205, 2017, NeuroImage.

Jenkinson M, Bannister P, Brady JM, et al., *"Improved Optimisation for the Robust and Accurate Linear Registration and Motion Correction of Brain Images",* Chapter:17 (2), Pages: 825-841, 2002, NeuroImage

Jezzard, P., Clare, S, *"Sources of distortion in functional MRI data".* Hum. Brain Mapp. 8, 80–85, 1999, PubMed

Johansson C.B., Momma S., Clarke D.L., et al. "Identification of a neural stem cell in the adult mammalian central nervous system". Chapter: 96, Pages: 25–34, January 1999, PubMed

King-Stephens D., Chapter 49 – *"Epilepsy: Anatomy, Physiology, Pathophysiology, and Disorders",* Neuromodulation 2009, Pages: 619-623, Google Scholar

Lee M.H., Smyser C.D. and Shimony J.S., *"Resting-State fMRI: A Review of Methods and Clinical Applications"*, Chapter:34 (10), Pages: 1866-187, American Journal of Neuroradiology October 2013

Le Bihan D., Mangin J.-F., Poupon C., et al. *"Diffusion Tensor Imaging: Concepts and Applications"*, Journal of magnetic resonance imaging Volume: 3, Pages:534–546, 2001, PubMed

Lienhard, Dina A., *"Roger Sperry's Split-Brain Experiments (1959–1968)".* Embryo Project Encyclopedia (2017) Pages: 12-27.

Liu G., Slater N., Perkins A., *"Epilepsy: Treatment Options",* Am Fam Physician. 2017; Chapter: 96(2), Pages:87-96, PubMed

Luat A. F., Asano E., Kumar A., et al. *"Corpus callosotomy for intractable epilepsy revisited: the Children's Hospital of Michigan series J Child Neurol*"; Volume: 32(7), Pages: 624–629, 2017, PubMed

Matthews P.M., Jezzard P., *"Functional magnetic resonance imaging"*, Journal of Neurology, Neurosurgery & Psychiatry; Chapter: 75, Pages: 6-12, 2004, PubMed.

Mingoia G.,Wagner G., Langbein K., et al., *"Default mode network activity in schizophrenia studied at resting state using probabilistic ICA",* Schizophrenia Research Chapter: 138, Pages:143–149, 2012, Elsevier, Scopus

Mohr J. P., Pessin M. S., Finkelstein S., et al., *"Broca aphasia, Pathologic and clinical"*, Chapter: 28 (4) Page:311; DOI: 10.1212/WNL.28.4.311, Neurology Apr 1978, Google Scholar

Moini J., Piran P., *"Cerebral cortex, Functional and Clinical Neuroanatomy, A Guide for Health Care Professionals"*, Chapter 6, Pages 177-240, 2020, Scopus

Moini J., Piran P., *"Split-brain syndrome"*, Chapter: Cerebral cortex, Functional and Clinical Neuroanatomy, 2020, Science Direct, Scopus

Nashef L., *"Sudden unexpected death in epilepsy: terminology and definitions"*, Epilepsia, 1997; Chapter: 38(11 suppl): Pages: S6-S8, Google Scholar

National Clinical Guideline Centre (January 2012). *"The Epilepsies: The diagnosis and management of the epilepsies in adults and children in primary and secondary care",* London: Royal College of Physicians (UK); 2012 Jan, Google Scholar

Ogawa S., Lee T.M., Kay A.R., et al., *"Brain magnetic resonance imaging with contrast dependent on blood oxygenation."* Proceedings of the National Academy of Sciences of the United States of America Volume:87(24), Pages:9868- 9872, 1990

Okanishi T., Fujimoto A., *"Corpus Callosotomy for Controlling Epileptic Spasms: A Proposal for Surgical Selection"*, 1 December 2021, PubMed

Palmer H., Berntsen E. M, *"Reduced Fractional Anisotropy Does Not Change the Shape of the Hemodynamic Response in Survivors of Severe Traumatic Brain Injury",* Journal of Neurotrauma Volume:27, Pages: 853–862 (May 2010), ResearchGate

Petelin Gadže Ž., *"Epilepsy in children – clinical and social aspects"*, August, 2011, Google Scholar

Poldrack R., Mumford J., Nichols T.*, "Handbook of Functional MRI Data Analysis",* Cambridge University Press, Chapter 3, Pages: 37-40 and Chapter 8 Pages: 138-140, 2011.

Prete G., Tommasi L., Progress in Brain Research, Chapter 10 – *"Split-brain patients: Visual biases for faces"*, Volume 238, Pages 271-291, 2018, Scopus

Purves D., Augustine G.J., Fitzpatrick D., et al. Sunderland: *"Neuroscience. 2nd edition*". Sinauer Associates, Chapter: The Ventricular System, 2001, Google Scholar

Rangaprakash D., Dretsch M. N., Yan W. et al. *"Hemodynamic response function parameters obtained from resting-state functional MRI data in soldiers with trauma".* 2017, PubMed

Rangaprakash D., Tadayonnejad R., Deshpande G., *et al. "FMRI hemodynamic response function (HRF) as a novel marker of brain function: applications for understanding obsessive-compulsive disorder pathology and treatment response."* Brain Imaging and Behavior, Volume:15, Pages:1622–1640 (2021).

Robert E, Kelly Jr, Alexopoulos GS, et al., *" Visual inspection of independent components: Defining a procedure for artifact removal from fMRI data"*, Chapter:189 Pages: 233-245, 2010, Journal of Neuroscience Methods.

Russell J., Wanda D., Webb G., *"Neurology for the Speech-Language Pathologist"* (Second Edition), Pages 183-23310 - The Central Language Mechanism and Its Disorders, 1992, PubMed

Sahayaraj S., *"Knowledge Discovery through computations on EEG and fMRI data",* October 2015, ResearchGate

Scelsi C.L., Rahim T.A., Morris J.A., et al. *"The Lateral Ventricles: A Detailed Review of Anatomy"*, April 2020, PubMed

Seitun A*., "Neurologia di Fazio-Loeb",* Volume 2, Capitolo 40, Epilessia, Pages: 1295-1375, Società Universo Editrice, V edizione, 2019

Smith S. M., Fox P.T., Millera K. L., et al., "Correspondence of the brain's functional architecture during activation and rest", Volume 106, Pages: 13040-13045, 2009, PubMed

Smith S. M., Jenkinson M., Woolrich M.W., et al. , *"Advances in functional and structural MR image analysis and implementation as FSL",* NeuroImage Chapter:23, Pages: 208–219, 2004, Scopus

Soares J. M., Marques P., Alves V. et al. *"A hitchhiker's guide to diffusion tensor imaging",* Frontiers Neuroscience, 12 March 2013

Sperry R.W., *"Hemisphere deconnection and unity in conscious awareness",*American Psychologist, Volume: 23 (10), Pages:723-733, 1968.

Sporns O*., "Structure and function of complex brain networks*", Pages: 247-262, 2013 PubMed

Stafstrom C.E., Carmant L., *"Seizures and epilepsy: an overview for neuroscientists"*, Cold Spring Harb Perspect Med. 2015 Jun 1;5(6): a022426, PubMed

Stejskal E. O. and Tanner J. E., *"Spin Diffusion Measurements: Spin Echoes in the Presence of a Time-Dependent Field Gradient",* 2004, AIP Publishing, The Journal of Chemical Physics

Stinnett T. J.; Reddy V.; Zabel M. K., *"Neuroanatomy, Broca Area"*, August 15, 2021, PubMed

Stone J. V., *"Independent component analysis: an introduction",* Volume 6 No.2, Chapter 8, Pages: 59-64, February 2002, PubMed

Uddin L. Q.*, "Complex relationships between structural and functional brain connectivity*", Volume: 17, No. 12, 2013, PubMed

Uddin L.Q., Mooshagian E., Zaidel E.,et al..*, "Residual functional connectivity in the split-brain revealed with resting-state functional MRI"*, Chaper:19(7) Pages::703-9, 2008, Neuroreport

University of Michigan, "*Andy's Brain Book"*, Chapter 1: Brain Extraction (also known as "skullstripping"), GitHub, 2022

Vaddiparti A., Huang R., Blihar D., et al., *"The Evolution of Corpus Callosotomy for Epilepsy Management"*, World Neurosurgery 145: 455-461, January 2021, PubMed

Vago D.R., Wallenstein G.V., Morris L.S., "*Encyclopedia of the Neurological Sciences"* (Second Edition), Pages 566-570, Hippocampus, 2014, Google Scholar

van Geuns R.-J. M., Wielopolski P. A., de Bruin H. G. et al., *"Basic Principles of Magnetic Resonance Imaging",* Progress in Cardiovascular Diseases, Volume: 42, No. 2 (September/October), Pages: 149-156, 1999

van den Heuvel M. P. , Hillek E. , Hulshoff P. , *"Exploring the brain network: A review on resting-state fMRI functional connectivity"*, 23 March 2010, Pages: 520-534, Scopus

Waxman S.G., “The ventricular system”, Cancer Neuroanatomy 26th, October 2020

West K. L., Zuppichini M. D. ,Turner M. P. et al., *“BOLD hemodynamic response function changes significantly with healthy aging”,* Volume 188, Pages: 198-207, March 2019, Neuro-Image

Woolrich M. W., Jbabdi S., Patenaude B. et al., *“Bayesian analysis of neuroimaging data in FSL”,* NeuroImage Volume 45, Pages: 173–186, 2008, Scopus

Acknowledgements

Innanzitutto, desidero ringraziare la mia correlatrice, la Prof.ssa Mara Fabri, che ha accettato di seguirmi ed è stata di fondamentale importanza nella stesura della tesi. Voglio ringraziare inoltre la mia correlatrice la Dott.ssa Ilaria Marcantoni, che è sempre stata presente e paziente, dandomi consigli puntuali ed indispensabili.

Un altro speciale ringraziamento è dedicato alla Prof.ssa Laura Burattini, che mi ha indirizzato sulla scelta dell'argomento, e dal quale ho potuto trarre molto entusiasmo nello svolgere questo elaborato.

Un altro ringraziamento va a Giusi Piccolantonio e alla sua infinita disponibilità, perché senza il suo aiuto sarei ancora lontana dal traguardo.

Ho il piacere di ringraziare anche chi non ho conosciuto in prima persona, ma senza i quali non avrei mai potuto svolgere questo lavoro. Queste persone sono il Prof. Gabriele Polonara, direttore di Neuroradiologia, la Dott.ssa Mojgan Ghoushi, dirigente medico di Neuroradiologia, Luigi Imperiale e Lucio Montesi, Tecnici di Neuroradiologia (acquisizione e salvataggio dati), Marco Valenti e Luca Reversi, fisici del Servizio di Neuroradiologia, la Dott.ssa Nicoletta Foschi, dirigente medico di Neurologia, referente per i pazienti epilettici e la Dott.ssa Simona Lattanzi, ricercatrice Clinica Neurologica, referente per i pazienti epilettici.